creative commons

COMMONS DEED

저작자표시-비영리-변경금지 2.0 대한민국

이용자는 아래의 조건을 따르는 경우에 한하여 자유롭게

- 이 저작물을 복제, 배포, 전송, 전시, 공연 및 방송할 수 있습니다.

다음과 같은 조건을 따라야 합니다:

저작자표시. 귀하는 원저작자를 표시하여야 합니다.

비영리. 귀하는 이 저작물을 영리 목적으로 이용할 수 없습니다.

변경금지. 귀하는 이 저작물을 개작, 변형 또는 가공할 수 없습니다.

- 귀하는, 이 저작물의 재이용이나 배포의 경우, 이 저작물에 적용된 이용허락조건을 명확하게 나타내어야 합니다.
- 저작권자로부터 별도의 허가를 받으면 이러한 조건들은 적용되지 않습니다.

저작권법에 따른 이용자의 권리는 위의 내용에 의하여 영향을 받지 않습니다.

이것은 이용허락규약(Legal Code)을 이해하기 쉽게 요약한 것입니다.

Disclaimer

dCollection

조선대학교
CHOSUN UNIVERSITY

[UCI]I804:24011-200000265163

February 2016

Phd Dissertation

A Comparative Analysis of Image Denoising Techniques for Efficient Interpolation in Noisy Color Channel

Graduate School of Chosun University

Department of Information and Communications Engineering

Ramesh Kumar Lama

조선대학교
CHOSUN UNIVERSITY

A Comparative Analysis of Image Denoising Techniques for Efficient Interpolation in Noisy Color Channel

February 25 2016

Graduate School of Chosun University

Department of Information and Communications Engineering

Ramesh Kumar Lama

Collection @ chosun

조선대학교
CHOSUN UNIVERSITY

A Comparative Analysis of Image Denoising Techniques for Efficient Interpolation in Noisy Color Channel

Advisor: Prof. Goo-Rak Kwon

This thesis is submitted to Chosun University in partial fulfillment of the requirements for a PhD Dissertation

October 2015

Graduate School of Chosun University

Department of Information and Communications Engineering

Ramesh Kumar Lama

Collection @ chosun

조선대학교
CHOSUN UNIVERSITY

라마 라메쉬 쿠마의 박사학위논문을 인준함

위원장 조선대학교 교수 변재영 (인)

위 원 조선대학교 교수 한승조 (인)

위 원 동국대학교 교수 정승원 (인)

위 원 (주)성광 연구소장 김종우 (인)

위 원 조선대학교 교수 권구락 (인)

2015 년 12 월

조선대학교 대학원

Collection @ chosun

조선대학교
CHOSUN UNIVERSITY

Contents

Collection @ chosun

조선대학교
CHOSUN UNIVERSITY

Collection @ chosun

조선대학교
CHOSUN UNIVERSITY

Collection @ chosun

조선대학교
CHOSUN UNIVERSITY

List of Figures

Collection @ chosun

조선대학교
CHOSUN UNIVERSITY

Collection @ chosun

조선대학교
CHOSUN UNIVERSITY

Collection @ chosun

조선대학교
CHOSUN UNIVERSITY

Collection @ chosun

조선대학교
CHOSUN UNIVERSITY

List of Tables

,

Collection @ chosun

조선대학교
CHOSUN UNIVERSITY

Acronyms

CFA	Color Filter Array
CCD	Charged Couple Device
RGB	Red Green Blue
CMOS	Complementary Metal Oxide Semiconductor
MOSFET	Metal Oxide Semiconductor Field Effect Transistor
PCA	Principal Component Analysis
CDM	Color Demosaicking
SVD	Singular Value Decomposition
HD	High Definition
HMM	Hidden Markov Model
DTCWT	Dual Tree Complex Wavelet Transform
LL	Low Low
LH	Low High
HL	High Low
HH	High High
MDC	Multiple Description Coding
HDTV	High Definition Television
POCS	Projection onto Convex Sets
HMT	Hidden Markov Tree
DWT	Discrete Wavelet Transform
CWT	Complex Wavelet Transform
GMM	Gaussian Mixture Model
EM	Expectation Maximization
DCT	Discrete Cosine Transform
ADWT	Adaptive Directional Wavelet Transform
ADL	Adaptive Directional Lifting
NEDI	New Edge Directed Interpolation
FFT	Fast Fourier Transform
MSE	Mean Square Error
PSNR	Peak Signal to Noise Ratio

Collection @ chosun

조선대학교
CHOSUN UNIVERSITY

Abstract

A Comparative Analysis of Image Denoising Techniques for Efficient Interpolation in Noisy Color Channel

Ramesh Kumar Lama
Advisor: Prof. Goo-Rak Kwon, Ph.D
Department of Information Communication Engineering,
Graduate School of Chosun University

Most of the existing image interpolation schemes assume that the low resolution image is noise free. This assumption is invalid in practice because image is corrupted by noise during the image acquisition process. This thesis presents a implementation of denoising and interpolation sequentially. For each noisy sample, we propose an efficient noise reduction technique designed to work with Color Filtering Array (CFA) data acquired by CCD/CMOS image sensors. CFA image neighborhood vectors are first projected on the principal component analysis (PCA) bases. The PCA bases are obtained by eigenvalue decomposition. The denoising is performed by the shrinkage of coefficients of patches which we obtain from principal components. The effectiveness of the shrinkage depends on the selection of threshold and transform to sparsely represent the true image data, thus separating it from the noise. The proposed method estimates the optimized threshold value based on the local statistical characteristics of the patch. Final color image is generated by color demosaicking (CDM). Once the CDM is accomplished, the low resolution image is interpolated to fit on the high resolution display

Collection @ chosun

조선대학교
CHOSUN UNIVERSITY

devices. In this dissertation we implement various wavelet based interpolation schemes which are adaptive directional wavelet transform, hybrid implementation of discrete wavelet transform and discrete cosine transform (DCT) and dual-tree complex wavelet transform (DT-CWT) and hidden Markov model (HMM). The adaptive directional wavelet transform is the lifting implementation of wavelet transform. This method is able to transform an image along multiple directions as well as conventional horizontal and vertical orientations. In the proposed method the high-frequency sub band images are obtained by adaptive wavelet transforms (ADWT). We interpolate high-frequency sub band images and the input low resolution image, and finally the high resolution image is generated by combining the interpolated subimages in the inverse ADWT process. In hybrid implementation of wavelet transform and DCT, the high frequency wavelet coefficients are interpolated using the zero pad method in DCT domain. The upscaled image is generated using inverse DWT of interpolated coefficients and original image. Finally in DT-CWT based method, we use DT-CWT is to decompose the low-resolution image into different subbands. The proposed method estimates the higher band coefficients by learning the correlation between the coefficients across the scale. In this paper, the relationship between the wavelet coefficients across the scale is described by HMM, and each wavelet coefficient is modelled by a Gaussian mixture having multiple means and variances. Experimental results demonstrate that the proposed methods are competitive with state-of-the-art methods despite its simplicity. The proposed method is also suitable for implementation in low power mobile devices with imaging capabilities such as camera phones.

Collection @ chosun

조선대학교
CHOSUN UNIVERSITY

초 록

노이즈 색상 채널에서 효율적인 보간법을 위한 영상 디노이징 기술의 비교 분석

라마 라메쉬 쿠마
지도교수: 권구락 교수, Ph.D
정보통신공학과, 대학원, 조선 대학교

기존의 대부분의 영상 보간 방식은 노이즈가 없는 것으로 가정한다. 노이즈가 영상 복호화 과정에서 사라지기 때문에 이러한 가정은 실제로 유효하다. 이 논문은 영상의 순차적인 잡음 제거와 보간 구현 방법에 대해 설명한다. 또한, 잡음 샘플(noisy sample)을 위해, CCD / CMOS 영상 센서에서 얻어진 컬러 필터링 어레이(CFA)에 적용할 수 있는 효율적인 잡음 감소 기법을 제안한다. 화상 이웃 벡터는 PCA 베이스 상에 투사된다. PCA 베이스는 고유 분해에 의해 얻을 수 있다. 잡음 제거는 영상의 주 성분으로부터 여러번 패치된 된 계수의 수축에 의해 수행된다. 수축 효과는 임계치의 선택과 노이즈로부터 원본 영상을 분리하려는 변환 과정에 의존한다.

제안하는 방법은 패치의 통계적인 특성들에 기초하여 최적화 된 임계 값을 추정한다. 한번 CDM이 수행되고 나면, 저해상도 영상은 듀얼-트리 콤플렉스 웨이블릿 변환과 (DT-CWT) 히든 마르코프 모델(HMM)을 기초하여 고해상도의 표시 장치에 적합하도록 보간된다. 제안한 방법의 DT-CWT는 상이한 서브밴드의 저해상도 화상을 분해하는데에도 사용된다. 웨이블릿 도메인 보간에서 주어진 영상은 고해상도 영상의 웨이블릿 계수의 저주파 LL 서브밴드로 간주된다. 제안한 방법을 통해 전체 스케일 계수간 상관 관계를 학습하여 보다 큰 크

Collection @ chosun

조선대학교
CHOSUN UNIVERSITY

기를 가진 밴드 계수들을 추정한다. 이 과정에서 스케일 사이간 웨이블릿 계수의 관계는 HMM에 의해 기술되고, 각각의 웨이블릿 계수들은 여러 수단 및 분산을 갖는 가우시안 혼합에 의해 모델링된다.

실험 결과를 통해 제안한 알고리즘은 기존의 다른 방법들에 비해 선명한 이미지를 얻을 수 있음을 증명한다. 그리고 기존 방법보다 단순하면서 보다 향상된 성능을 보여준다.

또한 제안한 방법은 카메라 폰 등의 촬상 기능을 가진 저전력 모바일 장치에서 구현하기에 적합하다.

Collection @ chosun

조선대학교
CHOSUN UNIVERSITY

Chapter 1

Introduction

Image interpolation is a process that is often used for image enlargement from its down-sampled version [34] or simply resizing the image from one pixel grid grid to another. Interpolation has been widely used in many image processing applications such as facial reconstruction, multiple description coding (MDC), super resolution and digital high-definition television (HDTV) [35]- [37]. The rapid advancements in hardware and display devices have made it possible to process high-resolution digital color images as shown in Figure 1.1. In order to utilize the display power of these state of-the-art viewing devices efficiently, input signals from a lower-resolution source must be upscaled to higher resolutions through interpolation. Most of the existing image interpolation schemes assume that the image is noiseless. However, this assumption is invalid in practice because image is corrupted by the noise during the image acquisition process specifically when the color channels are noisy.

Image denoising and interpolation are important tool in image processing. Since most of digital cameras are composed of a 2D grid of widely dissimilar imaging sensors, these methods are inherent to digital image acquisition. Thus, the noise must be removed prior to interpolation of image. The multichannel nature of color images demands efficient signal processing algorithms that take into account the existing inter-channel correlations when performing image size expansion and noise reduction. In [6], an algorithm of joint denoising and interpolation was proposed by using the directional interpolation technique. In [7], Zhang et al proposed joint denoising and demosaicking scheme using a directional filtering and wavelet transform. The whole algorithm is comprises two steps. The first step estimates the filter coefficients to denoise the noisy low resolution pixels. in the second stage,Similarly the weights calculated in first stage for denoising are employed directly for image interpolation and thus increasing the resolution of image simultaneously. The joint denoising and interpolation

Collection @ chosun

조선대학교
CHOSUN UNIVERSITY

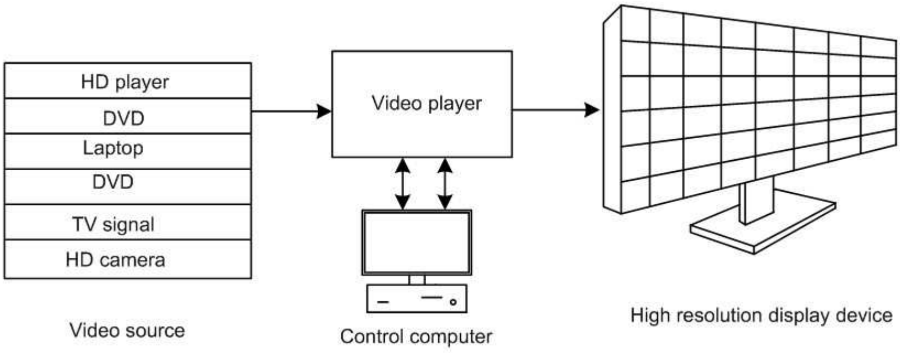

Figure 1.1: High resolution video wall display system.

method, can generate less artifacts. However the well designed denoise first and interpolation can also generate better results. In [25] Zhang et al proposed principal component analysis (PCA) based spatially-adaptive denoising algorithm. This method processes directly the CFA data using a variable sized window to analyze the local image statistics. The spatial and spectral correlations existed in the CFA image are exploited. Thus this method is capable of preserving the color edges and details while suppressing the noise.

1.1 Contributions of Dissertation

This thesis presents a new and efficient scheme for interpolating the noisy color image and noiseless color image. The overall system comprises two stages. In the first stage, denoising is performed while in the second stage the denoised and complete noiseless images are interpolated. In most of the real time scenario, image is corrupted by noise during the acquisition process. Thus the we propose effective denoising method to reduce the sensor noise in color filter array (CFA) in this dissertation. The mathematical tool of principle component analysis (PCA) [26], [54], is employed to analyze the local structure of each CFA blocks, which contains color components from different channels. We compute the co-variance matrix of each block. The noisy CFA image data is transformed

Collection @ chosun

조선대학교
CHOSUN UNIVERSITY

into another space by using PCA. In new space the signal energy is better clustered thus making easier to remove the noise more effectively. Since there can be a varying structures in each local window, to improve the estimation accuracy of PCA transformation matrix we divide the large sized patches into number of smaller blocks based on structural similarity. In the second stage, we interpolate the denoised image based on different wavelet transform techniques. We employ lifting based adaptive directional wavelet transform and the dual-tree complex wavelet transform (DT-CWT) to decompose the low-resolution image into different subbands. In wavelet domain interpolation, the given low resolution (LR)image and high frequency subband images are interpolated. Low resolution image is used instead of low frequency subband image. For adaptive directional wavelet transform (ADWT), we follow the general approach of interpolating the low resolution high frequency subbands images to generate high resolution subband images. In hybrid approach, the high resolution high frequency subband images are estimated using discrete cosine transform(DCT) based zero padding. Finally, for DT-CWT we generate the high resolution wavelet coefficient by learning the correlation between the coefficients across the scale. In this dissertation, the relationship between the wavelet coefficients across the scale is described by HMM, and each wavelet coefficient is modeled by a Gaussian mixture having multiple means and variances. Moreover, the each algorithms can be implemented together or they can be implemented separately as per requirement.

1.2 Organization of Dissertation

The remainder of this thesis is organized in modular chapters. Chapter 2 presents overview of the image acquisition using color filter array and describes the degradation of image by noise. System to reduce the noise is presented in Chapter 3. Chapter 4 demonstrates the reduction of noise reduction present in the CFA image by the proposed algorithm through simulation result. Interpolation of image in noisy channel is introduced in chapter 5 followed by review of wavelet transform on chapter 6 and dual tree complex wavelet transform based image interpolation

Collection @ chosun

조선대학교 CHOSUN UNIVERSITY

in chapter 7. Thesis is concluded in the last chapter with wrapping text for the summary of this research in chapter 8.

Collection @ chosun

조선대학교
CHOSUN UNIVERSITY

Chapter 2

Image acquisition

The modern digital camera captures the image by using a variety of sensor architectures based on charge-coupled device (CCD) and Complementary metal oxide semiconductor (CMOS) integrated circuit (IC) technologies [1]. This IC technology comes with either single sensor or separate color sensors for each color [2]. Since the single sensor architecture requires less number of image sensor cells this architecture is cheaper than multiple sensor architecture. The single sensor architecture places a color filter array (CFA), on top of the conventional single CCD/CMOS sensor to capture all three primary Red, Green and Blue (RGB) colors simultaneously [3]- [5]. Each sensor cell consists of spectrally selective filter, thus storing a single color measurement. Therefore, the CFA image constitutes a mosaic like grayscale image with only one color element available in each pixel location. In such scenario, a digital processing solution called the demosaicing is use to estimate the two missing colors from the adjacent pixels [7]- [9]. The image formation process through demosaicing may contain noisy artifacts in low cost devices such as mobiles phones and PDAs mainly due to low light conditions.

2.1 Introduction to CFA Images

To produce a color image, each pixel location requires at least three color samples. The conventional approach is to project the image onto three separate sensors using beam splitters along the optical path [4]. With this approach, three full-channel color images are obtained using a color filter in front of each sensor. However, the sensors have to be aligned precisely and moreover; this is a costly approach as it requires three CCD sensors [5]. The cost effective solution is to put a CFA in front of the sensor to capture one color component of a pixel and then interpolate the missing two color components [6]. A color reconstruction

Collection @ chosun

조선대학교
CHOSUN UNIVERSITY

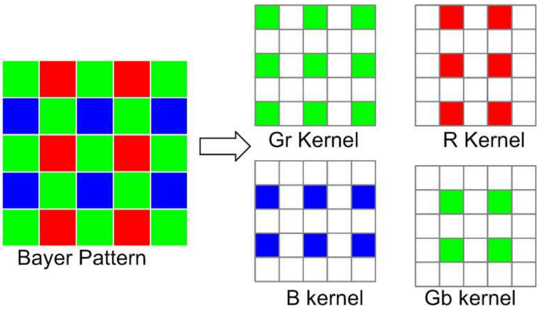

Figure 2.1: Filter mask for Bayer pattern data.

algorithm interpolates the missing information at each location and reconstructs the full RGB image [9]. Since the human eye is more sensitive to gren color, the green color component is twice the number of red and blue pixels. Thus the green color has higher weight while computing the luminance. We can implement post processing techniques [2] or increase the resolution [3]), or take multiple shot acquisitions to optimize the final perceived quality of images [4], [5]. All these operations are performed taking into account that the raw image is acquired in Bayer pattern [6].

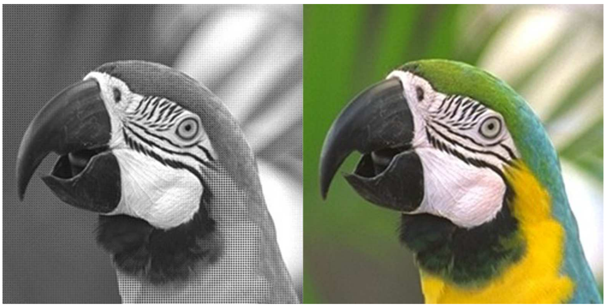

Figure 2.2: Single-sensor imaging concept: (a) a CFA image; (b) demosaicked full-color version of (b).

Collection @ chosun

조선대학교
CHOSUN UNIVERSITY

2.2 Raw Images Noise Model

Noise is a stochastic phenomenon that can neither be compensated nor eliminated. Numerous sources cause the generation of noise in CCD and CMOS sensors. Primarily, they can be classified into four types. (1) The photon noise also known as Poisson noise caused by a random nature of photons incident on photosite [62]; (2) the Photon Response non uniformity occurs due to small sensitivity differences between photosites; (3) the dark current noise which is occurred due to thermally generation of minority carriers in the sensor wells; and (4) the readout noise; resulting from thermal noise caused by MOSFET amplifiers. However in general, noise in raw images has basically two main sources:

1. N_p: caused by the discrete nature of light itself (Poisson distributed).
2. N_G: caused by the electric and thermal noise of image (Gaussian distributed)

The N_p term is related to the number of photons impinging on the image which is not constant over time but follows a Poisson distribution. Poisson noise, also called the photon noise is a signal-dependent noise. This type of noise is caused by the uncertainty associated with the measurement of light. In real imaging systems, the number of photons incident on the image sensor defines the light energy time impinging on the image sensor [62]. The fundamental statistical nature of photon production is random in nature. This random nature of individual photon leads to photon noise [63]. Thus the individual photon detection resembles the independent events that follow a temporal distribution. As a result, photon counting is a classic Poisson process, the probability distribution of N_p photons in an observation window of length t second is expressed as

$$p(N_p = k) = \frac{(\lambda t)^k \, e^{-\lambda t}}{k!} \tag{2.1}$$

where λ is the rate or the intensity parameter measured in photons per second. It is critical to understand that even if there were no other noise sources in the imaging

Collection @ chosun

조선대학교 CHOSUN UNIVERSITY

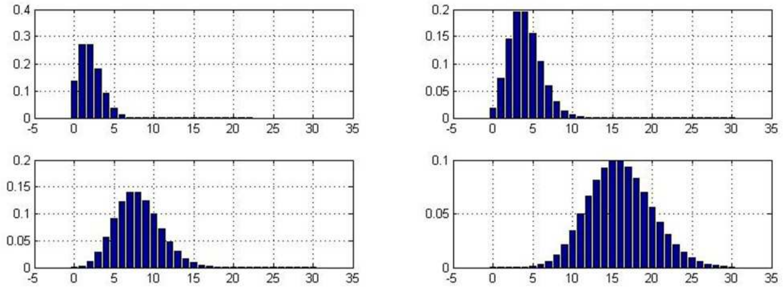

Figure 2.3: Poison distribution for different value of λ.

chain, the statistical fluctuations associated with photon counting over a finite time interval t would still lead to a finite signal-to-noise ratio(SNR). Because the incident photon count follows a Poisson distribution, it has the property that its variance is equal to its expectation, $E[N] = Var[N] = \lambda t$. This shows that photon noise is signal dependent, and that its standard deviation grows with the square root of the signal. In practice, photon noise is often modelled using a Gaussian distribution whose variance depends on the expected photon count. We usually model the other noise source as thermal noise, read-out noise, amplifier noise, and quantization noise as overlapped gausssians. A signal dependent noise is generated by the overlap of all type of noises. The standard deviation of such noise can be estimated

$$\sigma_i = \sqrt{a.i + b} \tag{2.2}$$

where: $a, b \epsilon R^+$ is signal intensity. To this end, we observe that the amount of light incident on image sensor characterizes the noise on the scene being captured. i.e. in order to obtain an acceptable image we must amplify the signal in low illumination condition. At sensor level, the signal amplification is obtained as a result of analog gains that boost the detected intensities. However, the noise level also boosts together with signal. One cannot amplify image signal without boosting noise levels. Which results to the amplification of signal and noise at higher analog gain applied at sensor level. In readout process a voltage value is read for each pixel. This voltage is read indicates the potential difference from a

Collection @ chosun

조선대학교
CHOSUN UNIVERSITY

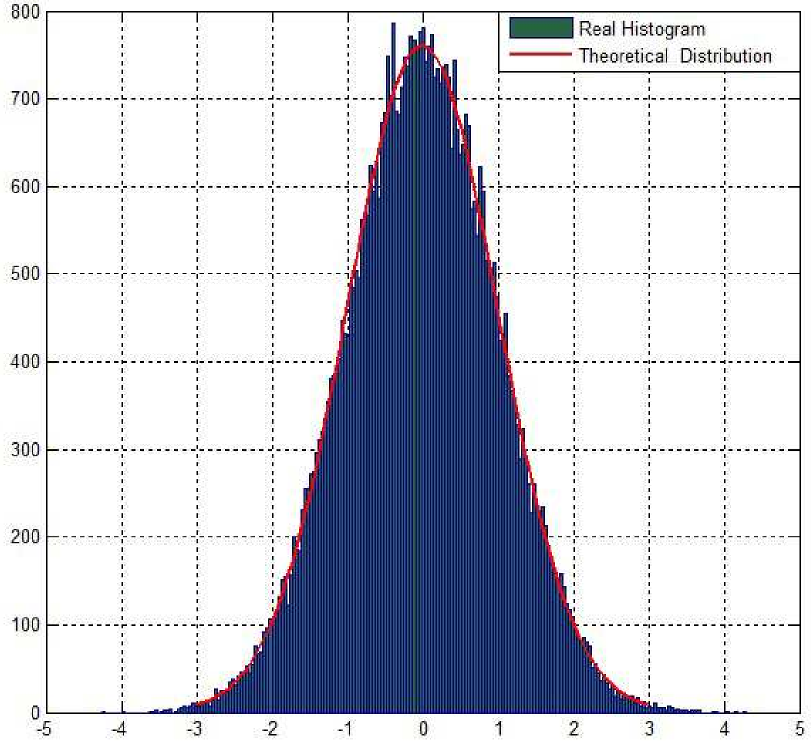

Figure 2.4: Additive noise distribution.

reference level. The absence of light and read noise typically follow a Gaussian distribution across all the pixels in the sensor. The readout noise typically follows a gaussian distribution across all the pixels in the sensor. Thus this readout noise can be expressed as an average value. Figure 2.4 shows the characteristics of a single data digitizer with a single Gaussian noise distribution. In CFA data the presence of noise not only deteriorates the visual quality of the captured image, but also the demosaicking artifacts are generated, regardless of the demosaicking technique.

Collection @ chosun

조선대학교
CHOSUN UNIVERSITY

2.3 CFA Sensor Noise

The Bayer pattern is widely used for analysis of noise in CFA images [1]. Thus we consider this pattern for noise reduction and the algorithm can be easily extended to other CFAs. The Bayer pattern is composed of interlaced red, green and blue samples, with the green channel having double sampling frequency compared to the red and blue channels. In order to produce full- color image from the CFA sensor readings the interpolation of two missing color components at each pixel location in the CFA image is employed known as known as color demosaicking (CDM). Most CDM algorithms assumes that the CFA data is noise free. However, this assumption is invalid in real time practice. Digital color imaging devices, ranging from the low cost and/or resource constrained ones (e.g.,wireless camera phones) to the high-end ones (e.g.,digital cinema cameras) produce images with modest to severe noise especially in low light condition. The main source of noise on the color channel is the image sensor itself. The digital camera sensor comprises a incredibly small photocells, especially with high-resolution compact camera sensors. Most compact camera sensors are of the 1/2.3 inch type, but commonly have over 10 million individual photocells crammed into an area of less than 30 square millimeters.Since the light sensing cells are so tiny, they may not be able to collect sufficient number of photons in low light conditions. Thus the random statistical fluctuation in photon density may occur, which results to effect on level of the electric signal produced by photo cell. Thus the physically larger sensors generates better image quality than by smaller ones especially when the light is low. With the introduction of noise in raw images, the quality of photograph is downgraded. Denoising of such image can be performed by modelling the sensor noise either a signal dependent or independent of signal. Foi et al. [27] modelled the sensor noise as signal-dependent. Poisson or multiplicative model can be used to model the noise in such scenario. Similarly, Hirakawa [29] proposed the raw sensor output as additive noise model with combination of gaussian and sensor dependent parameters. However this algorithm works with demand of high computational cost. The widely used and

Collection @ chosun

조선대학교
CHOSUN UNIVERSITY

simple noise model is additive noise model which is signal independent. This model has been widely used because of it's simplicity in literatures [19]; [24];. The signal-dependent noise characteristic can be compensated by estimating the noise variance adaptively in each local area [33]. In [24], Zhang et al. proposed additive noise model, to denoise the CFA image. In this method different types of color filters in the CFA are considered. The noise signals in the red, green and blue locations of the CFA image are assumed channel-dependent and expressed as

$$\hat{y_r} = s_r + n_r, \hat{y_g} = s_g + n_g, \hat{y_b} = s_b + n_b \tag{2.3}$$

where n_r, n_g, and n_b are the noise signals in the red, green and blue locations of the CFA image. The terms s_r, s_r, and s_b are the desired sample values to be recovered from their noisy versions $\hat{y}_r$, $\hat{y}_g$, and $\hat{y}_b$.

As in [24], we model the channel dependent noise in the the proposed CFA image denoising algorithm. Since a given type of sensors behaves differently in different wavelengths, the noise statistics are assumed to vary in different channels.

Collection @ chosun

조선대학교
CHOSUN UNIVERSITY

Chapter 3

System to Reduce CFA Noise

In this chapter, we describe a system to reduce noise in CFA image based on PCA. The proposed algorithm attempts to reduce the noise artifact by selecting the appropriate threshold value of based on noise statistics.

3.1 Noise on CFA Sensor

In image denoising problem, we assume the observed data vector Y_i as an unobserved deterministic vector S_i, corrupted by the noise N_i. As in previous literature [24], we assume the noise as an Additive White Gaussian Noise (AWGN). Thus, we express the observed noisy image Y_i as,

$$Y_i = S_i + N_i \tag{3.1}$$

where $i = 1, 2, ...M$ gives the number of pixels. The goal of the proposed denoising algorithm is to estimate of from CFA under the assumption that noise N is independent of S. Noise in CFA image can be reduced in several ways. A conventional solution to perform denosing operation after CDM on the demosaicked full color image. However, the noise caused color artifacts can be very hard to remove in the subsequent denoising process if the noise is discarded in the demosaicking step. The CDM process will complicate the noise characteristics by blending the noise across channels. Some joint demosaicking-denoising schemes have been reported [27], [30]. Both demosaicking and denoising operation share a common feature in terms of sample estimation. Both estimates the new sample from their neighboring pixels. Hirakawa and Parks [27] proposed the joint denoising method. They designed a filter which adaptively computed a filter coefficient by using the TLS technique under some constraints of the CFA pattern. Another method proposed by Zhang et al. [30] estimates the color difference

Collection @ chosun

조선대학교
CHOSUN UNIVERSITY

signal from the noisy CFA image at the first stage. Next, the green channel is reconstructed. A specific wavelet denoising algorithm is employed in this method. Finally, the red/blue channel is reconstructed. Both schemes perform better than many demosaicking first and denoising later methods. Denoising before demosaicking is another widely used strategy to remove noise from CFA data. This technique is capable of reduction of noise caused by noise-caused color artifacts. At the same time denoising and demosaicking algorithms can be independently designed. However, the red, green and blue interlaced CFA pattern. Because of this specific pattern many existing effective monochromatic image denoising methods may not perform effectively. One simple solution is to partition, for example, the big Bayer pattern CFA image into one red, one blue and two greens sub-images and then denoise them separately as gray level images. This solution, however, does not exploit the spectral correlation within red, green and blue channels.

3.2 Literature review on CFA image denoising

The straight forward method to remove noise is to perform post-processing the demosaicked images. Conventional algorithms developed for grayscale imaging, for example [23], can be applied to each channel of the demosaicked color image separately where as some color image filtering techniques [29] process color pixels as vectors. Similarly, wavelet denoising attempts to remove the noise present in the signal while preserving the signal characteristics, regardless of its frequency content. Numerous wavelet based denoising methods have been proposed to reduce the noise when noise is described by a Gaussian or Poisson process. Donoho et al. [16] proposed a soft thresholding to obtain a minimax mean-squared error estimate of wavelet coefficients. Wang [17] developed moving window based double Haar wavelet transform for local multi-scale analysis. In this method the wavelet transform is embedded in a moving window. DWT has been successfully used for image denoising. However, shortcomings such as shift variance, aliasing and lack of directionality compelled to use more efficient

Collection @ chosun

CHOSUN UNIVERSITY 1946 조선대학교 CHOSUN UNIVERSITY

transformation tools. Dual Tree Complex Wavelet Transform (DT-CWT) is introduced to overcome these limitations [15]- [16]. Similarly, the Non-local means (NL-means) is a popular technique for image denoising developed by Buades et al. [22]. This algorithm defines the neighborhood of a pixel by based on the similarity of whole neighborhood rather than a single pixel close to it. Its efficiency and conceptual simplicity have made it very popular, but its main drawback is its high computational complexity. The above mentioned filter techniques are successfully implemented on greyscale images. However, the noisy sensor readings are roots of many color artifacts in demosaicked images and those artifacts are difficult to remove using denoising the demosaicked full color data. In general the CFA readings corresponding to the different color components have different noise statistics. The CDM process blends the noise contributions across channels, thus producing compound noise that is difficult to characterize. This makes the design of denoising algorithms for single-sensor color imaging very difficult. Recently, some schemes that perform demosaicking and denoising jointly have been proposed [27] [33]. In [2], Trussell and Hartig presented a mathematical model for color demosaicking using minimum mean square error (MMSE) estimator. The additive white noise is considered in the modeling. Ramanath and Snyder [13] proposed a bilateral filter based demosaicking method. Since bilateral filtering exploits the similarity in both spatial and intensity spaces, this scheme can handle light noise corrupted in the CFA image. Hirakawa and Parks [9] developed a joint demosaicking-denoising algorithm by using the total least square (TLS) technique where both demosaicking and denoising are treated as an estimation problem with the estimates being produced from the available neighboring pixels. The filter used for joint demosaicking-denoising is determined adaptively using the TLS technique under some constraints of the CFA pattern. In , Hirakawa et al. proposed two wavelet based schemes that can perform CDM simultaneously with denoising. The joint demosaicking-denoising scheme developed by Zhang et al. first performs demosaicking-denoising on the green channel. The restored green channel is then used to estimate the noise statistics in order to restore the red and blue channels. In implementing the algorithm, Zhang et al. es-

Collection @ chosun

조선대학교
CHOSUN UNIVERSITY

timated the red-green and blue-green color difference images rather than directly recovering the missing color samples by using a linear model of the color difference signals. Inspired by the directional linear minimum mean square-error estimation (DLMMSE) based CDM scheme in [9], Paliy et al. [31], [32] proposed an effective nonlinear and spatially adaptive filter by using local polynomial approximation to remove the demosaicking noise generated in the CDM process and then adapted this scheme to noisy CFA inputs for joint demosaicking-denoising. The third way to remove noise from CFA data is to implement denoising before demosaicking. However, due to the underlying mosaic structure of CFAs, many existing effective monochromatic image denoising methods can not be applied to the CFA data directly. To overcome the problem, the CFA image can be divided into several sub-images using the approach known from the CFA image compression literature, e.g., [30]. Since each of the sub-images constitutes a gray-scale image, it can be enhanced using denoising algorithms from gray-scale imaging. The desired CFA image is obtained by restoring it from the enhanced sub-images. Nonetheless, such a scheme does not exploit the interchannel correlation which is essential to reduce various color shifts and artifacts in the final image [12] [13]. Since the volume of CFA images is three times less than that of the demosaicked images, there is a demand to develop new denoising algorithms which can fully exploit the interchannel correlations and operate directly on CFA images, thus achieving higher processing rates. Similarly, Zhang et el, [24] proposed a scheme for denoising CFA images. The technique of PCA is employed to analyze the local structure of each CFA variable block, which contains color components from different channels. By adaptively computing the covariance matrix of each variable block, the PCA could transform the noisy signal into another space, in which the signal energy is better clustered and the noise is removed. Since there can be different and varying structures in each local training window, to improve the estimation accuracy of PCA transformation matrix we select the similar blocks to the underlying one and use them only, instead of all blocks, for PCA training. Such a training sample selection procedure can better preserve the image local structures. This method to reduce noise in CFA is more accurate and

Collection @ chosun

조선대학교
CHOSUN UNIVERSITY

allows the adaptation of the fine structure in the image. However the algorithm goes through the sliding window operation of patches together with PCA. These operations lead to huge computational complexity. Therefore, this method may be inappropriate for low-speed devices.

3.3 Principal Component Models

Principal component analysis (PCA) [26] is a mathematical procedure that transforms a number of correlated variables into a number of uncorrelated variables called principal components (PCs). It is the purpose of PCA to derive new variables (in decreasing order of importance) that are linear combinations of the original variables. The first few components will account for most of the variance in the original data, and these can be used to reduce the dimensionality of the data. The rule is that the first principal component accounts for as much of the variability in the data set as possible, and each succeeding component accounts, in turn, for as much of the remaining variability as possible. Consider a data set $[y_1, y_2, ...y_m]^T$ component variable. We denote the variable as

$$\begin{bmatrix} y_1^1 & y_1^2 & .... & y_1^n \\ y_2^1 & y_2^2 & .... & y_2^n \\ . & . & .... & . \\ y_m^1 & y_m^2 & ...... & y_m^n \end{bmatrix}$$

The sample matrix of y, where $j = 1, 2, ...n$ are discrete samples of variable y_i, $i = 1, 2, ..m$. The i_{th} row of matrix y denoted as $Y = [y_1, y_2....y_m]$ is called the sample vector of x_i. The centralized sample vector μ is estimated by subtracting the mean value μ from sample vector y i,e,

$$\overline{y}_i = y_i - \mu_i \tag{3.2}$$

where $\mu = \frac{1}{N}\sum_{n=1}^{N} y_n$ The centered covariance matrix of the dataset is calculated from $\overline{y}_i$ as

$$C = \frac{1}{N}\overline{y}\overline{y}^T \tag{3.3}$$

Collection @ chosun

조선대학교
CHOSUN UNIVERSITY

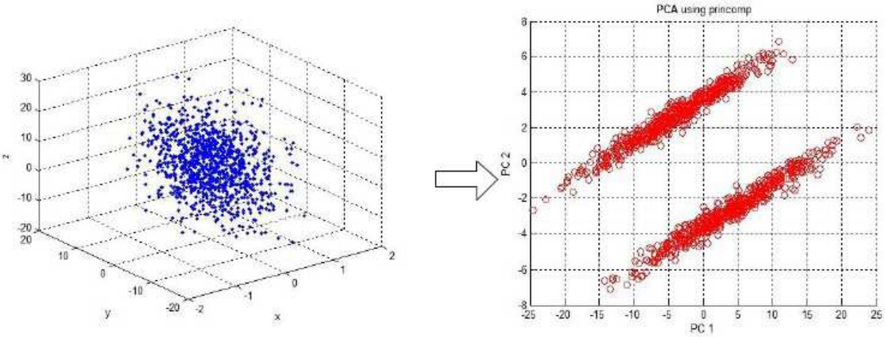

Figure 3.1: Dimensionality reduction using PCA.

As the covariance matrix is symmetrical, it can be further decomposed using singular value decomposition (SVD). The decomposition results in a product of three matrixes U, λ and U^T.

$$C = U\lambda U^T \tag{3.4}$$

$U_i = U_1, U_2, ...U_m$ is the orthogonal matrix of eigenvector, $\lambda = \lambda_1, \lambda_2.....\lambda_m$ is the diagonal matrix of eigenvalues arranged in $\lambda_1 \geq \lambda_2.... \geq \lambda_m$. Principal components are the coordinates in the Eigenvector basis. the amount of variance in the direction of U equals the size of an Eigenvalue corresponding to an Eigenvector $U$of C. Furthermore, the directions of the first Eigenvectors corresponding to the biggest Eigenvalues cover as much variance as possible by orthogonal directions. By setting $P = U^T$, the projection of data y_n can be expressed as

$$\overline{x} = P\overline{y} \tag{3.5}$$

There are several reasons to perform PCA One of the most important ones is to produce a low-dimensional representation with minimum loss of information so that the data may easily be understood and the structure in the data can also be identified easily as shown in Figure 3.1. In PCA domain, several leading Principal components capture the most of the scene signals in image patches, while the last few components are composed mostly of noise.

Collection @ chosun

조선대학교
CHOSUN UNIVERSITY

3.3.1 Singular Value Decomposition (SVD)

SVD [54], [55] is used to factorize a rectangular, real or complex matrix in linear algebra.

3.3.2 Mathematical definition of Singular Value Decomposition

Let X denote a $m \times n$ data matrix of rank m, with $m > n$. We decompose X using SVD i.e.

$$X = U\lambda V^T \tag{3.6}$$

where, U is an $m \times n$ orthogonal matrix $U^T U = I$, contains the eigenvectors of the matrix XX^T. The columns of U are called the left singular vectors [53] u_k,λ, is a $m \times n$ diagonal matrix containing the non-negative singular values [53] of matrix X. V^T is a row orthonormal matrix VV^T, containing the eigen vectors of the symmetric matrix XX^T. The elements of λ are only nonzero on the diagonal and are called the singular values. Thus

$$\lambda = \begin{bmatrix} \lambda_{1,1} & .. & .. & .. & .. \\ .. & \lambda_{1,2} & .. & .. & .. \\ \vdots & \vdots & \vdots & \vdots & \vdots \\ .. & .. & .. & .. & \lambda_{m,n} \end{bmatrix} \tag{3.7}$$

The ordering of the singular vectors is determined by high-to-low sorting of the singular values, with the highest singular value in the upper left entry of matrix λ. The SVD can be calculated by first calculating V^T and λ by diagonalizing $X^T X$:

$$X^T X = V\lambda^2 V^T \tag{3.8}$$

In next step, U can be calculated as

$$U = XV\lambda^{-1} \tag{3.9}$$

Collection @ chosun

조선대학교 CHOSUN UNIVERSITY

where the $(r+1)_{th}, ...n_{th}$ columns of U^T for which $\lambda_{kk} = 0$ are ignored in the matrix multiplication of the equation $U = XU^T\lambda^{-1}$.

3.3.3 Relationship between Principal Component Analysis and Singular Value Decomposition

There is a direct relation between PCA and SVD. We use SVD to perform PCA. Once we decompose a matrix X using SVD and write the covariance matrix as

$$C = \frac{1}{n}XX^T = \frac{1}{n}U\lambda^2U^T \tag{3.10}$$

where U is a $n \times m$ matrix. The SVD routine orders the singular values in descending order. In the case of $n < m$, the first n columns in U corresponds to the sorted eigenvalues of C. For $m \geq n$, the first m corresponds to the sorted non-zero eigenvalues of C. We can write transformed data as

$$Y = \hat{U}^T X = \hat{U}^T U\lambda V \tag{3.11}$$

where $\hat{U}^T U$ is a simple $n \times m$ matrix which is one on the diagonal matrix. Finally, the transformed data can be written in terms of the SVD decomposition of X.

3.4 System to Reduce CFA Noise

We consider the widely used Bayer pattern image in this paper. RGB samples are interlaced in Bayer pattern. The CDM interpolates the two missing color components at each pixel location in the CFA image, which produces the color image from a gray scale image. Most of the CDM are developed under the assumption of a noise free CFA image. However, the realtime images generated by low cost devices are contaminated with moderate or heavy noise, making the digital photographs visually unpleasing. Zhang. [26], proposed a CDM with a channel dependent noise model. It is accepted that the corrupted noise in CCD and CMOS sensors is independent of the magnitude of the signal. In a signal

Collection @ chosun

조선대학교
CHOSUN UNIVERSITY

independent model, the signal contaminated with the noise can be expressed in terms of additive gaussian white noise model (AGWN) as

$$\begin{aligned} \hat{r} &= r + n_r \\ \hat{g} &= g + n_g \\ \hat{b} &= b + n_b \end{aligned} \tag{3.12}$$

where, $\hat{r}$, $\hat{g}$ and $\hat{b}$ are the red, green and blue locations of the CFA image. n_r, n_g and n_b represent the noise contamination on the noiseless samples r, g and b respectively. Numerous methods can be implemented to remove the noise in CFA images. These methods involve denoising after CDM, denoising prior to CDM and denoising jointly with CDM. In the proposed method, we implement the pre-CDM model. The main advantage of this model is, that the noise caused by color artifacts can be reduced and demosaicking model can be designed independent of the denoising method.

3.4.1 Patch based Denoising in Principal Component Analysis Domain

To simplify the denoising algorithm, we employ a channel-dependent noise model where the sensor noise is independent of the signal within each channel. PCA is used as a mathematical tool to remove noise from y_i. In CFA images, the red, green and blue color samples are interlaced, which makes denoising difficult, while existing monochromatic image denoising methods are applied. A simple way to deal with this problem is to partition a big Bayer pattern CFA image into red, blue and green sub-images and denoise them separately as gray scale images. In Ref. [30], Zhang proposed a PCA based denoising for CFA images in which a variable block, which consists of at least one red, one green and one blue color sample, is defined. This method defines another block with more samples than the variable block for training. Wherever any part of the training block matches with the variable block, the pixels of that part are taken as the samples the variable block. As this method is based on applying the sliding window approach

Collection @ chosun

조선대학교
CHOSUN UNIVERSITY

to training block, the time complexity increases substantially with the increase in the size of the image. A time efficient alternative to sliding window approach is to consider the global samples with large block as training window. However the local feature of the image patches cannot be extracted with this approach. Thus, we propose a method that divides the large sized patches into number of smaller blocks based on structural similarity. The basic idea is to divide the image into four non overlapping blocks and arrange arrange all the image patches into a quad tree as depicted in Figure 3.2. The root node contains all the image patches. Performing the K-means clustering with $k = 2$ splits the image into two clusters. These two clusters are further divided into four clusters by repeating the same clustering procedure. Each cluster represents the image patch. Each of these patches can be further split recursively via K-means clustering. This way we can recursively build a quad tree. The division is stopped as soon as the block size is less than the specified size or all the blocks are structurally similar. The structural similarity of the blocks is measured by means of distance between the clusters. K-means algorithm takes linear time to find a local optimum. Next,

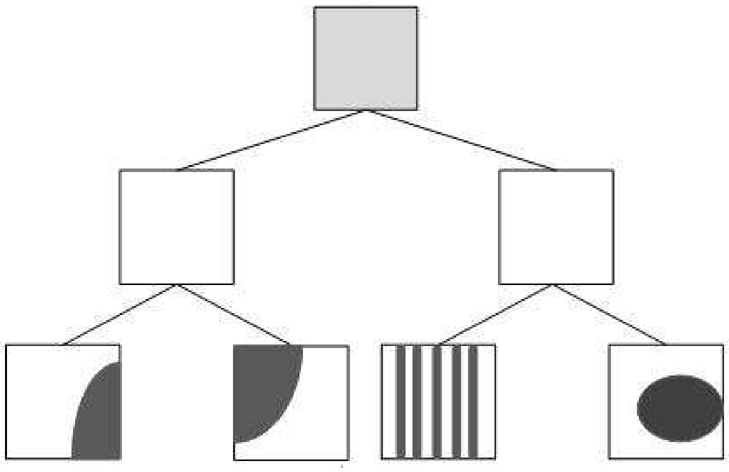

Figure 3.2: Image patch clustering based on textural pattern.

We create an orthonormal basis by performing PCA on the entire collection of patches extracted from the noisy CFA image. Let G be the row vector containing

Collection @ chosun

조선대학교 CHOSUN UNIVERSITY

all the samples associated with green color in a patch. Similarly, R and B represent the row vector of red and blue color samples. The entire data set can be written as,

$$Y = \begin{bmatrix} R^T & G_1^T & G_2^T & B^T \end{bmatrix} \tag{3.13}$$

Let μ_r, μ_{g_1}, μ_{g_2} and μ_b represent the mean values of variables, the mean vectors can be thus denoted as $\mu = [\mu_r \quad \mu_{g_1} \quad \mu_{g2} \quad \mu_b]$. Thus the zero mean centralized value of Y can be estimated as $\overline{Y} = Y - \mu$. With the additive Gaussian noise model, the observed noisy signal can be expressed as

$$\hat{y} = y + n \tag{3.14}$$

where $n = [n_r \quad n_{g_1} \quad n_{g_2} \quad n_b]^T$. Since the noise exhibits the zero mean characteristics, the mean vector of $\hat{y}$ is the same as that of y. Thus, the mean μ for both $\hat{y}$ and y is calculated as $E\left[\hat{y}\right]$. Similarly, we estimate the zero mean centralized vector of noisy signal $\overline{\hat{y}} = \hat{y} - \mu$ and $\overline{\hat{y}} = \overline{y} - \mu + n$. Similar to Y, we can express the noise in terms of signal independent noise as $N = [N_r \quad N_{g_1} \quad N_{g_2} \quad N_b]^T$. Then the measured signal $\hat{Y}$ is expressed as

$$\hat{Y} = Y + N. \tag{3.15}$$

and the zero mean centralized dataset of $\overline{\hat{y}}$

$$\overline{\hat{Y}} = \overline{Y} + N \tag{3.16}$$

For each patch having a patch size of $M = m \times m$, the covariance C_p is estimated as

$$C_p = \frac{1}{M} \sum_{i=1}^{M} \left[\overline{\hat{y}}_i - \mu\right] \left[\overline{\hat{y}}_i - \mu\right]^T \tag{3.17}$$

The SVD decomposition of the covariance matrix C_p gives the projection matrix P_q. The frequently used approach of denoising with PCA assumes that the noise is spread out uniformly in all directions. Hence, the projection of the patch onto the first $l' < l$ axes results in noise reduction, as a low dimensional subspace contains more information about the image.

Collection @ chosun

조선대학교
CHOSUN UNIVERSITY

$$\bar{x}_k = \sum_{i=1}^{l'} P_i(\tilde{\bar{y}}_i - \mu) \tag{3.18}$$

The reconstruction ensures the maximization of the variances of among all the subspaces of dimension. However, the axes that are assumed to hold the image feature are not unable to represent the significant information of patches. As a result, reconstruction of image is as compared to other alternative techniques. Instead of considering as noise the axes carrying low variance, it appears better to consider all axes as relevant for modeling the patches $y = [y_1, y_2....y_m]$. For the given set of patches of the sample value y_i, few axes are relevant, but the relevant axes may vary from one patch to another. Therefore, a reasonable strategy is to process the coefficients according to their magnitude. This leads to the general form of estimators.

$$\bar{x}_k = \sum_{i=1}^{l} \theta \left\langle P_i(\tilde{\bar{y}}_i - \mu) \right\rangle \tag{3.19}$$

where θ represents a shrinkage function. The classical methods include soft thresholding and hard thresholding. In most of the cases soft thresholding is preferred over hard thresholding for several reasons. However the proposed method employs the semisoft thresholding methods. This method yields more visually pleasant results than other thresholding methods because the latter are discontinuous and yield abrupt artifacts in recovered images, especially when the noise is abrupt. Semisoft thresholding method to the coefficients is expressed as,

$$\hat{\bar{x}}_k = \begin{cases} 0, & |\bar{x}_k| \leq T_1 \\ sgn\left(\bar{x}_k\right) \frac{T_2(|\bar{x}_k| - T_1)}{T_2 - T_1}, & T_1 < |\bar{x}_k| \leq T_2 \\ \bar{x}_k, & |\bar{x}_k| > T_2 \end{cases} \tag{3.20}$$

where T_1 and T_2 represent the upper and lower bound threshold values and $\hat{\bar{x}}_k$ represents the thresholded coefficients. We estimate T_1 and T_2 from the threshold value T and tuning parameter δ as $T_1 = T - \delta$ and $T_2 = T + \delta$. While the idea of thresholding is simple and effective, determining the optimal threshold is not an

Collection @ chosun

조선대학교
CHOSUN UNIVERSITY

easy task. The main concern in thresholding is the selection of appropriate threshold. When the optimal threshold value in PCA domain, effective noise reduction is achieved. By computing the covariance matrix C_y the optimal threshold value can be estimated. However the available dataset y_n is corrupted by noise such that C_y cannot be computed directly. In such scenario a, we use the linear noise model of equation Equation (3.12) to estimate the covariance. Assuming that N training samples are available from all patches, the covariance matrix of these samples can be estimated using a maximal likelihood.

$$\begin{aligned} C_y = \frac{1}{M}\sum_{i=1}^{M}\left[\overline{\hat{y}}_i - \mu\right]\left[\overline{\hat{y}}_i - \mu\right]^T \\ \approx \frac{1}{M}\overline{\hat{Y}\hat{Y}}^T \\ = \frac{1}{M}\left(\overline{YY}^T + \overline{Y}N^T + N\overline{Y}^T + NN^T\right) \end{aligned} \tag{3.21}$$

The components $\overline{Y}N^T$ and $Y\overline{Y}^T$ can be replaced by zero as the signal Y and noise N are independent of each other. Hence the above expression can be expressed as,

$$= \frac{1}{M}\left(\overline{YY}^T + NN^T\right) \tag{3.22}$$

where $\overline{YY}$ and NN^T are the covariance of Y and N respectively. Thus the covariance of the observed signal can be expressed as C

$$C_y = C_s + C_n \tag{3.23}$$

Estimating C_s from C_y requires the knowledge of C_n. We use the noise vector under the assumption that these noise elements are uncorrelated with each other.

$$C_n = diag\left\langle \sigma_r, \sigma_g, \sigma_b \right\rangle \tag{3.24}$$

where $\sigma_r, \sigma_g and \sigma_b$ are standard deviations of the channel dependent noise n_r, n_g and n_b. With Equation (3.23) and (3.24) the covariance can be estimated as $C_s = C_y - C_n$. Thus, the threshold value can be defined as,

$$T = TM.C_s \tag{3.25}$$

Collection @ chosun

조선대학교
CHOSUN UNIVERSITY

The thresholding is optimal in a minimax mean square error(MSE) sense over a class of signals, and the noise in the PCA coefficients can be further reduced by using the optimal minsquare error (MSE) processing. The thresholding filter approximates the LMMSE filter for large coefficients and smaller coefficients are replaced by zero. Thus error occurs at intermediate coefficients whose value lies between T_1 and T_2. Thus we use the optimal LMMSE Wiener filter and the coefficient of this filter is obtained as

$$w_k = \frac{C_s}{C_s + C_n} \tag{3.26}$$

The filtered coefficient can be estimated as

$$\tilde{x_k} = w_k.\hat{\bar{x}}_k \tag{3.27}$$

The filtered pixels of the image are obtained by inverse transform of PCA as

$$y_k = P^{-1}\tilde{x_k} \tag{3.28}$$

where P^{-1} is an inverse PCA function. Finally, reformatting the patches results in the denoised CFA block. In the proposed method, two parameters,need to be set: the size of the patch and the threshold parameter.

Collection @ chosun

조선대학교
CHOSUN UNIVERSITY

Chapter 4

Performance Evaluation

In this section, we describe the tests performed to assess the quality of the proposed algorithm. First we illustrate the comparison of output between the proposed filter and other denoising schemes using the CFA images.

Next, we evaluate the denoising outputs in terms of demosaiced color image. The given noisy CFA image is filtered and full color image is generated using a color demosaicing method. We provide qualitative and quantitative evaluation of the proposed method using benchmark images corrupted with different noise levels. For the quantitative analysis, we use peak to signal noise ratio (PSNR) defined by,

$ObjectiveQuality.$
$SubjectiveQuality.$

$$PSNR = 20log_{10}\frac{255}{\sqrt{(MSE)}} \tag{4.1}$$

Here, MSE is the averaged mean square error between the original image and the filtered image. Although, PSNR is not directly correlated with the quality of the human visual system however it is taken into account for the evaluation of performance of algorithms.

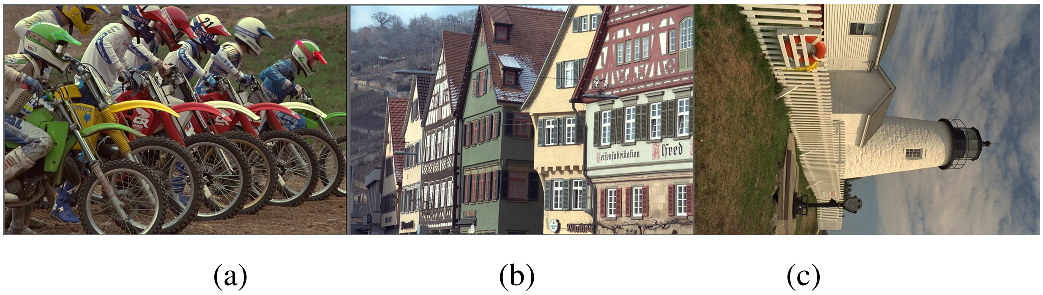
(a) (b) (c)

Figure 4.1: Test images. (a) Auto-bike (b) House (c) Fence

Collection @ chosun

조선대학교
CHOSUN UNIVERSITY

4.1 CFA Image Denoising

In this section, we describe the performance evaluation of the proposed method with other noise reduction algorithms based on wavelet [15], NLM [22], PCA based NLM [23] and spatially adaptive PCA [24] for comparison in terms of CFA images. Performance was evaluated in terms of gray scale image, since we view the CFA images as monochromatic images.

Table 4.1: Comparative results.

Image	Noisy Image PSNR (dB)	Denoising Method	PSNR Results (dB)
Fence	28.11	NLM [22]	28.14
		DTWT [15]	29.50
		NLM-PCA [23]	31.05
		SAPCA [24]	31.86
		Proposed	32.97
House	28.14	NLM [22]	26.81
		DTWT [15]	28.67
		NLM-PCA [23]	29.695
		SAPCA [24]	30.16
		Proposed	31.13
Auto bike	28.11	NLM [22]	26.53
		DTWT [15]	26.68
		NLM-PCA [23]	29.47
		SAPCA [24]	30.42
		Proposed	31.28

We used a variety of test images of a resolution of 512×768 from Kodak dataset, as depicted in Fig. 4.1(a), 4.1(b) and 4.1(c). These test images are widely used in the literature for evaluating demosaicking algorithms. To generated the mosaic CFA image, we used Bayer pattern to subsample the test images, following the standard practise. Since we assume that the image was corrupted by

Collection @ chosun

조선대학교
CHOSUN UNIVERSITY

channel dependent noise, Gaussian white noise was added separately to the red, blue and green channels of the mosaic images. The visual evaluation of the proposed method in comparison with the other denoising schemes is presented in Fig. 4.2.Fig. 4.2(a) shows the mosaic image without noisy, Fig. 4.2(b) shows the noisy mosaic image. Fig. 4.2(c) to 4.2(f) show the filtered image using SAPCA [24] NLM-PCA [23], NLM [22] and the proposed method. Similarly, Table 4.1 shows the comparison of results in terms of PSNR values.

4.1.1 Color Interpolation and Color Filter Array Image Denoising

In this section we describe the evaluation of the proposed CFA denoising scheme in combination with demosaicking. In this approach, we partitioned a CFA image into three sub-images (i.e., one red, one blue and one green channel sub-images) and used them for denoising. Each sub-image is a true monochromatic image. First, we perform the denoising on grayscale image then a color image is generated using CDM. Finally, the the performance was evaluated in terms of the demosaicked color image.

Table 4.2: Comparative results for Fence.

Color	NLM [22]	DTWT [15]	NLM-PCA [23]	SAPCA [24]	Proposed
Red	27.15	29.01	30.50	31.72	32.00
Green	29.86	30.14	31.24	32.52	32.90
Blue	25.96	29.47	30.84	32.40	32.32

Table 4.3: Comparative Results for House.

Color	NLM [22]	DTWT [15]	NLM-PCA [23]	SAPCA [24]	Proposed
Red	25.49	27.75	28.67	29.29	29.43
Green	27.28	28.85	29.64	30.22	30.77
Blue	25.93	28.15	28.66	29.48	29.46

Collection @ chosun

조선대학교
CHOSUN UNIVERSITY

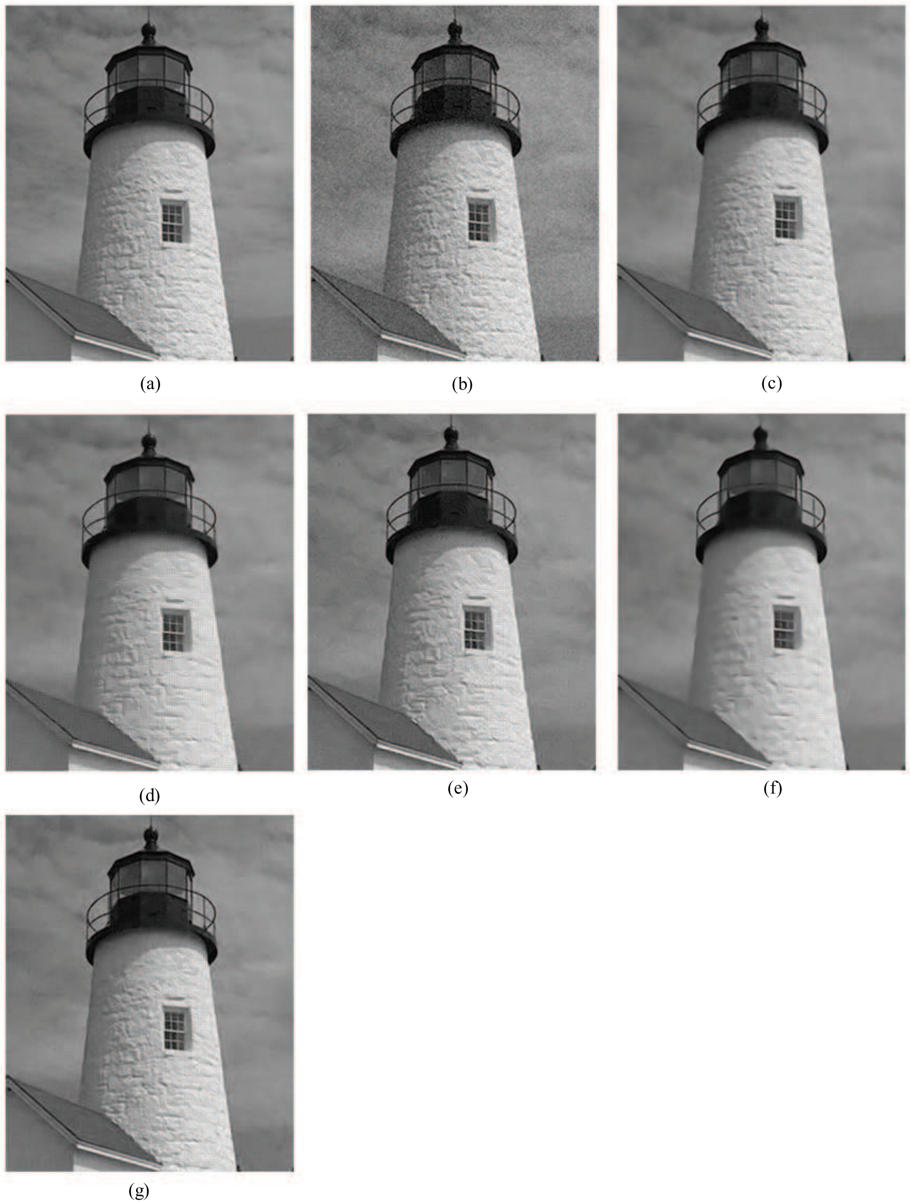

(a)

(b)

(c)

(d)

(e)

(f)

(g)

Figure 4.2: Denoising of CFA images"Fence"(a) Original image (b) noisy image (σ_r=10, σ_g=10, σ_b=10,) (c) denoised image using method NLM [22] (d) DTWT [15] (e) NLM -PCA [23] (f) Spatially Adataptive PCA [24] (g) the proposed PCA-based CFA denoising method.

Collection @ chosun

조선대학교
CHOSUN UNIVERSITY

Table 4.4: Comparative Results for Autobike.

Color	NLM [22]	DTWT [15]	NLM-PCA [23]	SAPCA [24]	Proposed
Red	25.63	26.55	28.79	30.06	30.17
Green	27.40	27.33	29.73	30.75	31.13
Blue	25.33	27.05	28.85	30.11	29.87

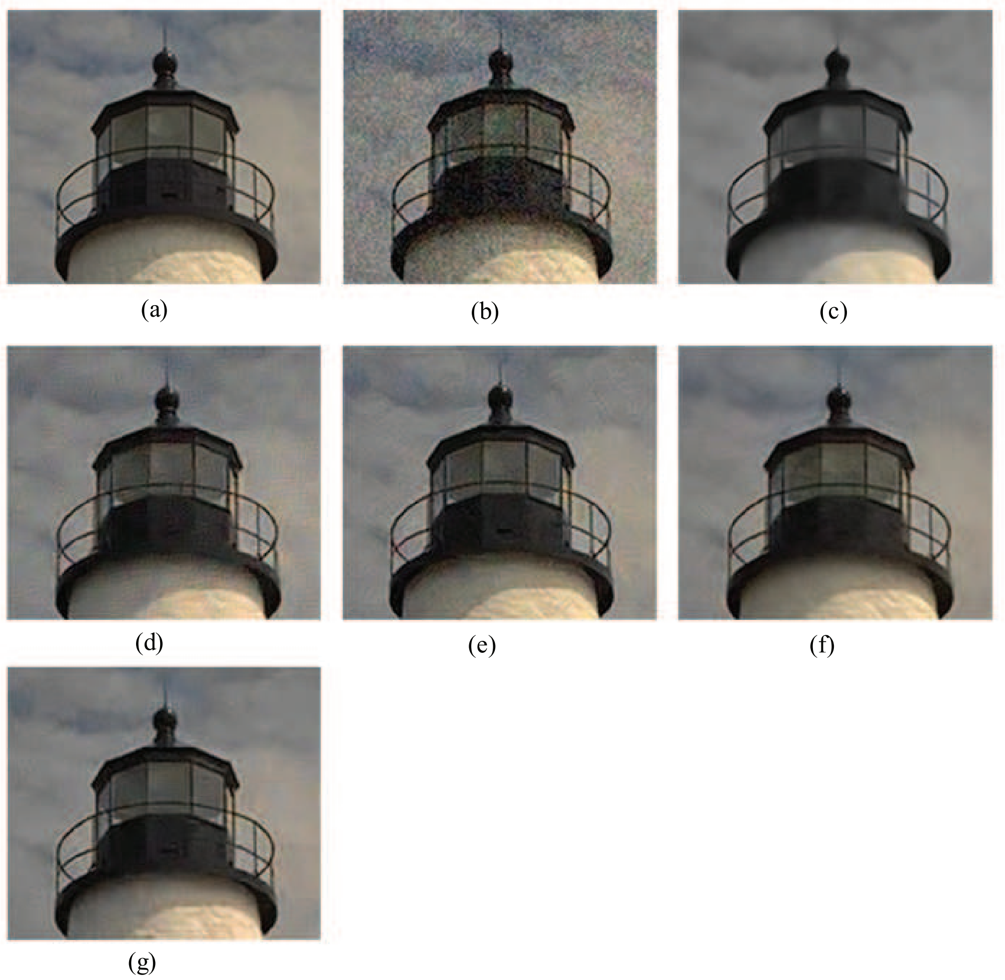

Figure 4.3: Denoised Color image of CFA images after demosaicing ”Fence ”(a) Original image (b) noisy image (σ_r=10, σ_g=10, σ_b=10,) (c) denoised image using method NLM [22] (d) DTWT [15] (e) NLM -PCA [23] (f) Spatially Adataptive PCA [24] (g) the proposed PCA-based CFA denoising method.

Collection @ chosun

조선대학교
CHOSUN UNIVERSITY

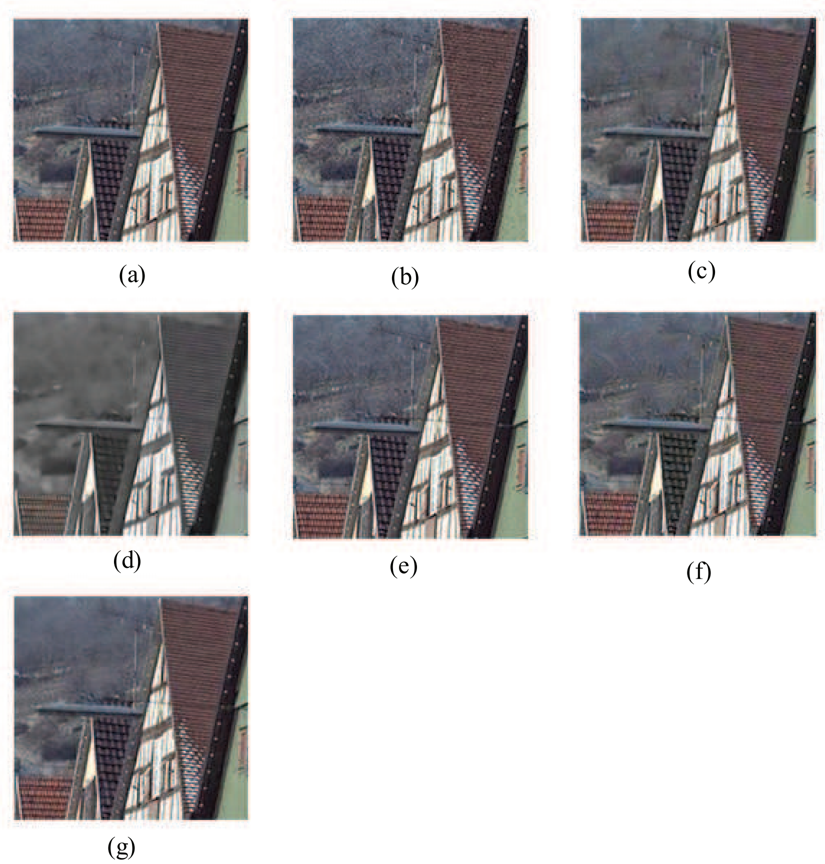

(a) (b) (c)

(d) (e) (f)

(g)

Figure 4.4: Denoised Color Image of CFA images after demosaicing ”House”(a) Original image (b) noisy image (σ_r=10, σ_g=10, σ_b=10,) (c) denoised image using method NLM [22] (d) DTWT [15] (e) NLM -PCA [23] (f) Spatially Adataptive PCA [24] (g) the proposed PCA-based CFA denoising method.

Collection @ chosun

조선대학교
CHOSUN UNIVERSITY

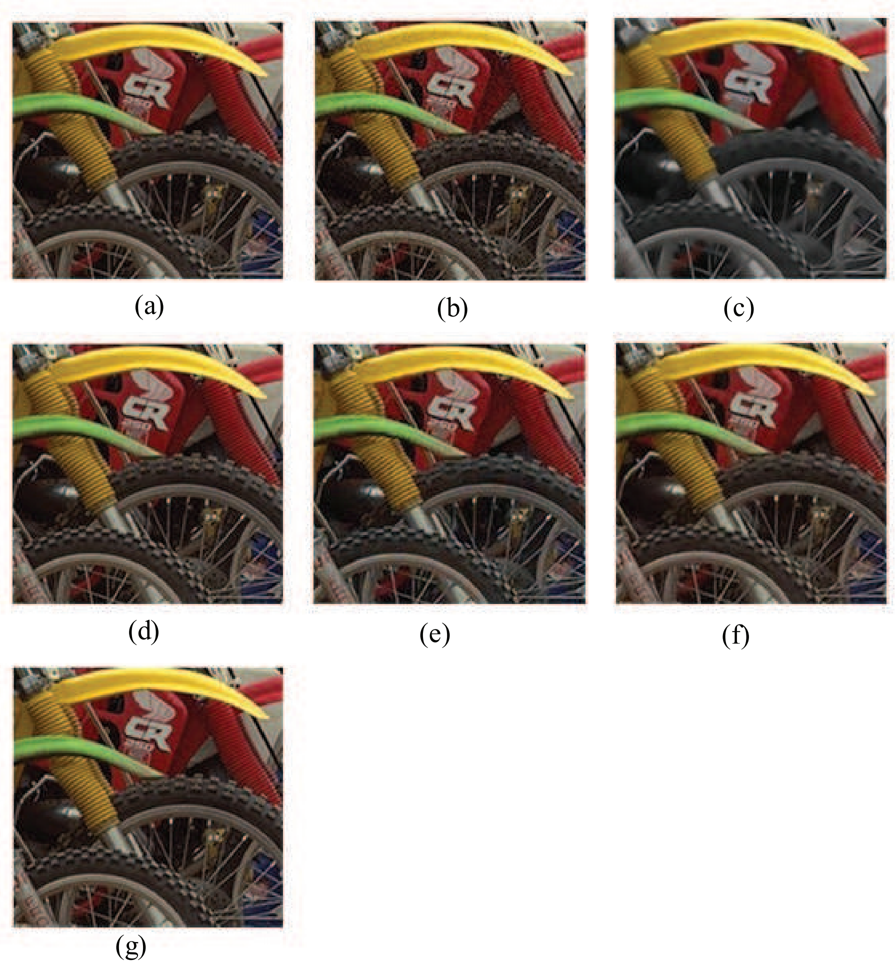

Figure 4.5: Denoised color image of CFA images after demosaicing ”Auto bike”(a) Original image (b) noisy image (σ_r=10, σ_g=10, σ_b=10,) (c) denoised image using method NLM [22] (d) DTWT [15] (e) NLM -PCA [23] (f) Spatially Adataptive PCA [24] (g) the proposed PCA-based CFA denoising method.

dCollection @ chosun

조선대학교
CHOSUN UNIVERSITY

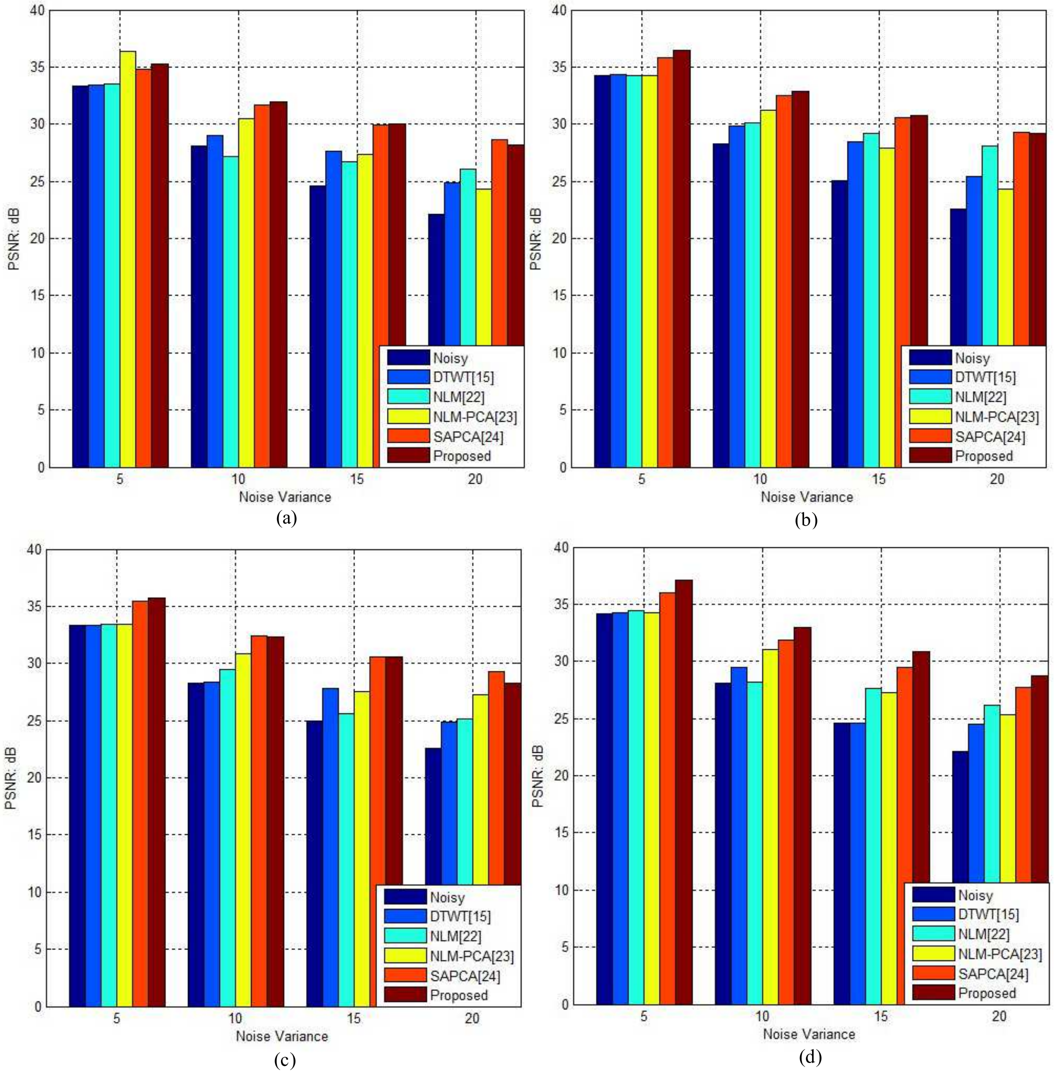

(a)

(b)

(c)

(d)

Figure 4.6: Graphical comparison in terms of PSNR reconstructed and noisy Fence image obtained for different values of noise variance(a) Red color (b) Green color (c) Blue color (d) Without demosaicking

Collection @ chosun

조선대학교 CHOSUN UNIVERSITY

The proposed approach was compared with three other approaches. As in the previous section, the example images in Figure 4.2(a), 4.2(b) and 4.2(c) were used in the experiments. The noisy CFA images were input to the competitive solutions to produce final restored images (i.e., demosaicked full-color data with suppressed noise). Table 4.2- 4.4 lists the achieved PSNR values by different schemes. A detailed examination of the results reveals that the proposed method produces very good results and outperforms many prior methods. When working with each one of the same demosaicking algorithm, the proposed PCA-based CFA denoising method almost always gives better result than the spatially adaptive PCA, non local means filter based and wavelet-based denoising schemes with the corresponding demosaicking algorithm. Figures(4.3- 4.5) prove that our claim in terms of subjective quality evaluation and Table 4.1 and Tables 4.2- 4.4 demonstrate the superiority of the proposed method in terms of objective quality. Similarly, Figure 4.6 shows the performance evaluation of proposed method of Fence image with other methods. We performed experiments on different values of noise variance ranging from 5 to 20. The proposed method generates better results on monochromatic image without demosaicking for all the noise variances. However, for demosaicked image PSNR values in some color component is not as good as spatially adaptive PCA [24].

4.2 Subsection Summaries

In this section, we described a method for the reduction of noise in CFA sensor images. The proposed method analyzes the pixel statistics properly and applies the filter appropriate for pixels of different classes. The experimental results show that the performance of this algorithm for a wide variety of images is satisfactory. Because of its non iterative and low complexity property, it can be applied for denoising in low power devices such as mobile phones and PDAs with minimal computational cost requirements. Moreover, with the application of an optimal linear MMSE filter it provides good results in both interms of subjective and objective quality metrics.

Collection @ chosun

조선대학교
CHOSUN UNIVERSITY

Chapter 5
Image Interpolation

This chapter introduces the description for the interpolation of a full high-definition (HD) image based on the dual-tree complex wavelet transform (DT-CWT) and hidden markov model (HMM). In the proposed method, the DT-CWT is used to decompose the low-resolution image into different subbands. In wavelet domain interpolation, given image is assumed as the low frequency LL subband of the wavelet coefficients of a high-resolution image. The proposed method estimates the higher band coefficients by learning the correlation between the coefficients across the scale. In this paper, the relationship between the wavelet coefficients across the scale is described by HMM, and each wavelet coefficient is modeled by a Gaussian mixture having multiple means and variances. Experimental results show that the proposed algorithm yields images that are sharper compared to several other methods that we have considered in this paper.

5.1 Introduction

Image interpolation has many applications in computer vision. It is the first of the two basic resampling steps and transforms a discrete matrix into a continuous image. Subsequent sampling of this intermediate result produces the resampled discrete image. Resampling is required for discrete image manipulations, such as geometric alignment and registration, to improve image quality on display devices or in the field of lossy image compression wherein some pixels or some frames are discarded during the encoding process and must be regenerated from the remaining information for decoding. In this work, we propose a new technique that generates sharper super-resolved images.

Collection @ chosun

조선대학교
CHOSUN UNIVERSITY

5.2 Literature review on image interpolation techniques

Various techniques have been proposed in order to scale the image from low resolution to high resolution and its reverse. Fundamentally, they can be classified into three categories:

1. Isotropic interpolation
2. Edge-directed, and
3. Transform-based methods.

5.3 Isotropic

The isotropic interpolation method [34]- [37] considers the source image as a sub-sampled discrete version of the original ”continuous” image. Nearest-neighbor, bilinear, and bi-cubic interpolation are some of the examples of this method.

5.3.1 Nearest Neighbor

In the nearest-neighbor method, the source image is scaled by sampling the nearest pixels in the source image [34]. This is also known as zero-order and point shift algorithm. It is a computationally efficient algorithm; however, the up-scaled image quality is degraded owing to the aliasing effect. The nearest neighbor interpolation algorithm kernel is expressed as

$$h(x) = \begin{cases} 1, & 0 \leq |x| < 0.5 \\ \\ 1, & 0 \leq |x| \end{cases} \tag{5.1}$$

Similarly, the frequency response of the nearest neighbor kernel can be defined as

Collection @ chosun

조선대학교
CHOSUN UNIVERSITY

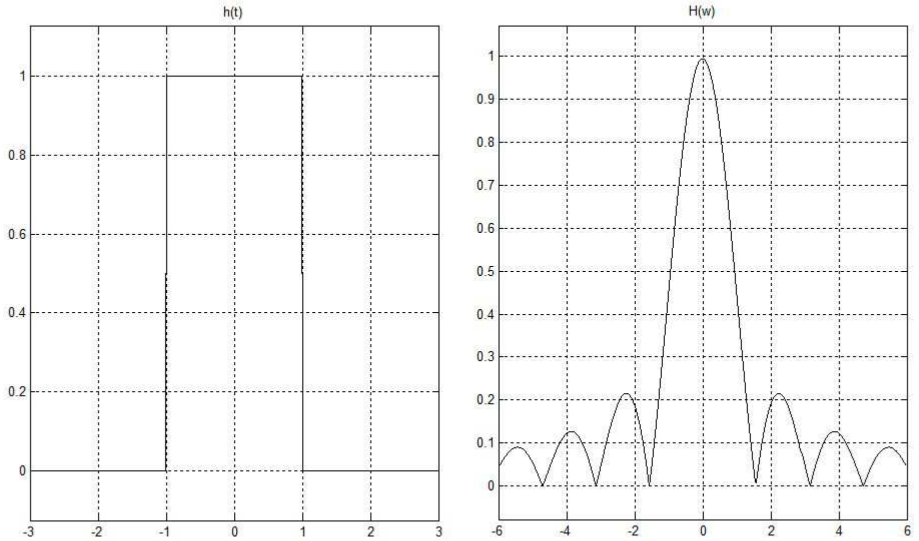

(a)

(b)

Figure 5.1: Nearest neighbor interpolation kernel.(a) Time domain (b) Frequency domain

$$H(w) = sinc\left(\frac{w}{2}\right) \tag{5.2}$$

Convolving an image with a rectangular function h creates the same effect on image as multiplying the spectrum of that image by the Fourier transform of the sinc function. However, Sinc function works as a poor low-pass filter due to the presence of prominent side lobes and infinite extent. Thus the magnification is achieved by pixel replication.

5.3.2 Bilinear

The bilinear interpolation estimates the new value from the neighbors by weighting their distance [35]. For separated bi-linear interpolation, the distance to the opposite point of interpolation weights the values of both direct neighbors. The linear approximation of the sinc function follows the triangular function. This method passes a straight line through every two consecutive points of the input

Collection @ chosun

조선대학교
CHOSUN UNIVERSITY

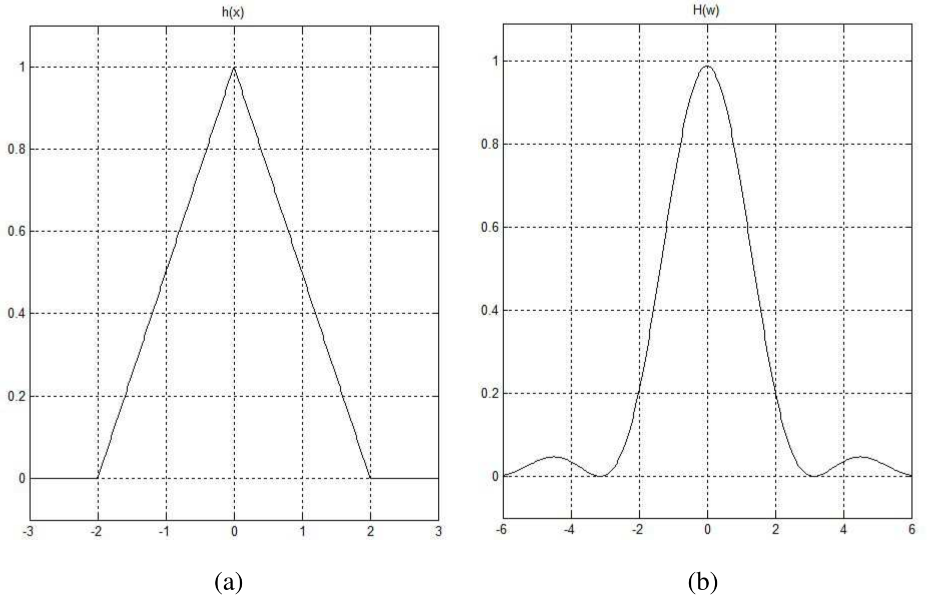

(a)

(b)

Figure 5.2: Bilinear interpolation kernel.(a) Time domain (b) frequency domain

signal. Thus this is a first degree method. In the spatial domain, linear interpolation can be obtained by convolving the sampled input with the following kernel.

$$h(x) = \begin{cases} 1 - |x|, & 0 \leq |x| < 0.5 \\ \\ 0, & elsewhere \end{cases} \tag{5.3}$$

The triangular function is equivalent to a modest low-pass filter in the frequency domain. However, linear interpolation comes with some disadvantages, attenuation occurs at the high-frequency components and the data beyond the cut-off point are aliased into the low frequencies. The frequency response of the filter is expressed as

$$H(w) = sinc^2\left(\frac{w}{2}\right) \tag{5.4}$$

Collection @ chosun

조선대학교
CHOSUN UNIVERSITY

5.3.3 Bi-cubic

Bicubic interpolation [35] is the cubic interpolation in two dimension. Bicubic interpolation can be realized using Lagrange polynomial, cubic splines, etc. Third degree cubic spline interpolation formula serve as a good approximation to ideal sinc function. The interpolated image so obtained is smoother than Nearest neighbor and bilinear interpolation. Bicubic interpolation takes a weighted average of the 16 pixels to calculate gray value of pixels Cubic Interpolation kernel is derived from interpolation formula for general cubic spline by imposing constraints. The cubic interpolation kernel is

$$h(x) = \begin{cases} (a+2)|x|^3 - (a+3)|x|^2 + 1, & 0 \leq |x| < 1 \\ \\ a|x|^3 - 5a|x|^2 + a|x| - 4a, & 0 \leq |x| < 1 \\ 0, & 2 \leq |x| \end{cases} \tag{5.5}$$

Similarly, the response in frequency domain is expressed as

$$H(w) = \frac{12}{w}\left(sinc^2\left(\frac{w}{2}\right) - sinc(w)\right) + a\frac{8}{w^2}\left(3sinc^2(w) - 2sinc(w) - sinc(2w)\right) \tag{5.6}$$

The value of a, and the frequency content of the image determines the performance of the interpolation kernel. Generally, the value of a are $a = -1, a = -0.75$ and $a = -0.5$.

5.4 Edge-Directed Interpolation(EDI)

Edge directed interpolation [38]- [40] uses the statistical sampling to ensure the quality while scaling an image. Instead of averaging pixels, as in bilinear interpolation, average of covariance of pixels is computed. Thus, the sharpness and the continuity of the edge are preserved compared to conventional Bilinear and Bicubic methods. Li [41] proposed new edge directed interpolation by using the statistical and geometrical properties to estimate the unknown pixel of an image. The algorithm in the literature [41] can be described as follows. Given the low

Collection @ chosun

조선대학교
CHOSUN UNIVERSITY

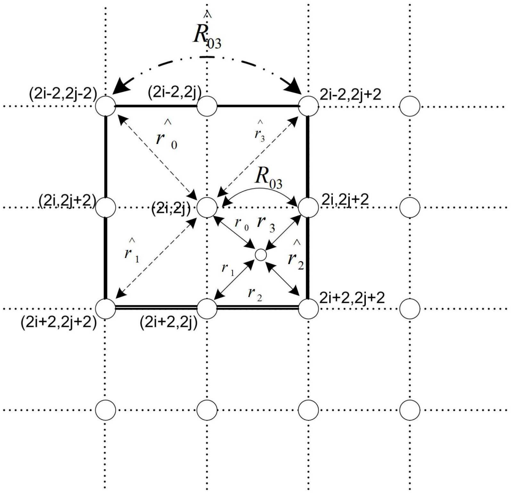

Figure 5.3: First step of NEDI

resolution image $Y_{i,j}$ of size $W \times H$. After the interpolation the corresponding high resolution image size is $aW \times bH$. Here a and b represents the scaling factor of width a and height b. Suppose we are going to scale the image by 2. We assume $a = 2$ and $b = 2$. Now the value of $Y_{2i,2j}$ can be easily determined as $Y_{2i,2j} = X_{i,j}$ for $i = 0, 1, 2....W$ and $j = 0, 1, 2....H$ as shown in Figure 5.3 and Figure 5.4. In order to obtain get the pixel values $Y_{2i+1,2j+1}$, $Y_{2i,2j+1}$, and $Y_{2i+1,2j}$, interpolation is performed. NEDI by estimates these pixels in two steps. In the first step unknown pixel $Y_{2i+1,2j+1}$ is estimated while in second step $Y_{2i,2j+1}$ and $Y_{2i+1,2j}$ are estimated. Using the fourth-order linear interpolation unknown pixel value is estimated from $Y_{2i,2j}$, $Y_{2i,2j+2}$, $Y_{2i+2,2j}$ and $Y_{2i+2,2j+2}$. The optimal MMSE linear interpolation coefficients are given by

$$Y_{2i+1,2j+1} = \sum_{k=0}^{1} \sum_{l=0}^{1} \alpha_{2k+l} Y_{2(i+k),2(j+l)} \tag{5.7}$$

A covariance of the pixel in a local block is required for the computation of the prediction coefficient. The optimal MMSE linear interpolation coefficients are given by

Collection @ chosun

조선대학교
CHOSUN UNIVERSITY

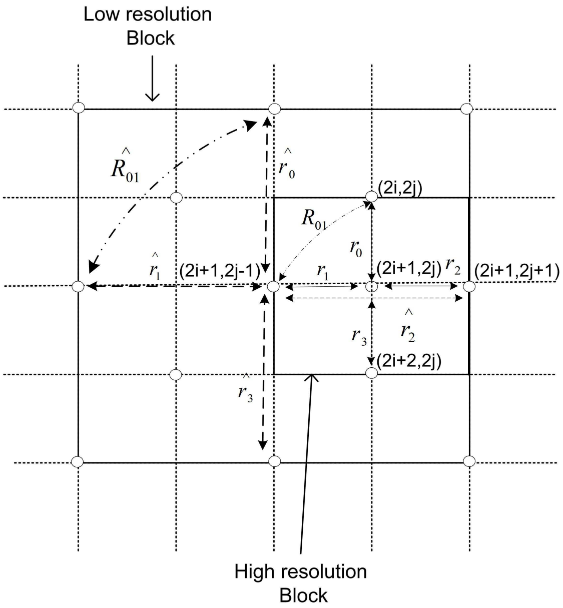

Figure 5.4: Second step of NEDI

$$\vec{\alpha} = R^{-1}\vec{r} \tag{5.8}$$

Here $\vec{\alpha} = [\alpha_0, ...\alpha_3], R = [R_{k,l}]for(0 \leq k, l \leq 3)$ and $r = [r_0, ...r_3]$. Since the computation of R_{kl} and r_k requires the knowledge of $Y_{2i+1,2j+1}$ which is obtained only after the interpolation. In order to overcome this problem geometric duality property is used. The covariance $\hat{r}_0$ is estimated from low resolution window and it is used as a substitute of r_0. Similarly the covariance $\hat{r}_k$ is used to substitute r_0. Now the unknown pixel is estimated using $\hat{r}_k$ and $\hat{R}_{kl}$ as indicated in Figure 5.3 in the first step. Now in second step the remaining unknown pixels $Y_{2i,2j+1}$ and $Y_{2i+1,2j}$ are estimated by same method with scaling of $2^{1/2}$ and a rotation factor of $\pi/4$ as shown in Figure 5.4. This algorithm works well for preserving the sharpness and continuity of the edges. However, one of the limitations of this approach is that it leads to the prediction error in interpolation coefficient, resulting error in interpolated pixels in first step when the small sized training window is taken. Since the estimation of unknown pixels is performed

Collection @ chosun

조선대학교
CHOSUN UNIVERSITY

based on the result of first step, the error of first step is propagated to second step. If large sized training window is taken, we consider larger neighborhood as a result the local characteristics of image will be lost and the image edge details of image will be unnecessarily blurred.

5.4.1 Modified Edge Directed Interpolation (MEDI)

One of the limitations of NEDI approach is that it leads to the prediction error in interpolation coefficient, resulting error in interpolated pixels in first step when the small sized training window is taken. Since the estimation of unknown pixels is performed based on the result of first step, the error of first step is propagated to second step. If large sized training window is taken, we consider larger neighborhood as a result the local characteristics of image will be lost and the image edge details of image will be unnecessarily blurred. A modified training window structure has been proposed in [42] in order to overcome this problem. The training window in the second step of NEDI is modified to the form of sixth order linear interpolation with a 5×9 training window for the interpolation of and . Even though an improved edge directed is proposed it still suffers from the covariance mismatch problem as in NEDI. M. Li [42] suggested the Markov random field (MRF) based model. Image is modeled with MRF model and edge estimation is extended in other directions by increasing the neighboring pixels in the kernel. This algorithm is able to preserve the sharpness of the edge in interpolated image.

5.5 Transform Based Interpolation

Transforms like Discrete Cosine Transform(DCT) and Discrete Wavelet Transform(DWT) are efficient tool for compressing the signal energy into a few transformed coefficients. As a result of multiplying these transformed coefficients, a scaled image can be obtained. More detailed description is presented in chapter 6.

Collection @ chosun

조선대학교
CHOSUN UNIVERSITY

Chapter 6
Wavelet Transform

In this section, we give a concise review of the real orthogonal wavelet transform in order to set up notation and to illustrate its lack of shift-invariance.

6.1 Wavelet Definition

The term wavelet refers to small waves of varying frequency and limited duration. This feature allows to describe the time frequency plane, with atoms of different time supports as shown in Figure 6.1. Fourier transform on the other hand provide only the frequency information. temporal or time information is lost in the transformation process.

6.2 Wavelet Characteristics

Wavelets are a mathematical tool, having specific properties that make them useful to extract information from many kinds of data, including audio signals and images. Mathematically, the wavelet ψ, is a function of zero average, having the energy concentrated in time:

$$\int_{-\infty}^{+\infty} \psi(t)dt = 0 \tag{6.1}$$

A family of wavelets is constructed from a function $\psi(t)$, known as the Mother Wavelet, which is confined in a finite interval. Daughter Wavelets, $\psi_{u,s}(t)$ are then formed by translation with a factor u and dilation with a scale parameter s:

$$\psi_{u,s}(t) = \frac{1}{\sqrt{s}}.\psi(\frac{t-u}{s}) \tag{6.2}$$

Collection @ chosun

조선대학교 CHOSUN UNIVERSITY

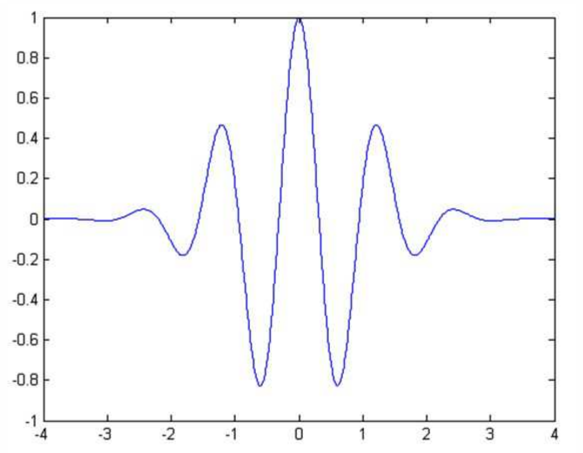

Figure 6.1: Wavelet basis

6.3 Wavelet Analysis

The wavelet analysis implies a multiplication and an integration. It is performed by projecting the signal to be analyzed on the the wavelet function [59]. We can use different scales and translations of the mother wavelet, depending on the signal characteristics of the signal to be analyzed. It allows us to change freely the size of the analysis function to make it suitable for the needed resolution, in time or frequency domain.

$$\langle f(t), \psi_{u,s}(t)\rangle = \int f(t)\psi_{u,s}(t)dt \tag{6.3}$$

For high resolution in time-domain analysis we want to capture all the sudden changes that appear in the signal, and we do that by using a contracted version of the mother wavelet. Conversely, for high-resolution in the frequency-domain we will be using a dilated version of the same function.

Collection @ chosun

조선대학교
CHOSUN UNIVERSITY

6.4 Wavelet Transform

The Wavelet Transform(WT) decomposes the signal over a set of dilated and translated wavelets based on the multi resolution analysis. The WT processes different frequencies in a different way. By using this technique, the time resolution is increased when we analyze a high frequency portion of the signal, and the frequency localization is increased when analyzing a low-frequency part of the same signal. This type of analysis is suitable for signals that have both low-frequency components with long time duration and high-frequency components with short time duration, which is the case of most signals. If we consider a function $f \in L^2(R)$ and for analysis we use the mother wavelet ψ, with its scaled and translated versions in equation 6.2, we can write the wavelet transform of $f(t)$ at time u and scale s as:

$$Wx(u,s) = \langle f, \psi_{u,s} \rangle = \int\limits_{-\infty}^{+\infty} f(t)\frac{1}{\sqrt{s}}.\psi(\frac{t-u}{s}) \tag{6.4}$$

For the continuous-time signal $f(t)$, the scale factor must be a positive real number, whereas the shift factor can be any real number. If the continuous wavelet $\psi_{u,a}$ meets the admissibility condition, we can use the computed wavelet coefficients to reconstruct the original signal $f(t)$. However, we seldom use the above integration to compute the CWT because of the following reasons:

The majority of real-world signals that you encounter are available as discrete-time samples. The analytical form of the signal $f(t)$ usually is not accessible. The closed-form solution of the integration does not exist except for very special cases.

For these reasons, you usually select a set of discrete values for the scales and shifts of the continuous wavelets and then compute the CWT numerically.

Collection @ chosun

조선대학교
CHOSUN UNIVERSITY

6.4.1 Discrete Wavelet Transform (DWT)

The 1D discrete wavelet transform (DWT) decomposes a signal in terms of a shifted and dilated mother wavelet and scaling function

$$f(t) = \sum_{l \in Z} u_{j_0,l}\phi_{j_0,l}(t) + \sum_{j \geq j_0} \sum_{l \in Z} w_{j,l}\psi_{j,l}(t) \tag{6.5}$$

where, $\phi_{j_0,l}(t) := 2^{j_0/2}\phi(2^{j_0/2}t - l)$ and $\psi_{j,l}(t) := 2^{j/2}\psi(2^{j/2}t - l)$. The scaling coefficients and wavelet coefficients can be calculated using the standard inner product :$\psi_{j,l}(t) := 2^{j/2}\psi(2^{j/2}t - l)$ if $\phi_{j_0,l}, \psi_{j,l}, j \geq j_0, l \in Z$. The wavelet transform is computed recursively using the filter bank structure shown in Figure 6.2. Given the scaling coefficients $u_{j+1,l}, l \in Z$ at scale $j + 1$, we compute the scaling coefficients $\{u_{j,l}, l \in Z\}$ and wavelet coefficients $\{w_{j,l}, l \in Z\}$ at scale j passing the $\{u_{j+1,l}, l\}$ through digital filters and and down sampling by a factor of two. The impulse responses $h_0[n]$, $h_1[n]$ of H_0 and H_1 are related to the scaling and wavelet basis functions in (6.1) by $\phi(t) = \sqrt{2}\sum_n h_0[n]\phi(2t - n)$and $\psi(t) = \sqrt{2}\sum_n h_1[n]\psi(2t - n)$. To reconstruct the signal from its wavelet (and scaling) coefficients, we apply the filter bank structure shown in Figure 6.2(b), which computes the scaling coefficients $u_{j+1,l}$ at scale $j+1$ by up-sampling $u_{j,l}$ and $w_{j,l}$, filter with G_0 and G_1 (whose impulse responses are just time reversed versions of h_0 and h_1 in the orthogonal case), and adding the results. In discrete time, we can interpret each sample of an N-point signal as a scaling coefficient at the nest scale $j = log_2 N$, and apply the filter bank structure in Figure 6.2 recursively to efficiently compute the wavelet transform with $O(N)$ computational complexity [57].

In 2D, the discrete wavelet transform decomposes an image $x(s)$ in terms of a set of shifted and dilated wavelet functions $\left\{\psi^{0°}, \psi^{90°}, \psi^{\pm 45°}\right\}$ and scaling function $\phi(s)$:

$$x(s) = \sum_{k \in Z^2} u\phi_{j_0,k}(s) + \sum_{b \in B} \sum_{j \geq j_0} \sum_{l \in Z} w^b_{j,l}\psi^b_{j,l(s)} \tag{6.6}$$

Collection @ chosun

조선대학교 CHOSUN UNIVERSITY

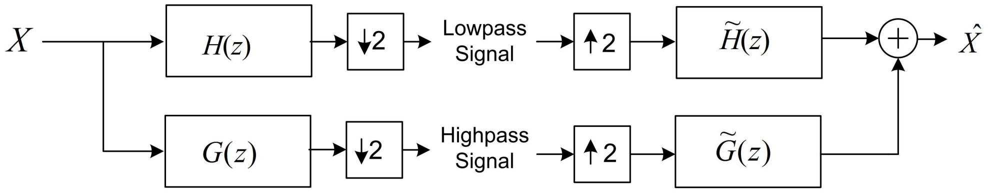

(a) (b)

Figure 6.2: Wavelet filter bank structure in 1D.

with $\phi_{j_0,l}(t) := 2^{j_0/2}\phi(2^{j_0/2}t - l)$ and $\psi_{j,l}(t) := 2^{j/2}\psi(2^{j/2}t - l)$ and $b \in B := \{0°, 90°, \pm 45°\}$ denote the subbands of the wavelet decomposition. In this paper, we will consider only separable 2D wavelet transforms, meaning we can write $\psi^{0°}(s) := \psi^{0°}(s_1, s_2) = \phi(s_1)\psi(s_2)$, $\psi^{90°}(s) = \psi(s_1)\phi(s_2)$, $\psi^{\pm 45°}(s) = \psi(s_1)\psi(s_2)$ where ϕ and ψ are 1D scaling and wavelet functions as in (6.1). A separable 2D DWT can be computed efficiently in discrete time by applying the associated 1D filter bank to each column of the image, and then applying the filter bank to each row of the result. A 2D wavelet basis function $\psi^b_{j,k}$ analyzes a local region of the image x. This region is a square centered on $2^{-j}k + 2^{-(j+1)}, k = (k_1, k_2) \in Z^2$ with width and hight proportion to 2^{-j}.

We will call this region the locale of basis function $\psi^b_{j,k}$. Salient feature of the image in this locale affect the behavior of $w^b_{j,k}$. At the next finest scale $j+1$, the locale of $w^b_{j,k} := w^b_{j,(k_1,k_2)}$ breaks into the four locales of $w^b_{j+1,(2k_1,2k_{2+1})}$, $w^b_{j+1,(2k_{1+1},2k_2)}$, and $w^b_{j+1,(2k_{1+1},2k_{2+1})}$. This allows each subband of the wavelet transform to be naturally arranged in a quad tree with each parent wavelet at scale j giving rise to four child coefficient at scale $j+1$ occupying the same spatial region. Roughly speaking, we can think of wavelets as local edge detectors in the horizontal ($0°$ subband), vertical $90°$ and diagonal ($\pm 45°$).

Collection @ chosun

조선대학교
CHOSUN UNIVERSITY

6.5 2D Wavelet Transform

In 2D wavelet transform, the transformed coefficient becomes two variable functions, denoted as $\phi(x, y)$ and $\psi(x, y)$. Thus, the scaled and translated basis functions are defined as

$$\phi_{j,m,n}(x, y) = 2^{j/2}\phi(2^j x - m, 2^j y - n) \tag{6.7}$$

$$\psi_{j,m,n}(x, y) = 2^{j/2}\psi(2^j x - m, 2^j y - n), i = H, V, D \tag{6.8}$$

where i identifies the tree different direction of directional wavelet functions, $\psi^H(x, y)$ $\psi^V(x, y)$ and $\psi^D(x, y)$. Conceptually, the scaling function is the low frequency component of the previous scaling function in 2 dimensions. Therefore, there is one 2D scaling function. However, the wavelet function is related to the order to apply the filters. If the wavelet function is separable, i.e. $f(x, y) = f_1(x)f_2(y)$. These functions can be easily rewritten as

$$\phi(x, y) = \phi(x)\phi(y) \tag{6.9}$$

$$\psi^H(x, y) = \psi(x)\phi(y) \tag{6.10}$$

$$\psi^V(x, y) = \psi(x)\psi(y) \tag{6.11}$$

$$\phi^D(x, y) = \psi(x)\psi(y) \tag{6.12}$$

The wavelet transform of image $f(x, y)$ of size M× N is then expressed as

$$W_\phi j_0, m, n = \frac{1}{\sqrt{MN}} \sum_{x=0}^{M-1} \sum_{x=0}^{M-1} f(x, y)\phi_{j_0,m,n}(x, y) \tag{6.13}$$

$$W_\psi j_0, m, n = \frac{1}{\sqrt{MN}} \sum_{x=0}^{M-1} \sum_{x=0}^{M-1} f(x, y)\psi^i_{j,m,n}(x, y), i = H, V, D \tag{6.14}$$

Similarly the $f(x, y)$ can be reconstructed from given wavelet coefficients W_ϕ

Collection @ chosun

조선대학교
CHOSUN UNIVERSITY

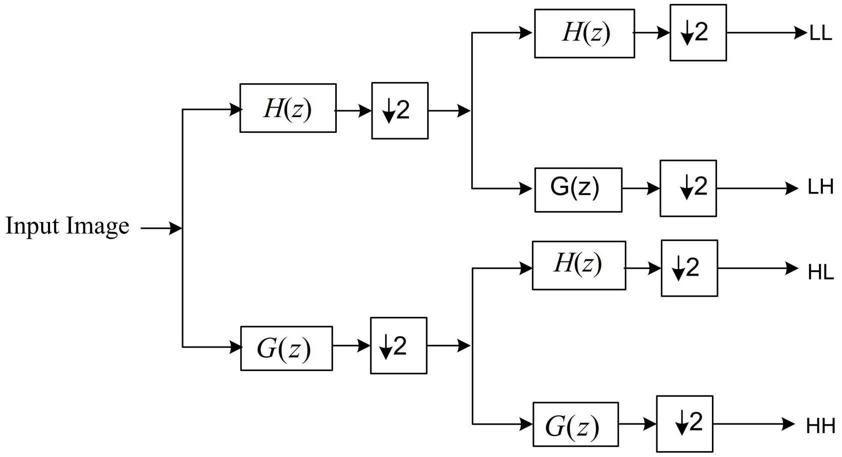

Figure 6.3: Wavelet filter bank structure in 2D.

and W_ψ via the inverse discrete wavelet transform

$$f(x,y) = \frac{1}{\sqrt{MN}} \sum_m \sum_n W_\phi j_0, m, n(x,y)\phi_{j_0,m,n}(x,y) + \frac{1}{\sqrt{MN}} \sum_{i=H,V,D} \sum_{j=j_o}^{\infty} \sum_m \sum_n W_\psi(j,m,n)\psi^i_{j,m,n}(x,y) \tag{6.15}$$

This is the general form of 2D wavelet transform. If the scaling and wavelet functions are separable, the summation can be decomposed into two stages. First step is along the x-axis and then calculate along the y-axis. For each axis, we can apply fast wavelet transform to accelerate the speed. A schematic diagram is shown in Figure 6.4. The two dimensional signal (usually image) is divided into four bands: LL(left-top), HL(right-top), LH(leftbottom) and HH(right-bottom). The HL band indicated the variation along the x-axis while the LH band shows the y-axis variation. Figure 7.5(a) and 7.5(b) show the decomposition of Lena image. The power is more compact in the LL subband.

Collection @ chosun

조선대학교
CHOSUN UNIVERSITY

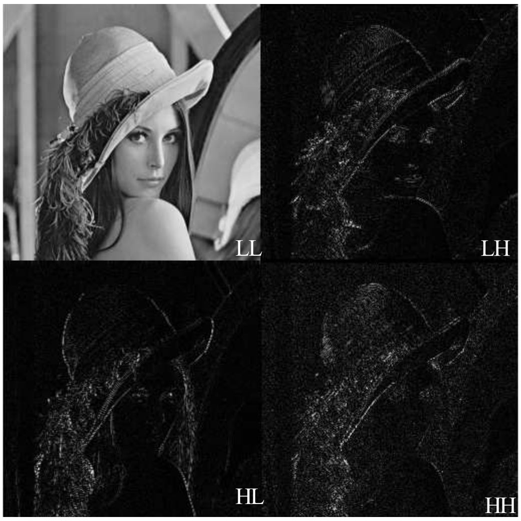

Figure 6.4: Wavelet decomposition of Lena image.

6.6 Wavelet Transform based Interpolation

The fundamental assumption in wavelet based interpolation methods is, low resolution image is obtained as low pass subband of 2D wavelet transform from high resolution image. The main goal is to exploit the regularity of edges across resolution scales to estimate the high-frequency information of missing subbands from the available LR image.

6.6.1 General Approach

This is a straight forward method to estimate the missing high frequency subbands from available LR image. DWT separates the image into different sub band images, namely, $LL, LH, HL,$ and HH. In the wavelet domain, the low-resolution image is equivalent to low-pass filtering of the high-resolution image. In other words, low-frequency sub band images are the low resolution of the original image. The high frequency subband images are interpolated using isotropic interpolation methods such as bicubic or bilinear. Simultaneously, the input image is also interpolated separately. Finally, the high-resolution output image is

Collection @ chosun

조선대학교
CHOSUN UNIVERSITY

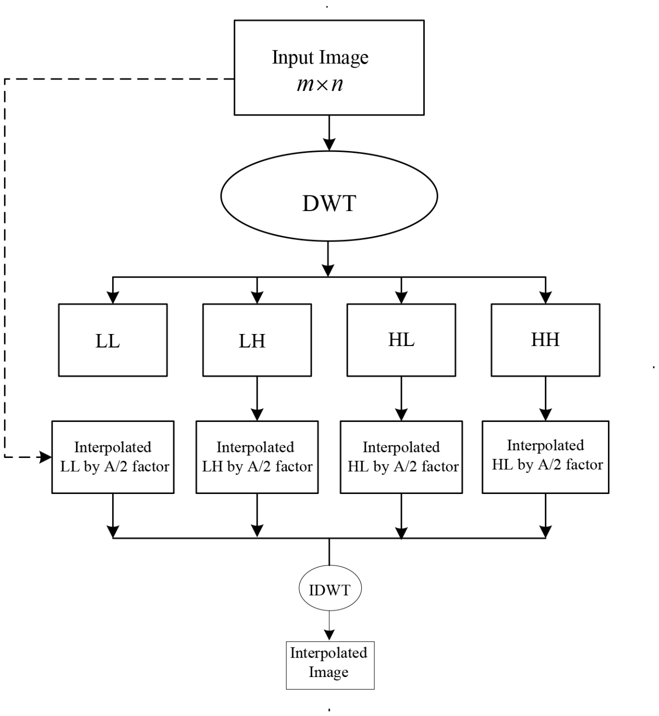
Input Image
$m \times n$
DWT
LL
LH
HL
HH
Interpolated LL by A/2 factor
Interpolated LH by A/2 factor
Interpolated HL by A/2 factor
Interpolated HL by A/2 factor
IDWT
Interpolated Image

Figure 6.5: Wavelet based interpolation

generated by combining the interpolated high-frequency subband images and interpolated input image by using inverse DWT (IDWT). The overall process of general wavelet based interpolation is shown in Figure 6.5. By interpolating original input image I by $A/2$, and interpolating HH, HL, and LH by A, and then applying inverse IDWT, the output image will contain sharper edges than the interpolated image obtained by interpolation of the image I directly. This is because the interpolation of isolated high-frequency components in HH, HL, and LH will preserve more high-frequency components after the interpolation of the respective subbands separately than interpolating I directly.

Collection @ chosun

조선대학교
CHOSUN UNIVERSITY

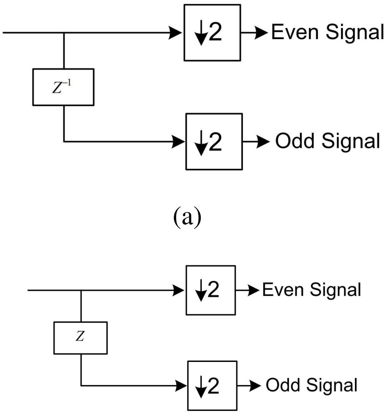

(a)

(b)

Figure 6.6: Polyphase decomposition types.(a) Type-I (b) Type-II

6.7 Lifting based Wavelet Transform

As defined in previous section, the multi resolution analysis can be view as cascade of several two channel filter banks. As shown in Figure $H(z)$ and $G(z)$ are low pass and high pass filters respectively. DWT is implemented in convolution based architecture with the direct structures of two channel filter banks. The convolution based architecture can be constructed by polyphase decomposition as shown in Figure 6.6. where, $H(z) = H_e(z^2) + z^{-1}H_o(z^2)$ and $G(z) = G_e(z^2) + z^{-1}G_o(z^2)$ if type-I decomposition is used and $H(z) = H_e(z^2) + zH_o(z^2)$ and $G(z) = G_e(z^2) + zG_o(z^2)$. The lifting based DWT methodology has been widely as computational efficient method as it requires less multiplications and additions [60].Any DWT filter having perfect reconstruction can be implemented using a finite sequence lifting steps. A lifting based architecture is composed of filters with one predict and one updated step. The output are generated in interleaved fashion. The basic principal of lifting based scheme is to factorize the polyphase matrix of wavelet filter into a sequence of alternating upper and lower triangular matrices and diagonal matrix. The corresponding polyphase matrices are defined as

Collection @ chosun

조선대학교
CHOSUN UNIVERSITY

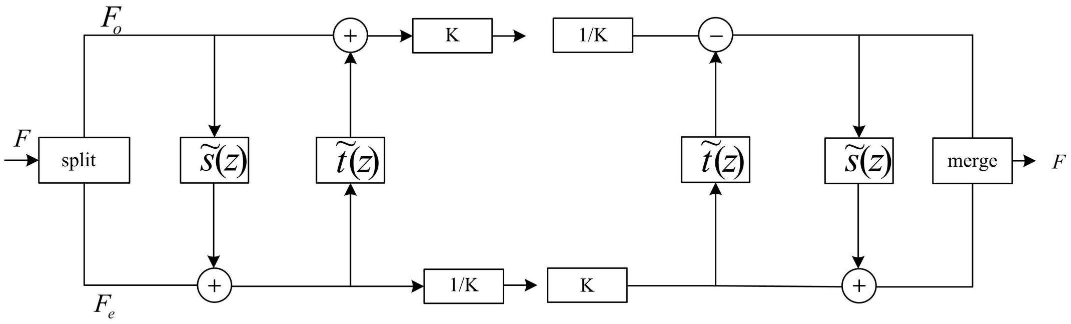

Figure 6.7: Lifting based wavelet transform

$$P(z) = \begin{bmatrix} K & 0 \\ 0 & \frac{1}{K} \end{bmatrix} \prod_{i=1}^{m} \begin{bmatrix} 1 & \hat{s}_i(z) \\ 0 & 1 \end{bmatrix} \begin{bmatrix} 1 & 0 \\ \hat{t}_i(z) & 1 \end{bmatrix} \tag{6.16}$$

or

$$P(z) = \begin{bmatrix} K & 0 \\ 0 & \frac{1}{K} \end{bmatrix} \prod_{i=1}^{m} \begin{bmatrix} 1 & \hat{s}_i(z) \\ 0 & 1 \end{bmatrix} \begin{bmatrix} 1 & 0 \\ \hat{t}_i(z) & 1 \end{bmatrix} \tag{6.17}$$

$$\hat{P}(z) = \begin{bmatrix} \hat{H}_e(z) & \hat{H}_o(z) \\ \hat{G}_e(z) & \hat{G}_o(z) \end{bmatrix} \tag{6.18}$$

and where K is a constant. The lifting scheme is shown in Figure 6.7. The complete factorization consists of three steps:

1. Predict step: where the even samples are multiplied by the time domain equivalent of and are added to the odd samples;

2. Update step: where updated odd samples are multiplied by the time domain equivalent of and are added to the even samples;

3. Scaling step: where the even samples are multiplied by

The inverse DWT is obtained by traversing in the reverse direction, changing the factor to K, factor to $1/K$, and reversing the signs of coefficients in $\hat{t}(z)$ and $\hat{S}(z)$.

Collection @ chosun

조선대학교
CHOSUN UNIVERSITY

The polyphase matrix of the (5,3) filter with highpass coefficients $(1/8, 2/8, 6/8, 2/8, -1/$ and low pass filter is

$$\hat{P}_1(z) \begin{bmatrix} -\frac{1}{8}z + \frac{6}{8} - \frac{1}{8}z^{-1} & \frac{2}{8} - \frac{2}{8}z \\ -\frac{1}{2} - \frac{1}{2}z^{-1} & 1 \end{bmatrix} \tag{6.19}$$

Similarly the polyphase matrix can be factorized as

$$\hat{P}_1(z) \begin{bmatrix} 1 & 0.25(1+z) \\ 0 & 1 \end{bmatrix} \begin{bmatrix} 1 & 0 \\ -0.5(1+z^{-1}) & 1 \end{bmatrix} \tag{6.20}$$

The implementation of lifting based wavelet transform, comprises the decomposition of the given signal into high and low sub-bands using 1-D wavelet transform direction in three steps. In the first step, the given signal is split into two parts: the even polyphase samples $f_e(m,n)$ and the odd polyphase samples $f_o(m,n)$ as shown in Figure 6.7 and expressed in time domain as

$$\begin{aligned} f_e(m,n) &= f(m,2n) \\ f_o(m,n) &= f(m,2n+1) \end{aligned} \tag{6.21}$$

In the prediction step, the odd polyphase samples located at integer positions are predicted from the neighboring even polyphase samples. The resulting prediction residuals, or high subband coefficients, are

$$y_{2i+1} = f_o(m,n) - P_e(m,n) \tag{6.22}$$

The predictor $P(.)$ is a linear combination of neighboring even subset

$$P_e(m,n) = \sum_i p_i f_i[m+i,n] \tag{6.23}$$

p_i represents the lifting coefficient for prediction step.

The third lifting step transforms the even subset $f_e(m,n)$ into a low-pass filtered and sub-sampled version of $f(m,n)$. This coarse approximation is obtained

Collection @ chosun

조선대학교
CHOSUN UNIVERSITY

by updating with a linear combination of the prediction residual $d(m, n)$. The $f_e(m, n)$is replaced with

$$c(m, n) = f_e(m, n) + U(d)(m, n) \tag{6.24}$$

where $U(.)$ is a linear combination of neighboring d values

$$U(d)(m, n) = \sum_j u_j d[m + j, n] \tag{6.25}$$

If the signal is numbered from 0 and if even terms are considered to be the lowpass values and the odd terms the highpass values, we can interpret the above matrices in the time domain as

$$\begin{aligned} y_{2i+1} &= -0.5(f_{2i} + f_{2i+2}) + f_{2i+1}; \\ y_{2i} &= 0.25(y_{2i+1} + y_{2i+3}) + f_{2i} \\ where \quad & 0 \leq i < N/2 \end{aligned} \tag{6.26}$$

6.7.1 Adaptive Directional Lifting

Lifting based wavelet transform also allows each subband of the wavelet transform to be naturally arranged in a quad tree with each parent wavelet at scale giving rise to four child coefficient at scale occupying the same spatial region. One of the draw backs of conventional lifting based wavelets is detection of edge along the horizontal, vertical and diagonal directions only. The adaptive direction lifting based however overcome these drawbacks by efficiently approximating the image signals of edge textures in arbitrary directions. The adaptive directional lifting(ADL) analyzes the local spatial correlation in all direction and then selects the pixels along the direction in which prediction error is minimum. As in conventional lifting, wavelet decomposition based on ADL also follows three steps.

1. Splitting: The splitting process follows same procedure as in conventional lifting based system defined in equation 6.21.

Collection @ chosun

조선대학교
CHOSUN UNIVERSITY

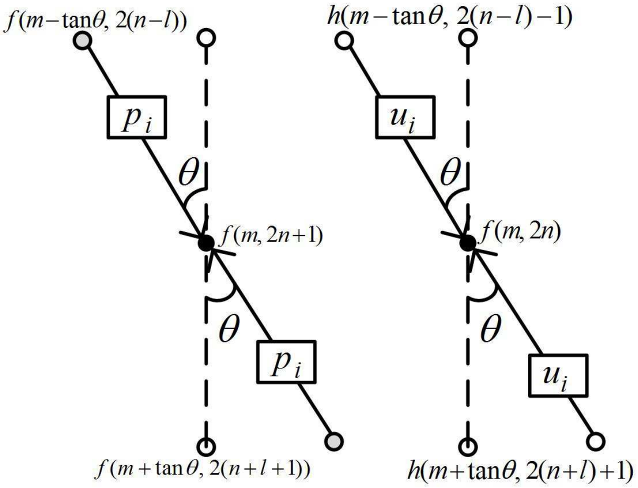
$f(m-\tan\theta, 2(n-l))$
p_i
θ
$f(m, 2n+1)$
θ
p_i
$f(m+\tan\theta, 2(n+l+1))$
$h(m-\tan\theta, 2(n-l)-1)$
u_i
θ
$f(m, 2n)$
θ
u_i
$h(m+\tan\theta, 2(n+l)+1)$

Figure 6.8: Adaptive directional lifting

2. Prediction: The fundamental difference between conventional lifting and ADL lies in the prediction. In contrast to the conventional lifting the high frequency coefficient along an arbitrary direction θ is estimated as

$$h(m, 2n+1) = f(m, 2n+1) - P(m, 2n) \tag{6.27}$$

where, $P(m, 2n) = P_i(x(m - tan\theta, 2n+1) + f(m + \tan\theta, 2(n, l+1))$. Here, P_i represents the lifting coefficient for prediction step. Similarly, in the update process, low frequency coefficient along direction θ is estimated as

$$l(m, 2n) = f(m, 2n) + U(m, 2n+1) \tag{6.28}$$

where $U(m, 2n+1)$ is update coefficient and expressed as

$$U(m, 2n+1) = U_i(h(m - tan\theta, (2n-1)-1) + h(m + \tan\theta, 2(n-1)+1)) \tag{6.29}$$

6.7.2 ADL based Interpolation

ADL performs lifting-based prediction and concentrates energy in image into a LL subband by using transformation along the direction of high pixel correlation.

Collection @ chosun

조선대학교
CHOSUN UNIVERSITY

The high frequency subband images are interpolated using bicubic interpolation. In parallel, instead of interpolating the LL subband the input image is interpolated separately. Finally, the interpolated high-frequency subband images and interpolated input image are combined by using inverse ADL (IADL) to achieve the high-resolution output image. The proposed technique has been compared with conventional and state-of-art image resolution enhancement.

6.7.3 Discrete Cosine Transform

Discrete Cosine Transform (DCT) attempts to decorrelate the signal data [61]. Like other transforms (DCT) expresses a finite sequence of data points in terms of a sum of cosine functions oscillating at different frequencies. DCT has been widely used by modern image and video coding standards, such as JPEG, MPEG, H.263, H.264 and H.265.

6.7.4 One Dimensional DCT

For a 1-D sequence of data with length N is, the DCT is expressed as

$$C(u) = \alpha(u) \sum_{i=0}^{N-1} f(i) \cos\left[\frac{(2i+1)u\pi}{2N}\right], \tag{6.30}$$

for $u = 0, 1, 2, ..., N-1$. Similarly, the inverse transformation is expressed as,

$$f(i) = \alpha(u) \sum_{i=0}^{N-1} C(u) \cos\left[\frac{(2i+1)u\pi}{2N}\right], \tag{6.31}$$

defined as for $i = 0, 1, 2, ...N-1$.

In both equations 6.30 and 6.31 $\alpha(u)$ is defined as

Collection @ chosun

조선대학교 CHOSUN UNIVERSITY

$$\alpha(u) = \begin{cases} \frac{1}{\sqrt{N}}, & for\, u = 0 \\ \\ \sqrt{\frac{2}{N}}, & for\, u = 1, 2....N-1. \end{cases} \tag{6.32}$$

Similarly, we can extend the 1-D DCT to 2-D and expressed as

$$C(u,v) = \alpha(u)\alpha(v) \sum_{i=0}^{N-1} \sum_{i=0}^{N-1} f(i,j) \cos\left[\frac{(2i+1)u\pi}{2N}\right] \times \cos\left[\frac{(2j+1)v\pi}{2N}\right] \tag{6.33}$$

for $u, v = 0, 1, 2, ...N-1$ and $\alpha(u)$ and $\alpha(v)$ are defined in equantion 6.30. The inverse transform is defined as

$$f(i,j) = \alpha(u)\alpha(v) \sum_{i=0}^{N-1} \sum_{i=0}^{N-1} C(u,v) \cos\left[\frac{(2i+1)u\pi}{2N}\right] \times \cos\left[\frac{(2j+1)v\pi}{2N}\right] \tag{6.34}$$

for $i, j = 0, 1, 2, , N-1$. The 2-D basis functions can be generated by multiplying the horizontally oriented 1-D basis functions with vertically oriented set of the same functions. Again, it can be noted that the basis functions exhibit a progressive increase in frequency both in the vertical and horizontal direction. The basis function at $u = 0$ and $v = 0$ results from multiplication of the DC component. Hence, this function assumes a constant value and is referred to as the DC coefficient.

6.8 Discrete Cosine Transform based Image Resizing

Image resizing in DCT domain is performed by either truncating the high frequency DCT coefficients or by zero-padding. Downsized image is obtained by truncation the coefficients and zero-padding is implemented to obtain upscaled image. We determine the number of truncated coefficients and number of zeros

Collection @ chosun

조선대학교 CHOSUN UNIVERSITY

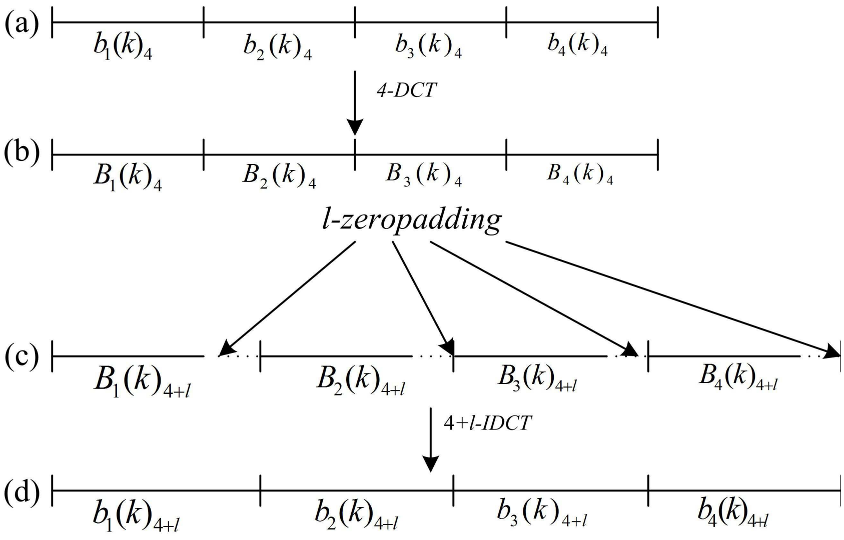

Figure 6.9: DCT based interpolation

according to resizing ratio. For simplicity we describe the 1-D resizing method, which can be applied to 2-D image in horizontal and vertical direction. In general, resizing is performed on block unit, each block having n length. First the n sample DCT is perfomed for each blocks. Zeropadding of l samples is performed on n DCT coefficients. The resized image can be obtained through $n + l$ length inverse DCT. The conceptual diagram of DCT based resizing is shown in Figure 6.9 In DCT based image resizing, resizing, N consecutive 4-sample blocks are converted to $N(4 + l)$ sample blocks. Therefore, N-sample blocks are grouped as shown on Figure. 6.9(a) $b_i(k)_4, (i = 1, 2....N)$ denotes 4 sample image pixels of the i^th block of group of N blocks. The total sample number of original N blocks is $4 \times N$. In order to perform the resizing, the proposed method first performs DCT on each block. $B_i(k)_4, (i = 1, 2....N)$ denotes 4 sample DCT coefficients in Figure. 6.9(b). Let

$$B = \begin{bmatrix} C_4 & 0_4 & 0_4 & \dots & 0_4 \\ 0_4 & C_4 & 0_4 & \dots & 0_4 \\ \vdots & \vdots & \vdots & \ddots & \vdots \\ 0_4 & 0_4 & 0_4 & \dots & C_4 \end{bmatrix} \begin{bmatrix} b_4^1 \\ b_4^2 \\ \vdots \\ b_4^M \end{bmatrix} = \begin{bmatrix} B_4^1 \\ B_4^2 \\ \vdots \\ B_4^M \end{bmatrix} \tag{6.35}$$

Collection @ chosun

조선대학교
CHOSUN UNIVERSITY

To perform resizing in DCT domain, we append l zeros to each block of transformed coefficients which can be expressed as

$$\hat{B} = \begin{bmatrix} B^1_{4+l} \\ B^2_{4+l} \\ \vdots \\ B^M_{4+l} \end{bmatrix} \tag{6.36}$$

where C_4 is the 4 sample DCT coefficients and 0_4 is the 4×4 zero matrix. Finally, the resized image can be obtained by inverse DCT of $\hat{B}$.

$$B = \begin{bmatrix} C_{4+l} & 0_{4+l} & 0_{4+l} & \dots & 0_{4+l} \\ 0_{4+l} & C_{4+l} & 0_{4+l} & \dots & 0_{4+l} \\ \vdots & \vdots & \vdots & \ddots & \vdots \\ 0_{4+l} & 0_{4+l} & 0_{4+l} & \dots & C_{4+l} \end{bmatrix} \begin{bmatrix} B^1_{4+l} \\ B^2_{4+l} \\ \vdots \\ B^M_{4+l} \end{bmatrix} \tag{6.37}$$

6.9 Interpolation Using the Combination of DWT and DCT

We integrate DWT and DCT transformations together in a hybrid architecture. With this hybrid structure, we can exploit the local characteristics within each region of image and the redundancy due to the correlation between adjacent blocks in image. For the finite sequence of data points, DCT of the differential signal generates less high frequency components than that of the original signal. i,e, the error on reconstructed signal is lower in differential based DCT. Thus, the video coding techniques employs the different types of predictions in intra mode codings. The proposed method follows the follows the same procedure as in DCT based interpolation to scale up low resolution image. In this paper, we obtain the differential value of image signal prior to DCT operation. We employ wavelet transform to obtain differential value. Since the wavelet transform decorelates the spatial corelation of pixels, the hybrid architecture enables us to exploit the local characteristics within image. The wavelet coefficients follow the Gaussian distribution, with majority of coefficients centered around the zero as shown in

Collection @ chosun

조선대학교
CHOSUN UNIVERSITY

Figure, the energy compaction property of DCT will concentrate all these signals around the low frequency region. Thus the high frequency region of DCT contains only the zero values.

The first step in the hybrid algorithm consists of wavelet decomposition of image into band of energy. For each level, the input signal is filtered along the rows, and the resulting signal is filtered along the columns. In this way, the 2-D decomposition of an input signal results to four subband images LL, LH, HL and HH. In second step, we interpolate the image by adding additional zeros in high frequency region. Since, majority of coefficients are zeros in except in low frequency region, occurrence of error is low in interpolated data. Thus the interpolated image is not affected by blurring and aliasing in high frequency region. For the efficient implementation of DCT, the structure of hybrid wavelet DCT is similar to classical fast fourier transform (FFT). The bit-reversal and odd-even index separation process is replaced by lifting based DWT. Figure 6.10 shows the block diagram of the last stage of the length-8 Wavelet-DCT. The data is separated into higher detail and lower detail parts via one scale wavelet transform before going through the length-4 DCT blocks. After that, the results of the DCT are combined using an equivalent butterfly operation.

$$B_k = \begin{bmatrix} C_{N/2} & 0 \\ 0 & C_{N/2} \end{bmatrix} \begin{bmatrix} I_{N/2} & 0 \\ 0 & (-1)^m I_{N/2} \end{bmatrix} W_N \tag{6.38}$$

where $C_N/2$ is the $N \times N$ DCT matrix, B_N is the $N \times N$ cross diagonal butterfly matrix, I_N is the $N \times N$ identity matrix and W_N is the $N \times N$ lifting coefficients which is given as.

$$\begin{bmatrix} Sz \\ Wz \end{bmatrix} = \begin{bmatrix} k & 0 \\ 0 & 1/K \end{bmatrix} \prod_{i=1}^{m} \begin{bmatrix} 1 & s_i z \\ 0 & 1 \end{bmatrix} \begin{bmatrix} 1 & 0 \\ t_i(z) & 1 \end{bmatrix} \begin{bmatrix} f_{even}(z) \\ f_{odd}(z) \end{bmatrix} \tag{6.39}$$

where k is a normalization factor. $s_i(z)$ and $t_i(z)$ are lifting coefficients and value of these coefficients is related to filter bank structure. Generally we obtain $s_i(z)$ and $t_i(z)$ by using factorization from filterbank. To perform resizing in DCT domain, we append l zeros to each block of transformed coefficients which

Collection @ chosun

조선대학교
CHOSUN UNIVERSITY

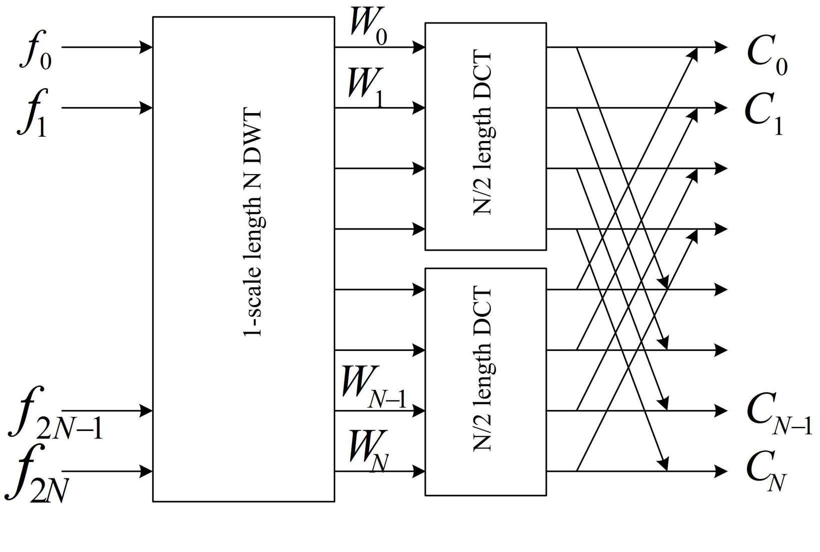

Figure 6.10: Implementation of DWT and DCT

can be expressed as

$$\hat{B} = \begin{bmatrix} B^1_{4+l} \\ B^2_{4+l} \\ \vdots \\ B^M_{4+l} \end{bmatrix} \tag{6.40}$$

where C_4 is the 4 sample DCT coefficients and 0_4 is the 4×4 zero matrix. Finally, the resized image can be obtained by inverse DCT of $\hat{B}$.

$$B = \begin{bmatrix} C_{4+l} & 0_{4+l} & 0_{4+l} & \dots & 0_{4+l} \\ 0_{4+l} & C_{4+l} & 0_{4+l} & \dots & 0_{4+l} \\ \vdots & \vdots & \vdots & \ddots & \vdots \\ 0_{4+l} & 0_{4+l} & 0_{4+l} & \dots & C_{4+l} \end{bmatrix} \begin{bmatrix} B^1_{4+l} \\ B^2_{4+l} \\ \vdots \\ B^M_{4+l} \end{bmatrix} \tag{6.41}$$

Simultaneously, the low resolution input image is interpolated separately. Finally, the interpolated high-frequency subband images and interpolated input image are combined by using inverse DWT to obtain the high-resolution output image. The overall block diagram of hybrid based interpolation is shown in Figure 6.11.

Collection @ chosun

조선대학교
CHOSUN UNIVERSITY

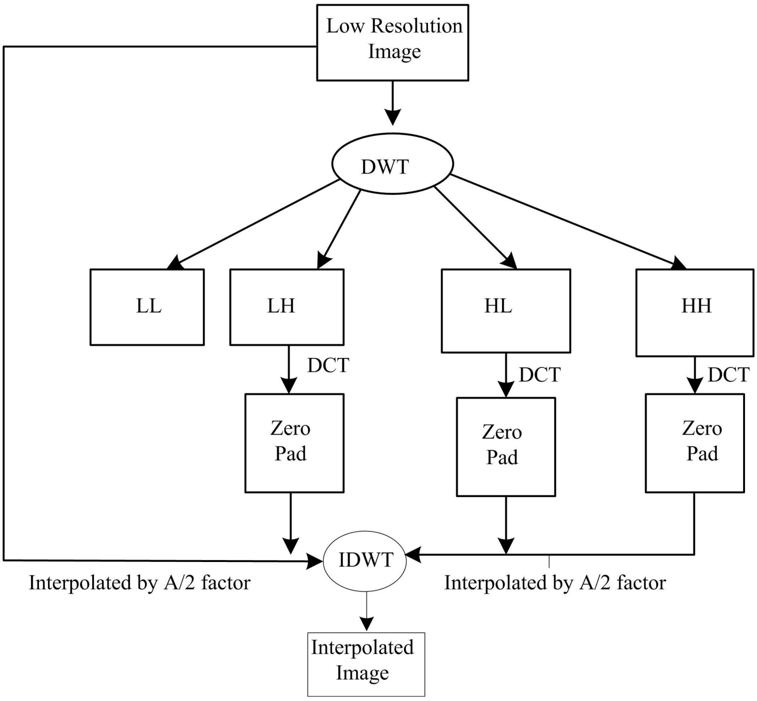

Figure 6.11: Block diagram of hybrid DWT and DCT based interpolation

Collection @ chosun

조선대학교
CHOSUN UNIVERSITY

6.10 Performance Evaluation

In this section, we present experimental results of evaluating the performance of the proposed algorithm using different test images. The performance is compared with several standard methods, such as bilinear interpolation, edge directed interpolation and in [39] and adaptive directional lifting based interpolation. We compared the test result in three different test environment, noise free, noisy and denoised images. For noise free environment, we have selected gray scale Lena image of size 512×512 and high resolution color image of size 1920×1080. Figure 6.12 shows the interpolation of Lena image using different interpolation method. Figure 6.12(a) shows the original image. Figure 6.12(b) shows an interpolated image using new edge directed interpolation (NEDI) [39]. Figure 6.12(c) shows a magnified image using the bilinear method. Figure 6.12(d) shows a magnified image using the adaptive directional lifting (ADL) based method. Finally, Figure 6.12(e) shows the image upscaled using the proposed method. Visually, experiments from the three different filters yield very similar results and conclusions, but the PSNR tells quite a different story. In order to obtain PSNR measurement, we take the $2N \times 2N$ and down sample then HR image to obtain $N \times N$ image. PSNR values of reconstructed images are shown in Table 6.1.

Table 6.1: Comparative Results

Image	Bilinear	NEDI [22]	ADL based Method [15]	Proposed
Rocket	27.01	27.36	28.00	28.19
Flower	27.60	27.35	27.98	28.10
Lena	30.16	30.12	30.65	30.81
Boat	27.50	27.18	27.73	29.23

Although the PSNR is not a good indication of image quality, it is nevertheless frequently used, and the results are tabulated in Table 6.1 for the bilinear interpolation, NEDI methods and ADL based method. Similarly, In Figure 6.13, we demonstrate the interpolation of high resolution color image using different methods and their comparison with the proposed method. One can see

Collection @ chosun

조선대학교
CHOSUN UNIVERSITY

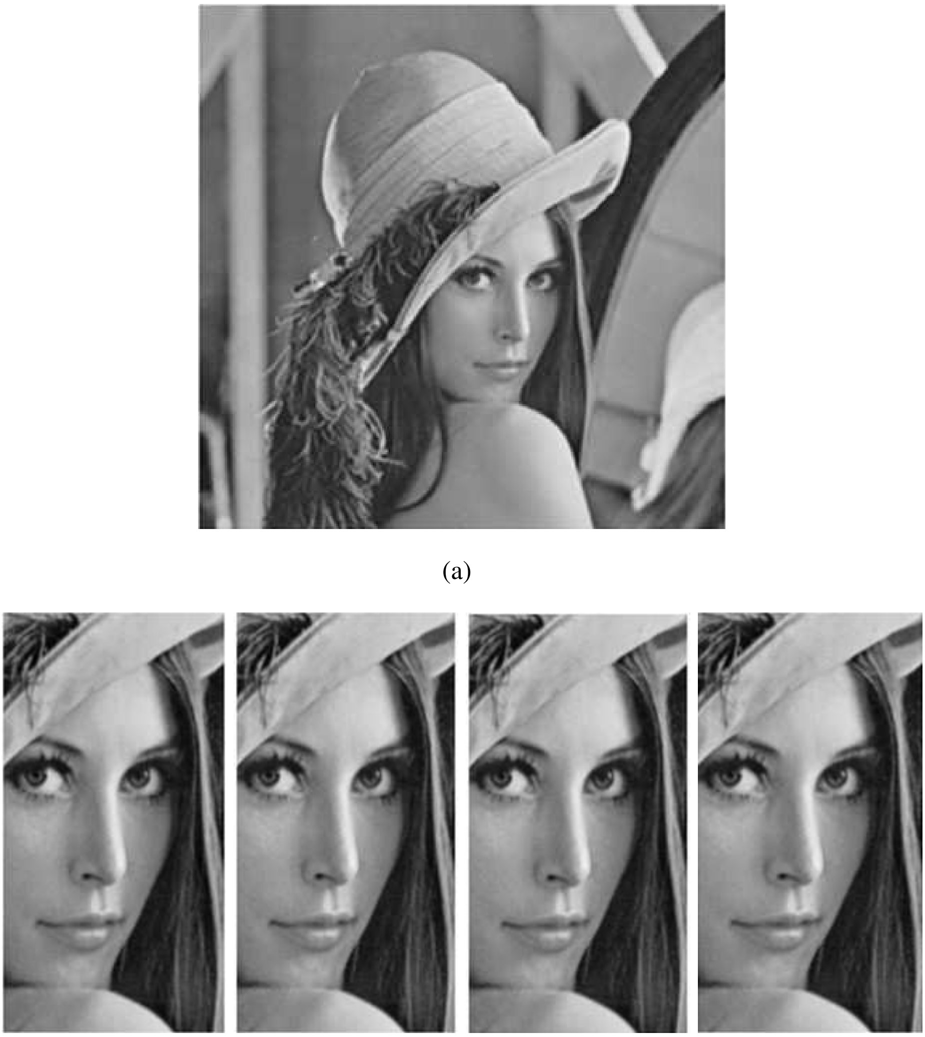

(a)

(b) (c) (d) (e)

Figure 6.12: Experimental results: (a) Original image Lena, (b) Interpolated image using the NEDI method, (c) Bilinear method, (d) ADL-based method, and (e) proposed method.

Collection @ chosun

조선대학교
CHOSUN UNIVERSITY

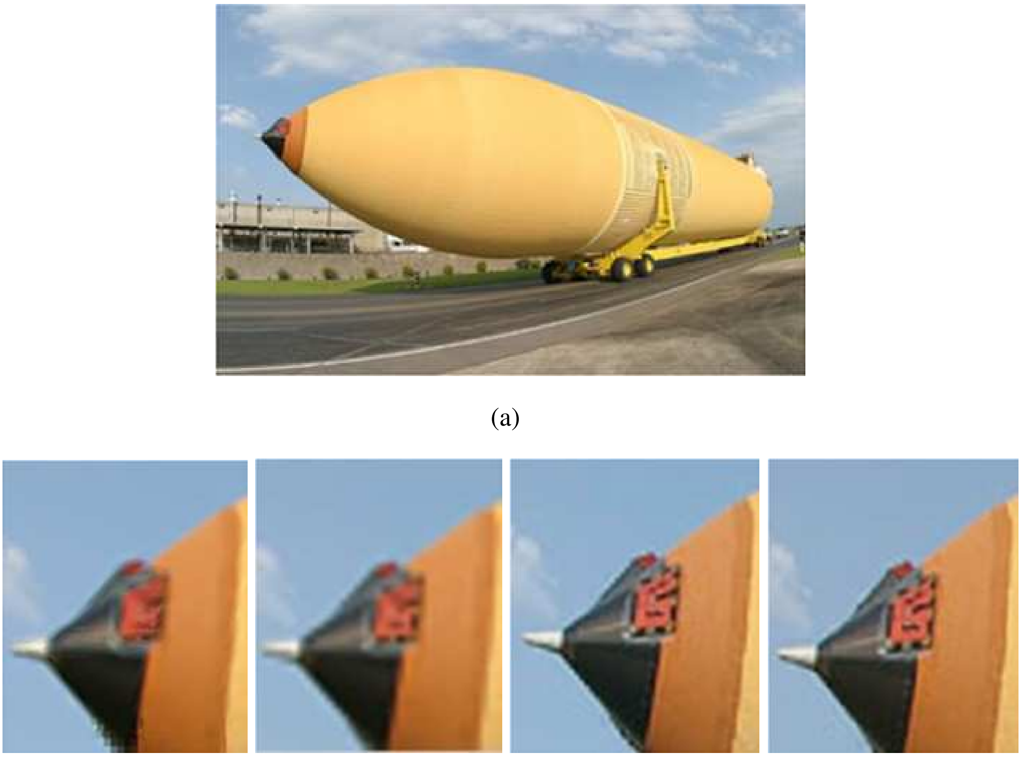

(a)

(b) (c) (d) (e)

Figure 6.13: Experimental results: (a) Original image, (b) Interpolated image using the NEDI method, (c) Bilinear method, (d) ADL-based method, and (e) proposed method.

Collection @ chosun

조선대학교
CHOSUN UNIVERSITY

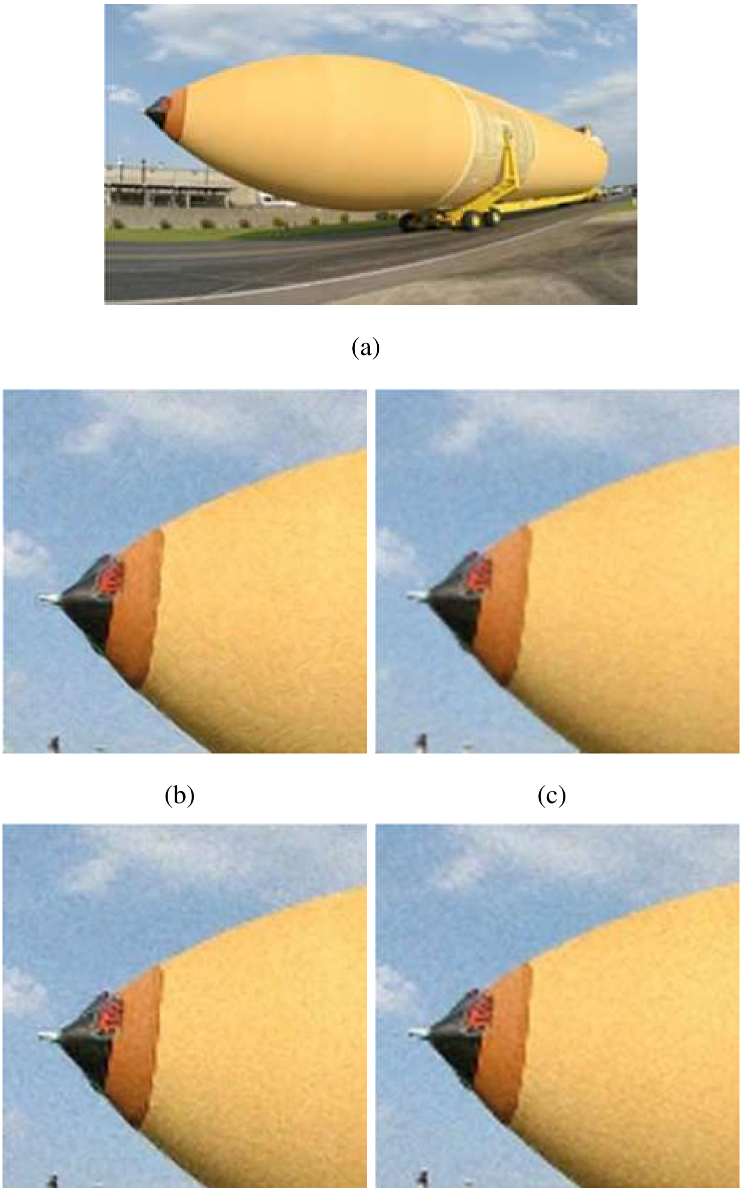

(a)

(b)

(c)

(d)

(e)

Figure 6.14: Experimental results: (a) Original image (b) Interpolated image using the NEDI method, (c) Bilinear method, (d) ADL-based method, and (e) proposed method.

Collection @ chosun

조선대학교
CHOSUN UNIVERSITY

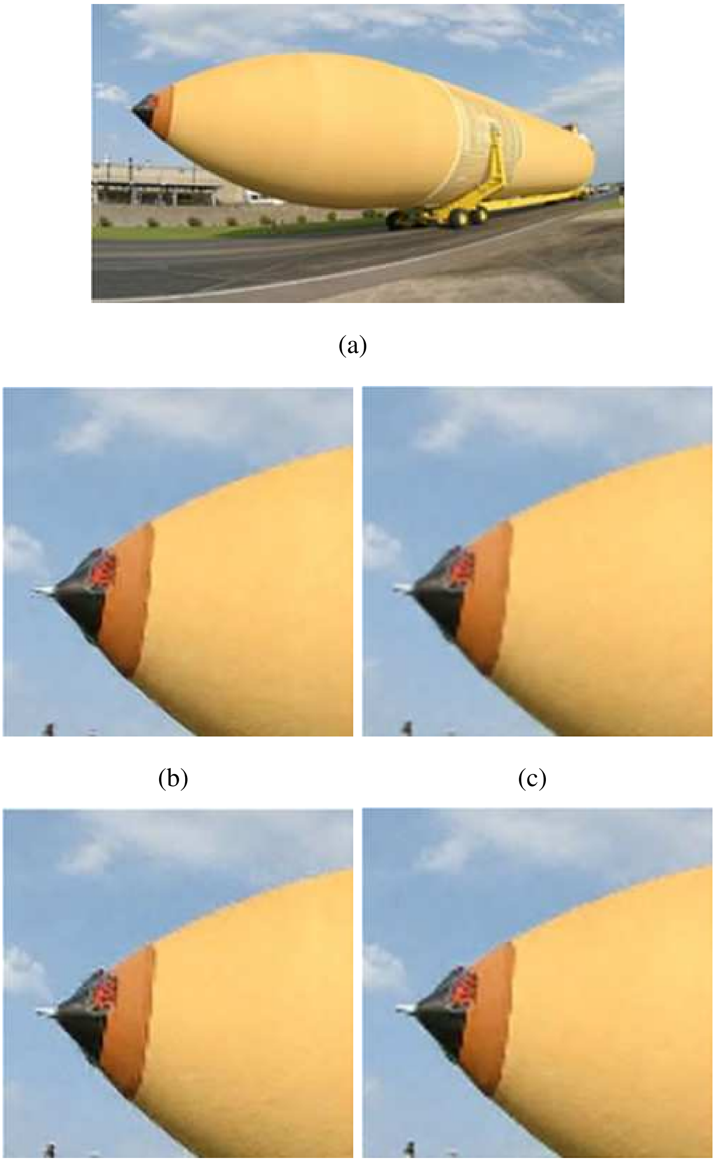

(a)

(b) (c)

(d) (e)

Figure 6.15: Experimental results: (a) Original image, (b) Interpolated image using the NEDI method, (c) Bilinear method, (d) ADL-based method, and (e) proposed method.

Collection @ chosun

조선대학교
CHOSUN UNIVERSITY

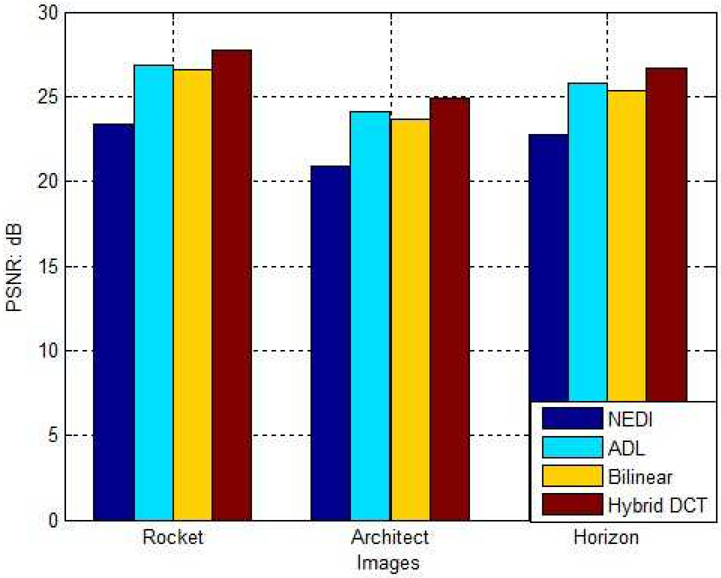

(a)

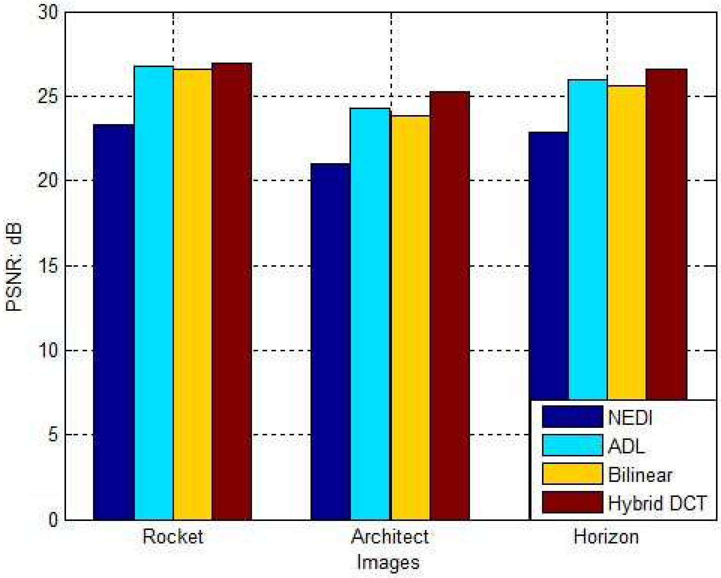

(b)

Figure 6.16: Performance evaluation in Red color channel on: (a) Noiseless image, (b) Denoised image using CDM.

Collection @ chosun

조선대학교 CHOSUN UNIVERSITY

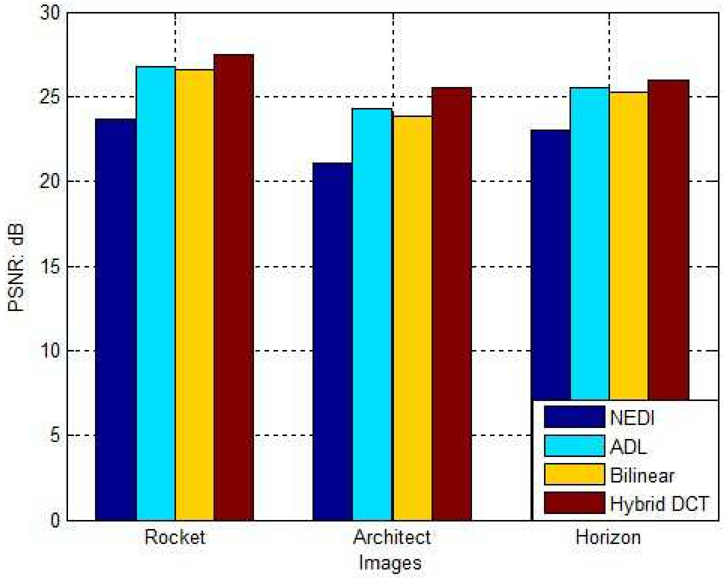

(a)

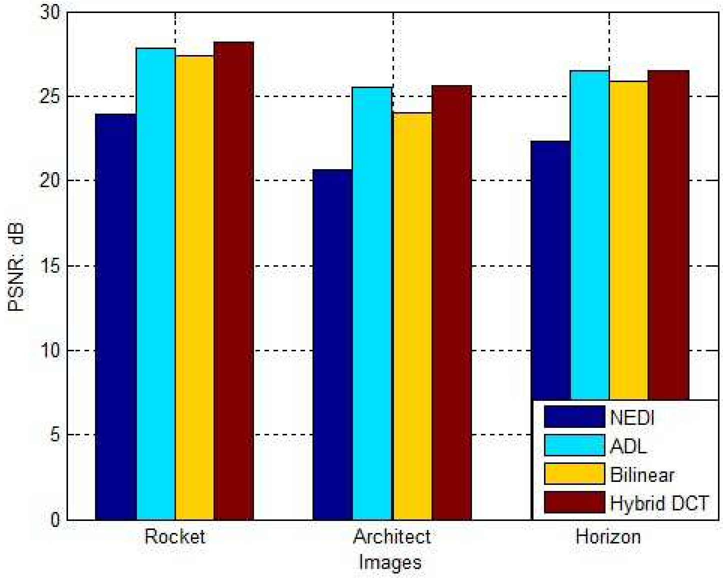

(b)

Figure 6.17: Performance evaluation in Green color channel on: (a) Noiseless image, (b) Denoised image using CDM.

Collection @ chosun

조선대학교
CHOSUN UNIVERSITY

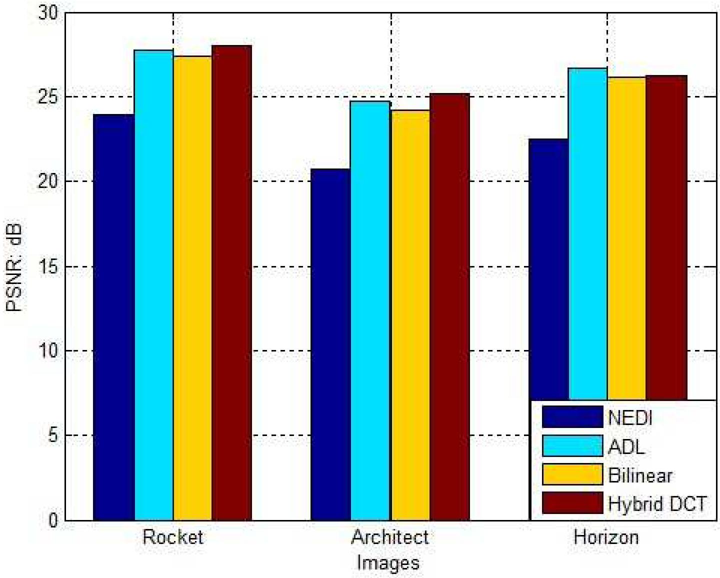

(a)

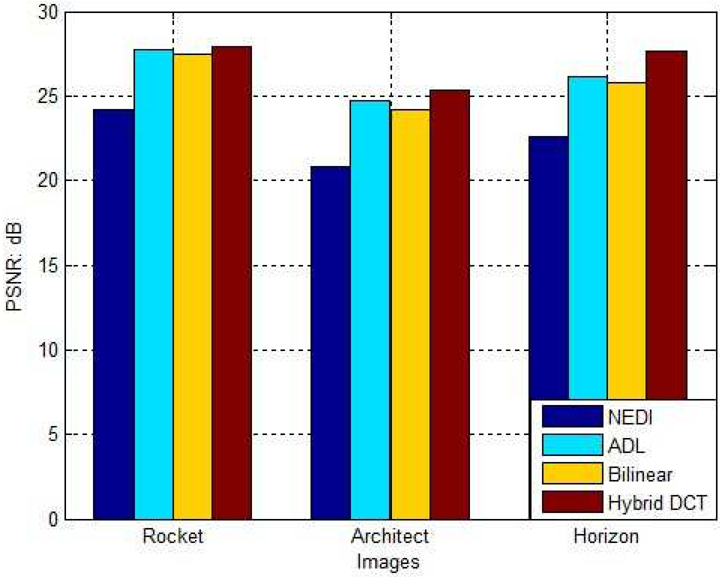

(b)

Figure 6.18: Performance evaluation in Blue color channel on: (a) Noiseless image (b) Denoised image using CDM.

Collection @ chosun

조선대학교 CHOSUN UNIVERSITY

that the proposed algorithm resizes the high-frequency component better without the ringing artifacts present in bilinear and other methods. We used a half-size downsampled image using nearest neighbor method to interpolate to the original size and compute the PSNR. For the noisy test environment, we performed experiments of noisy and denoised images. For this experiment, we added gaussian noise to the CFA image and performed denosing followed by CDM as described in section IV. Interpolation is performed on noisy and denoised images separately. Figures 6.14 shows interpolation of noisy image. Figure 6.14(a) shows the original image. Figure 6.14(b) shows an interpolated image using NEDI. Figure 6.14(c) shows a magnified image using the bilinear method. Figure 6.14(d) shows a upscaled image using the adaptive directional lifting (ADL) based method. Finally, Figure 6.14(e) shows the image upscaled using the proposed method. The corresponding PSNR values are shown in Figure 6.16(a), 6.17(a) and 6.18(a). Similarly, Figures 6.15 shows interpolation of denosied image. Figure 6.15(a) shows the original image. Figure 6.14(b) shows an interpolated image using NEDI. Figure 6.15(c) shows a magnified image using the bilinear method. Figure 6.15(d) shows a upscaled image using the adaptive directional lifting (ADL) based method. Finally, Figure 7.11(e) shows the image upscaled using the proposed method. The corresponding PSNR values are shown in Figure 6.16(b), 6.17(b) and 6.18(b).

6.11 Subsection Summaries

In this Section, we discussed on image up-sampling algorithm based on the combination of ADL and DCT. Since, the original image is used as LL subband and zero padding is used for the interpolation of the high frequency subband in DCT domain, the proposed method yields much better visual quality as well as objective quality compared to the current state of the art image resolution enhancement for noiseless and noise corrupted image. Finally, owing to the hybrid directional lifting and DCT concept of the proposed method, it can be efficiently used for the interpolation of noisy and noiseless color images.

Collection @ chosun

조선대학교
CHOSUN UNIVERSITY

Chapter 7
Complex Wavelet Transform Based Interpolation

7.1 Complex Wavelets

Discrete wavelet transform (DWT) has emerged as an efficient multi resolution analysis tool for images over the last decades. However, it comes with following limitations. DWT fails to provide a compact representation of edges or contours. The main reason for this inefficiency is the lack of shift-invariance and the spatial isotropy of the construction of the standard 2-D WT. Filtering and subsampling operations are applied equally along both the horizontal and vertical directions at each scale. An edge is essentially a singularity moving around in space may be represented on by three directions. However in DWT the corresponding filters, obtained as direct products of the 1-D counterparts, are isotropic at all scales. In this section, we will explored the additional features of complex wavelets [57], of providing an approximately shift-invariant multi scale representation, strengthen the two populations and persistence assumptions, which provides a more accurate characterization of edge structure.

7.2 The Dual-Tree Complex Wavelet Transform

The DT-CWT is an enhancement to the traditional critically sampled DWT to overcome the shortcomings with important additional properties: it is nearly shift invariant and offers higher directional selectivity [57]. The DT-CWT provides the explicit information about singularities in a broad range of orientations which allows the characterization of images more efficiently [58].

The DT-CWT of a signal $f(t)$ is implemented by using two critically sampled DWTs in parallel on the same data, for N point signals, it has generated $2N$ DWT

Collection @ chosun

조선대학교
CHOSUN UNIVERSITY

coefficients, the transform is doubly expansive. The decomposition of a signal $f(t)$ terms of a complex shifted and dilated mother wavelet can be expressed as,

$$f(t) = \sum_{l \in Z} u_{j_0,l} \phi_{j_0,l}(t) + \sum_{j \geq j_0} \sum_{l \in Z} c_{j,l} \psi_{j,l}(t) \tag{7.1}$$

where, $\phi_{j_0,l}$ and $\psi_{j,l}$ are complex basis functions composed of real basis functions and expressed as $\phi_{j_0,l} = \phi^r_{j_0,l} + \sqrt{-1}\phi^i_{j_0,l}$ and $\psi_{j,l} = \psi^r_{j,l} + \sqrt{-1}\psi^i_{j,l}$. Since $\phi^i_{j_0,l}$ and $\psi^i_{j,l}$ are real wavelets. A tight frame with 2× redundancy is formed in 1D by $\{\phi^r_{j_0,l}, \phi^i_{j_0,l}, \psi^r_{j,l}, \psi^i_{j,l}\}$. For the imaginary part, the real and imaginary parts of the dual-tree CWT are computed using separate filter bank structures with wavelets. The filters are designed in a specific way such that the sub-band signals of the upper DWT can be interpreted as the real part of a complex wavelet transform, and the sub-band signals of the lower DWT can be interpreted as the imaginary part. When designed in this way, the DT-CWT is nearly shift invariant, in contrast to the classic DWT. Similarly, in 2D the CWT decomposes an image $f(x, y)$ using dilations and translations of a complex scaling function and six complex wavelet functions

$$f(x, y) = \sum_{k \in Z^2} u_{j_0,k} \phi_{j_0,k}(s) + \sum_{b \in \theta} \sum_{j \geq j_0} \sum_{k \in Z^2} c^b_{j,k} \psi^b_{j,k}(s) \tag{7.2}$$

The six subbands of the 2D CWT are labeled $\theta = \{\pm 15°, \pm 45°, \pm 75°\}$ for the oriented direction of the wavelet function as shown in Figure 7.3(b). For a separable 2D CWT based on 1D complex ϕ, ψ, we have $\psi^{+15°}(s) = \phi(s_1)\psi(s_2)$, $\psi^{+45°}(s) = \psi(s_1)\psi(s_2)$, $\psi^{+75°}(s) = \psi(s_1)\phi(s_2)$, $\psi^{-15°}(s) = \phi(s_1)\overline{\psi(s_2)}$, $\psi^{-45°} = \psi(s_1)\overline{\psi(s_2)}$ and $\psi^{-75°(s)} = \psi(s_1)\overline{\phi(s_2)}$ as shown in Figure 7.2, where $\overline{\psi}$ is the complex conjugate of ψ.

The 2D CWT expansion $f(x, y))$ using a tight frame with 4×4 redundancy. The 2-D DT-CWT implementation consists of two fundamental steps. Firstly, an input image is decomposed up to a desired level by two critically sampled separable 2-D DWT in parallel as two branches, branch a and branch b as shown in Figure7.1(a) This decomposition leads to generation of six high pass subbands

Collection @ chosun

조선대학교
CHOSUN UNIVERSITY

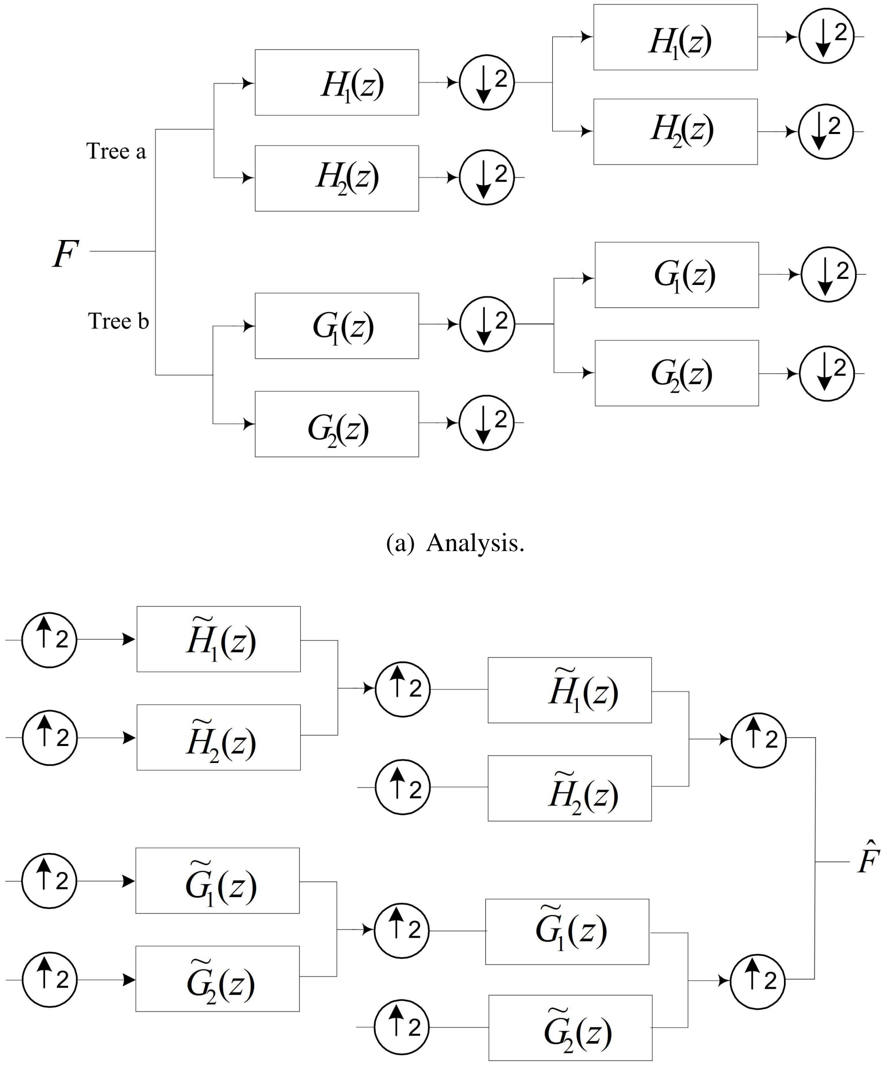

(a) Analysis.

(b) Synthesis

Figure 7.1: Dual-tree complex wavelet transform

Collection @ chosun

조선대학교
CHOSUN UNIVERSITY

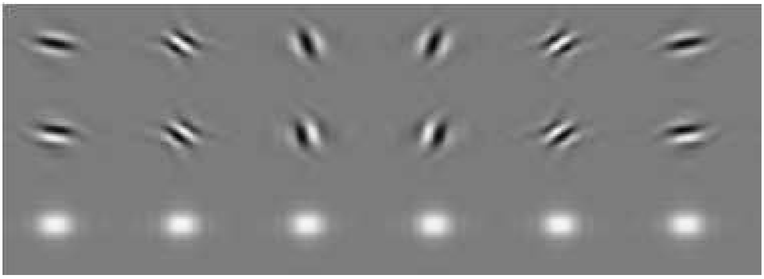

Figure 7.2: Dual-tree complex wavelet transform basis function

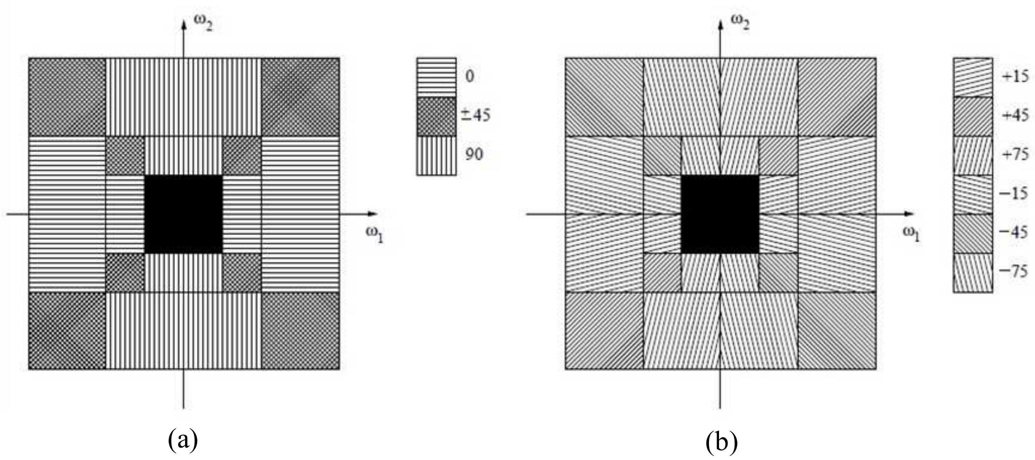

(a) (b)

Figure 7.3: An edge contour (a) in the plane reconstructed using wavelet coefficients at one scale j from (b) the real DWT and (c) the CWT.

dCollection @ chosun

조선대학교
CHOSUN UNIVERSITY

HL_a, LH_a, HH_a, LH_b, HL_b, HH_b and two low pass as LL_a and LL_b subbands at each level. In the next step, every two corresponding subbands having same pass bands are linearly combined by using both the averaging and differentiation operation.

$$\begin{aligned}(LH_a + LH_b)/\sqrt{2}, (LH_a - LH_b)/\sqrt{2}\\ (HL_a + HL_b)/\sqrt{2}, (HL_a - HL_b)/\sqrt{2}\\ (HH_a + HH_b)/\sqrt{2}, (HH_a - HH_b)/\sqrt{2}\end{aligned} \tag{7.3}$$

7.3 Statistical Modelling of Complex Wavelet Transform

The main idea of the wavelet domain interpolation is to exploit the properties of wavelet coefficients for estimating the extreme points in the higher frequency bands. First, the intra-scale characteristic of coefficients is studied. Within the same scale, coefficients representing the smooth region in an image have small magnitudes while large magnitudes represent singular regions. Each wavelet coefficient is modeled by a gaussian mixture model (GMM) that has multiple means and variances.

The overall marginal probability distribution function (PDF) is given by a two-state model with hidden states $(S_i = 1/2)$, where one Gaussian is used to model the coefficients around zero for small region, while another is used for the higher-magnitude coefficients which constitute the singularities. These two states are illustrated in Figure 7.4. Similarly, the PDF plot of wavelet coefficients of Lena image is shown in Figure 7.6. Each coefficient is assumed to fall into one of these distributions, and HMT model is trained by the expectation maximization (EM). Then, the overall density function is given by:

$$f(w_i) = p(S_i = m)f(w_i/S_i = m) \tag{7.4}$$

where, $p(S_i = m)$ is obtained using the EM. Given the state S_i, the conditional

Collection @ chosun

조선대학교 CHOSUN UNIVERSITY

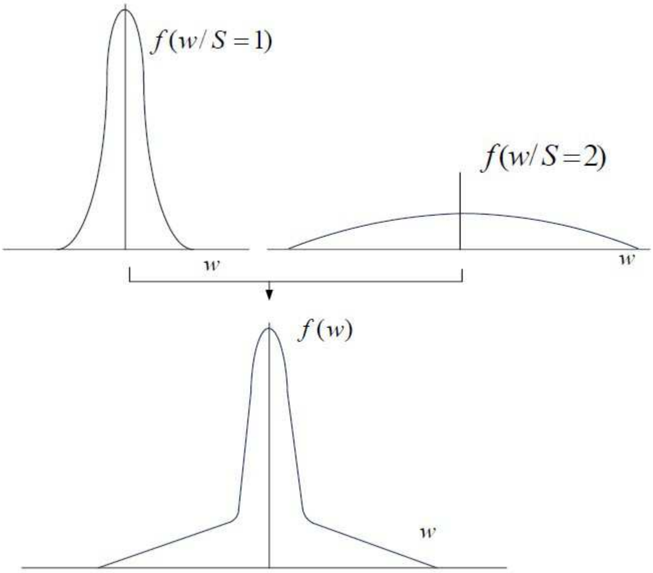

Figure 7.4: Two state Gaussian model.

probability $f(w_i/S_i = m)$ of the coefficient value corresponding to the Gaussian distribution is obtained as:

$$f(w_i/S_i = m) = \frac{1}{\sqrt{2\pi\sigma_{i,m}^2}} exp\left(-\frac{w_i^2}{2\sigma_{i,m}^2}\right) \tag{7.5}$$

Second, the unknown high-frequency coefficients are estimated by using the inter-scale relationship, which is defined by the Markov stochastic model. This model uses both the persistency and non-Gaussianity properties of the wavelet coefficients. For images, each parent wavelet coefficient in the HMT hierarchy has four children as shown in Figure 7.5(a). Owing to persistence, the relative size of the coefficients propagates across the scale. To describe these dependencies, the two-state HMT model uses the state transition probabilities $f(S_i = m/S_{p(i)} = n)$ between the hidden states S_i of the children, given that of the parent $S_{p(i)}$:

$$f(w_i/S_i = m) = \frac{1}{\sqrt{2\pi\sigma_{i,m}^2}} exp\left(-\frac{w_i^2}{2\sigma_{i,m}^2}\right) \tag{7.6}$$

Collection @ chosun

조선대학교
CHOSUN UNIVERSITY

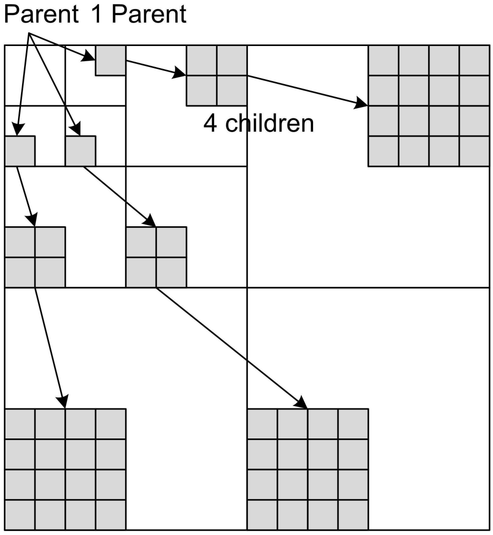

(a) Each wavelet coefficient analyzes a local region in the image.

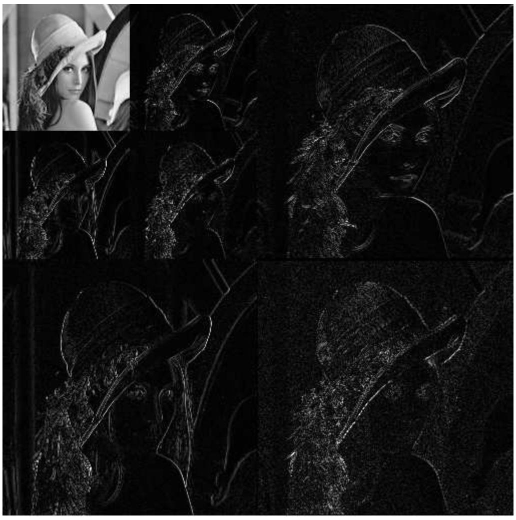

(b) Wavelet transform of the Lena test image wavelet coefficients with large magnitude are white, while those with small magnitude are black

Figure 7.5: Wavelet transform

Collection @ chosun

조선대학교 CHOSUN UNIVERSITY

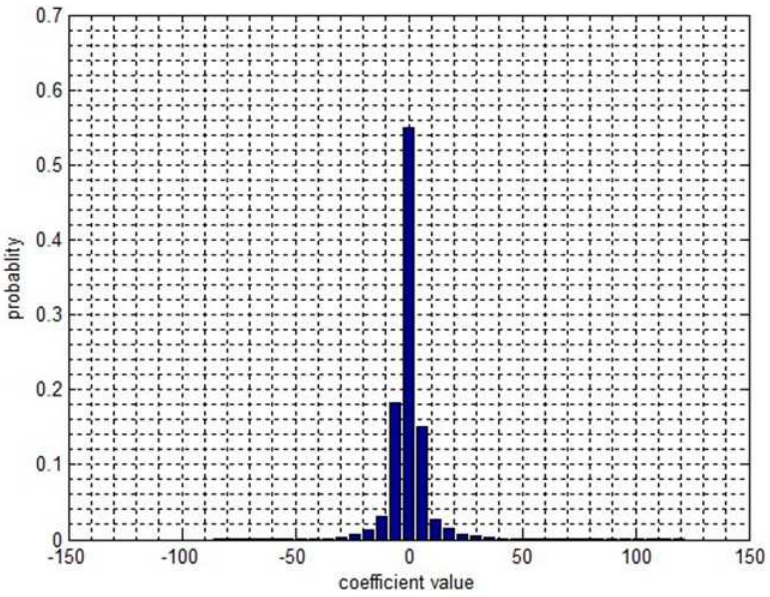

Figure 7.6: Two state Gaussian model.

where according to the persistence assumption, $f(S_i = 1|S_{p(i)} = 1)f(S_i = 2|S_{p(i)} = 1)$, and

$$f(S_i = 1/S_{p(i)} = 1) >> f(S_i = 2/S_{p(i)} = 1) \tag{7.7}$$

The probability that the large coefficient changes into the small coefficient converges to 0.5 across scales [51]. Thus the state probability can be expressed as,

$$f(S_i = 1/S_{p(i)} = 2) = 0f(S_i = 1/S_{p(i)} = 1) = 1 \tag{7.8}$$

Finally, state transition probabilities can be approximated by:

$$f(S_i = 1/S_{p(i)} = 2) = 1/2f(S_i = 2/S_{p(i)} = 2) = 1/2 \tag{7.9}$$

Similarly, the variance of child coefficients is obtained based on [47]. In this paper, the DWT wavelet coefficients are modeled using three independent HMT models. In this way, we tie together all trees belonging to each of the three detail subbands to decrease the computational complexity and prevent overfitting to the

Collection @ chosun

조선대학교
CHOSUN UNIVERSITY

data. For the DT-CWT coefficients, the complex wavelet coefficient comprise real and complex components $w = (w_r, w_c)$ Thus, the conditional probability for the complex coefficient $f(w_i/S_i = m)$ is expressed as:

$$\begin{bmatrix} \epsilon_{i,p(i)}^{1,1} & \epsilon_{i,p(i)}^{1,2} \\ \epsilon_{i,p(i)} & \epsilon_{i,p(i)}^{2,2} \end{bmatrix} = \begin{bmatrix} 1 & 0.5 \\ 0 & 0.5 \end{bmatrix} \tag{7.10}$$

Once the state of the child coefficient is confirmed, we generate corresponding coefficient values based on different interpolation methods. The state value of coefficients clearly indicates the pixel characteristics around the location i,e, the state value $S_i = 1$, indicates the coefficient belongs to low frequency region while the high $S_i = 2$ corresponds to high frequency regions. In the proposed method unknown coefficients values belonging to the high frequency region are generated using a linear interpolation instead of random values based on the variance. Coefficients along the direction yielding the lowest high frequency energy among all the directions are selected for interpolation. While, in case of low frequency region, pixel intensity of neighboring pixels are almost identical. Thus we generate the child coefficients based from the variance same as its parents.

7.4 Performance Evaluation

Some experimental results of the proposed algorithm are presented in this section. As in previous chapter, we performed experiments on 512×512 sized gray scale Lena image and high resolution color image of size 1920×1080 in three different test environment, noise free, noisy and denoised images. Several standard methods such as bilinear interpolation, edge directed interpolation and in [39] and adaptive directional lifting based interpolation are used for the performance evaluation. Figure 7.8 show the interpolation of Lena image using different interpolation method. Figure 7.8(a) shows the original image. Figure 7.8(b) shows the interpolated image using new edge directed interpolation (NEDI) [39]. Figure 7.8(c) shows a magnified image using the bilinear method. Figure 7.8(d) shows a magnified image using the ADL based method. Finally, Figure 7.8(e)

Collection @ chosun

조선대학교
CHOSUN UNIVERSITY

shows the image upscaled using the proposed method. Visually, experiments from the three different filters yield very similar results, but the PSNR tells quite a different story. In order to obtain PSNR measurement, we take the $2N \times 2N$ and downsample it to obtain $N \times N$ image. PSNR values of reconstructed images are shown in Table 7.1. The reconstructed images generally attain most of their quality in few iterations and practically do not change after 5 and 6 iterations of expectation maximization(EM), both in visual quality and in PSNR measurements. The log likelihood of high frequency coefficients estimated during expectation maximization remains constant after 5-6 iterations as shown in Figure 7.7.

Table 7.1: Comparative Results.

Image	Bilinear	NEDI [22]	ADL based Method [15]	Proposed
Rocket	27.01	27.36	28.00	28.19
Flower	27.60	27.35	27.98	28.10
Lena	30.16	30.12	30.65	30.81
Boat	27.50	27.18	27.73	29.23

Since we obtain the variances and mean of coefficients using only few iterations, the use of EM doesnt make the overall system more complex. Although the PSNR is not a good indication of image quality, it is nevertheless frequently used, and the results are tabulated in Table 7.1 for the bilinear interpolation, NEDI methods and ADL method. The best numbers are highlighted in bold. Similiary, In Figure 7.9, we demonstrate the interpolation of high resolution color image using different methods and their comparison with the proposed method. One can see that the proposed algorithm resizes the high-frequency component better without the ringing artifacts present in bilinear and other methods. We used a half-size downsampled image using nearest neighbor method to interpolate to the original size and compute the PSNR. For the noisy test environment, we performed experiments of noisy and denoised images. For this experiment, we added gaussian noise to the CFA image and performed denosing followed by CDM as described in section IV. Interpolation is performed on noisy and

Collection @ chosun

조선대학교
CHOSUN UNIVERSITY

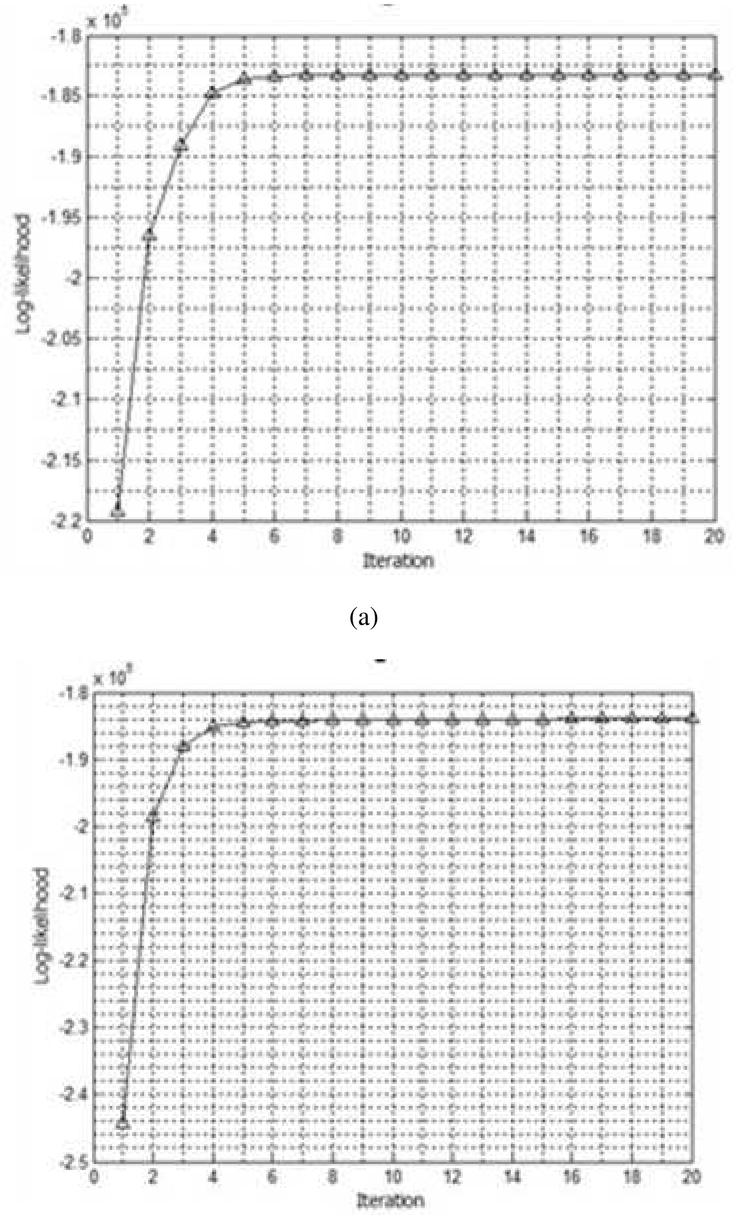

(a)

(b)

Figure 7.7: Log-likelihood vs number of iterations (a) Real HH coefficients (b) Imaginary HH coefficients

Collection @ chosun

조선대학교
CHOSUN UNIVERSITY

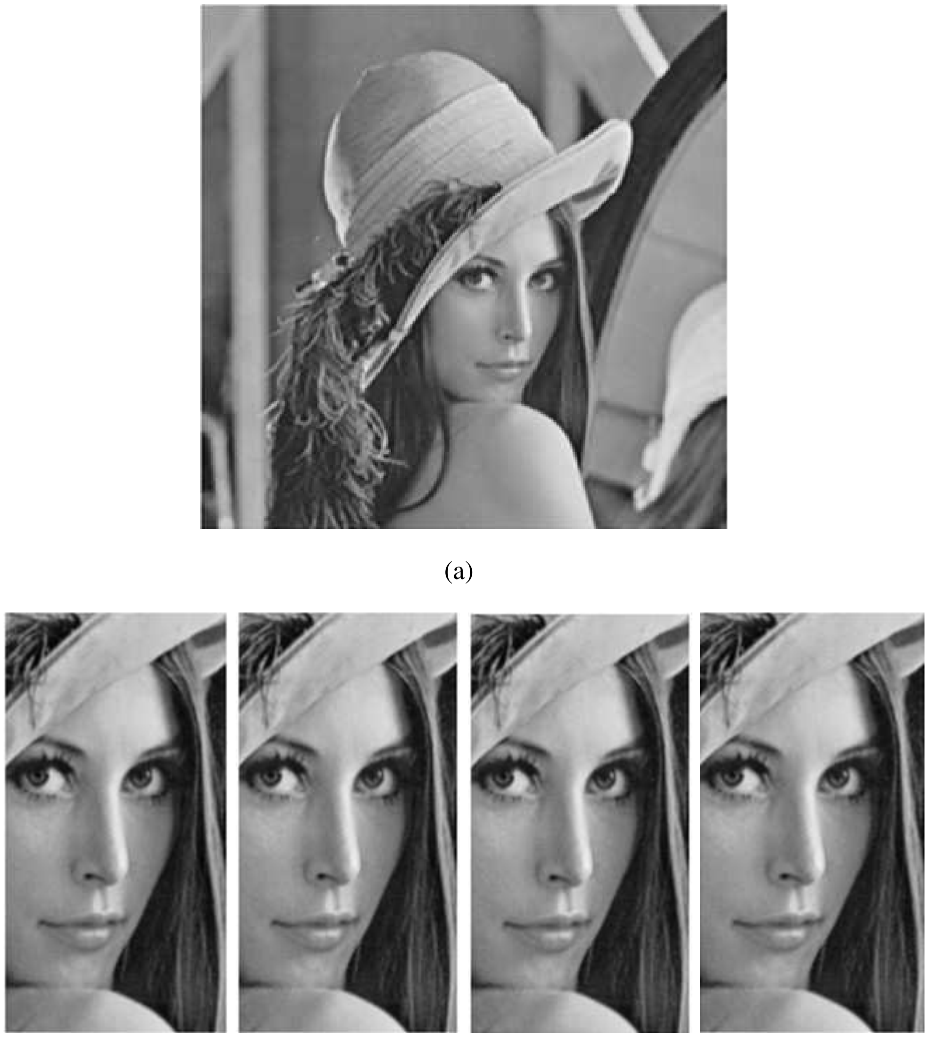

(a)

(b) (c) (d) (e)

Figure 7.8: Experimental results: (a) Original image Lena, (b) Interpolated image using the NEDI method, (c) Bilinear method, (d) ADL-based method, and (e) proposed method.

Collection @ chosun

조선대학교
CHOSUN UNIVERSITY

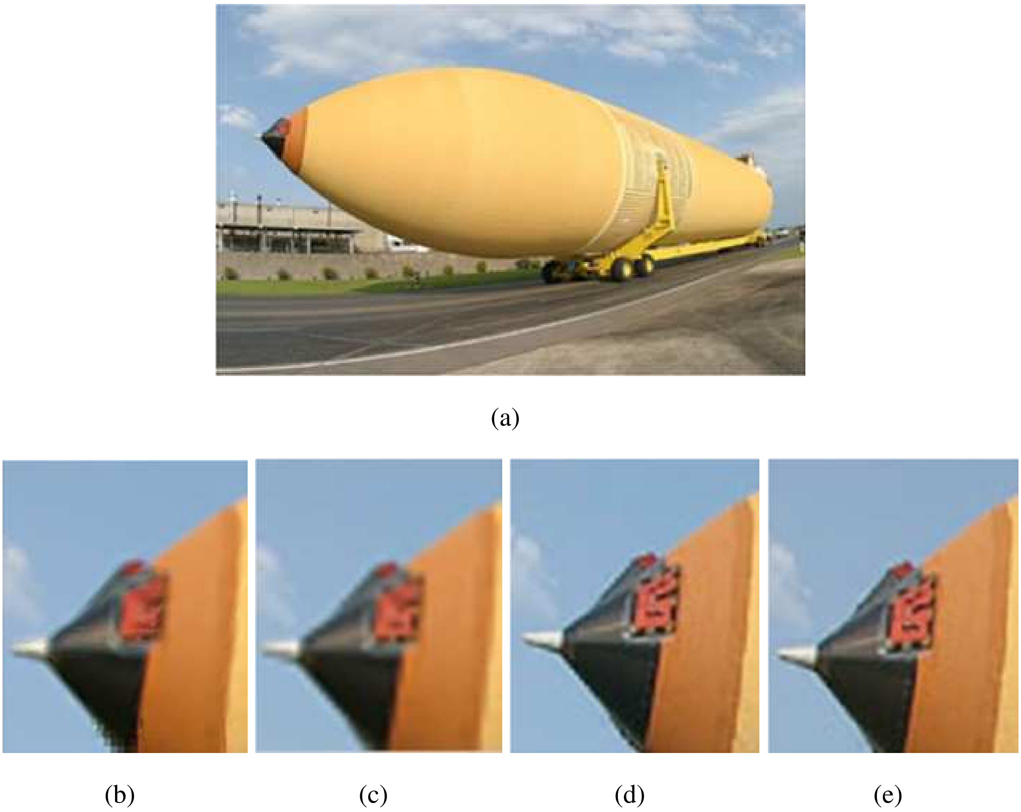

(a)

(b) (c) (d) (e)

Figure 7.9: Experimental results: (a) Original image, (b) Interpolated image using the NEDI method, (c) Bilinear method, (d) ADL-based method, and (e) proposed method.

dCollection @ chosun

조선대학교 CHOSUN UNIVERSITY

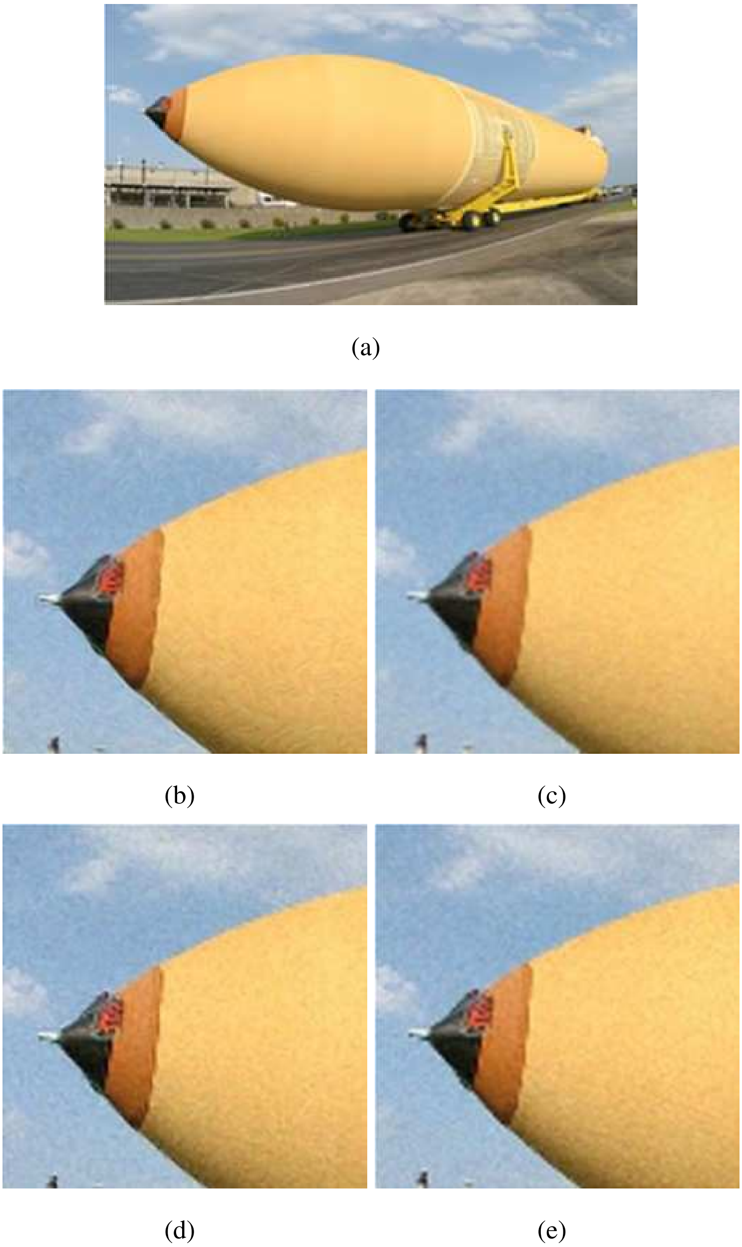

(a)

(b)

(c)

(d)

(e)

Figure 7.10: Experimental results: (a) Original image (b) Interpolated image using the NEDI method, (c) Bilinear method, (d) ADL-based method, and (e) proposed method.

Collection @ chosun

조선대학교
CHOSUN UNIVERSITY

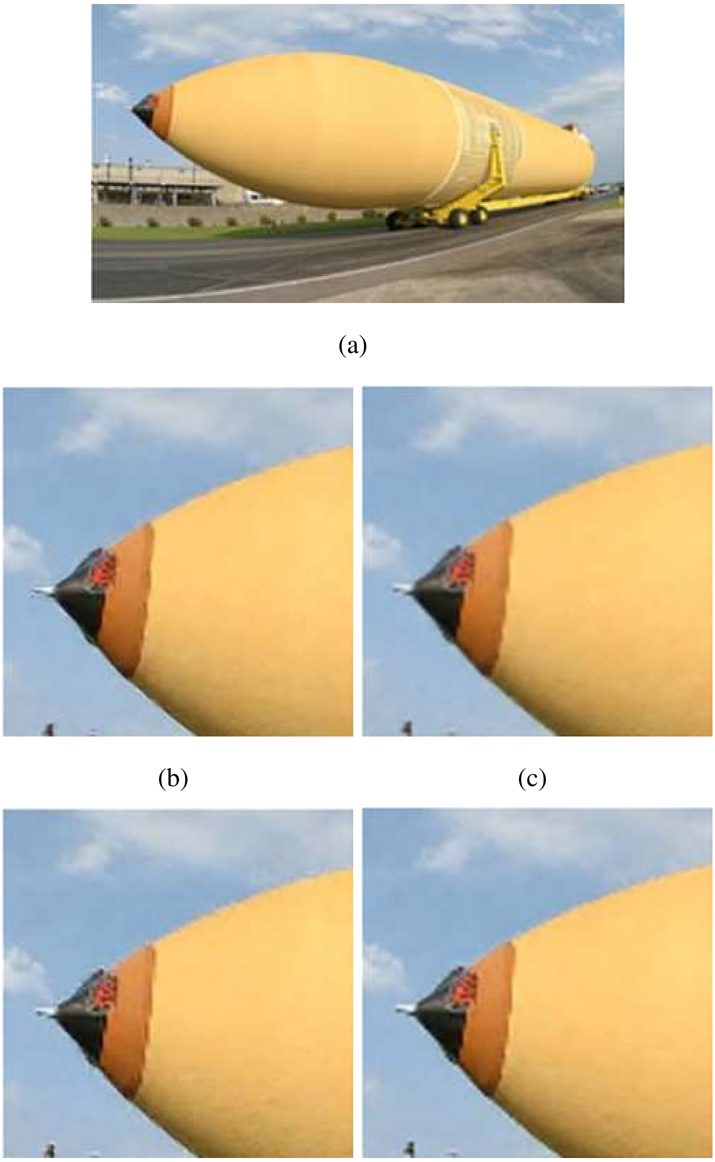

(a)

(b) (c)

(d) (e)

Figure 7.11: Experimental results: (a) Original image, (b) Interpolated image using the NEDI method, (c) Bilinear method, (d) ADL-based method, and (e) proposed method.

dCollection @ chosun

조선대학교
CHOSUN UNIVERSITY

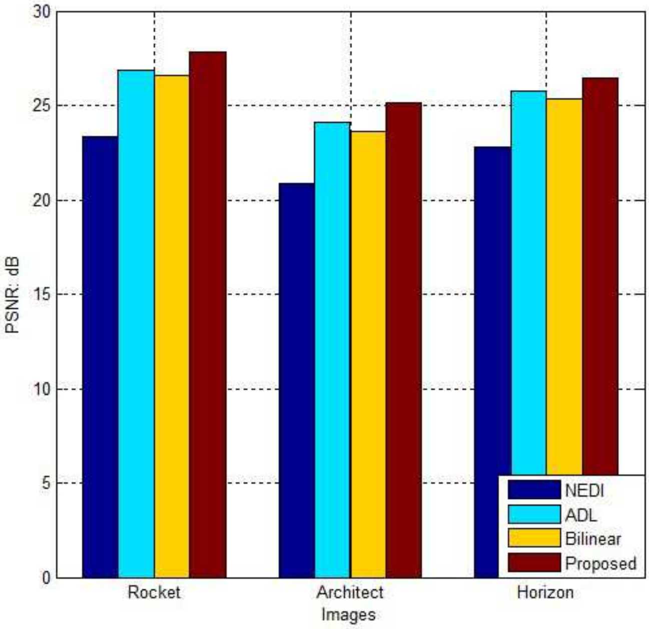

(a)

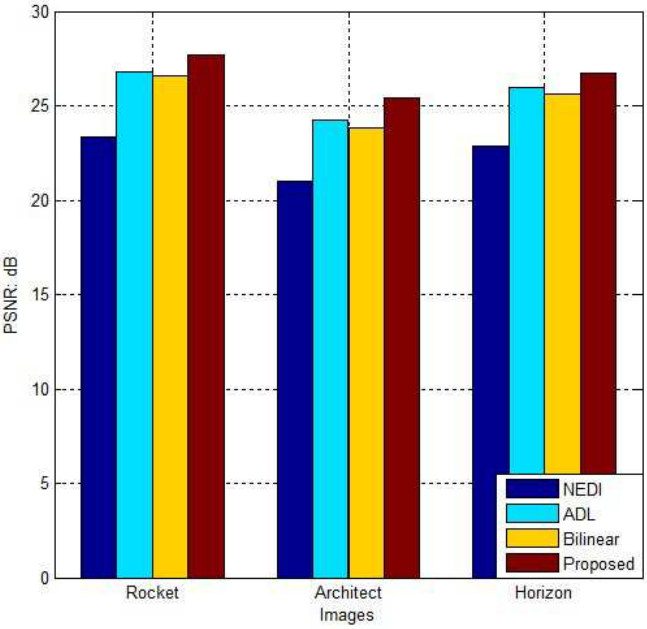

(b)

Figure 7.12: Performance evaluation in Red color channel on: (a) Noiseless image, (b) Denoised image using CDM.

Collection @ chosun

조선대학교
CHOSUN UNIVERSITY

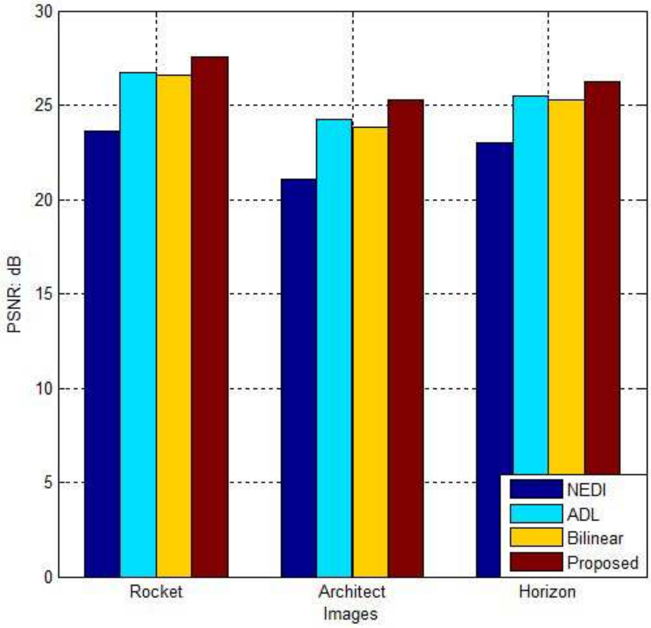

(a)

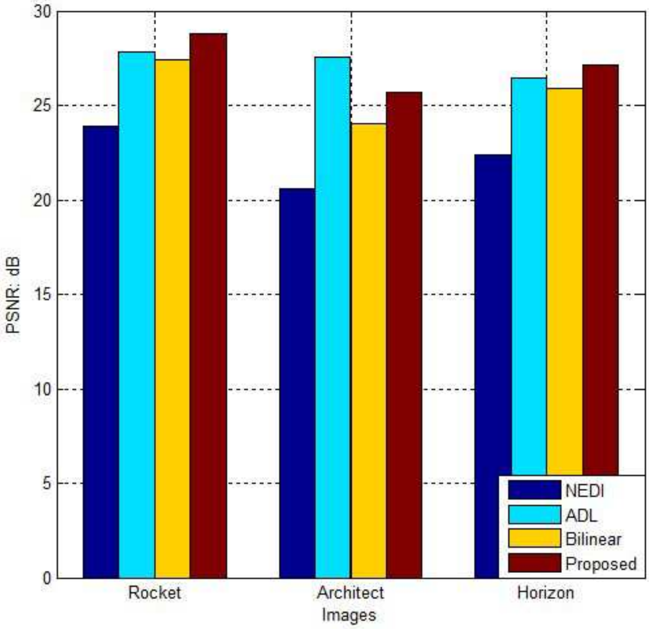

(b)

Figure 7.13: Performance evaluation in Green color channel on: (a) Noiseless image, (b) Denoised image using CDM.

Collection @ chosun

조선대학교 CHOSUN UNIVERSITY

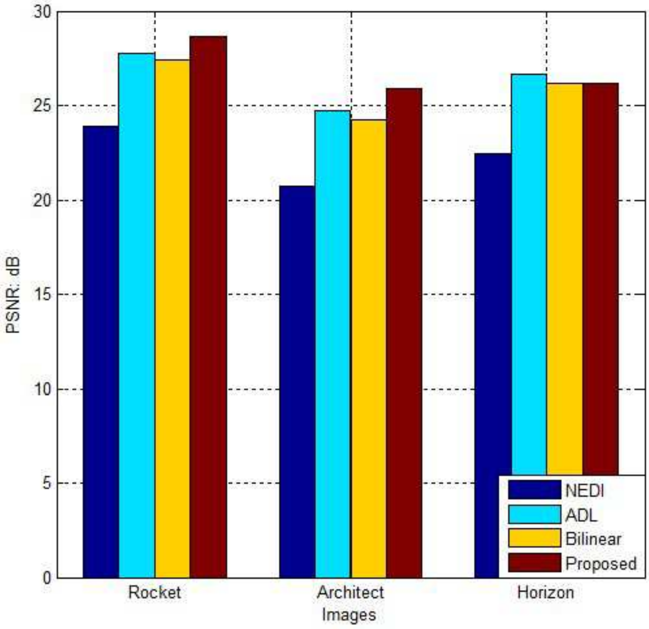

(a)

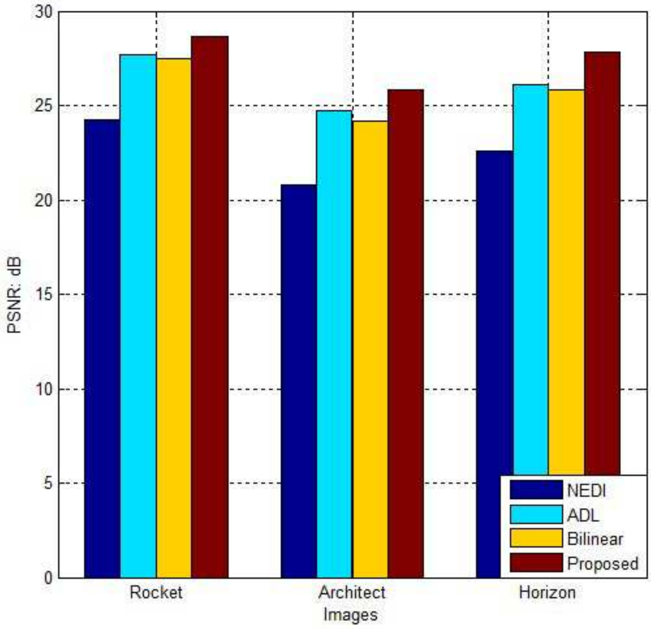

(b)

Figure 7.14: Performance evaluation in Blue color channel on: (a) Noiseless image, (b) Denoised image using CDM.

Collection @ chosun

조선대학교
CHOSUN UNIVERSITY

denoised images separately. Figures 7.10 shows interpolation of noisy image. Figure 7.10(a) shows the original image. Figure 7.10(b) shows an interpolated image using NEDI. Figure 7.10(c) shows a magnified image using the bilinear method. Figure 7.10(d) shows a upscaled image using the adaptive directional lifting (ADL) based method. Finally, Figure 7.10(e) shows the image upscaled using the proposed method. The corresponding PSNR values are shown in Figure 7.12(a), 7.13(a) and 7.14(a). Similarly, Figures 7.11 shows interpolation of denosied image. Figure 7.11(a) shows the original image. Figure 7.10(b) shows an interpolated image using NEDI. Figure 7.11(c) shows a magnified image using the bilinear method. Figure 7.11(d) shows a upscaled image using the adaptive directional lifting (ADL) based method. Finally, Figure 7.11(e) shows the image upscaled using the proposed method. The corresponding PSNR values are shown in Figure 7.12(b), 7.13(b) and 7.14(b).

7.5 Subsection Summaries

In this section, we discussed on image interpolation method based on the DT-CWT and HMM method. We used the DT-CWT is to decompose the low-resolution image into different subbands. In wavelet domain interpolation, given image was assumed as the low frequency LL subband of the wavelet coefficients of a high-resolution image. The proposed method estimates the higher band coefficients by learning the correlation between the coefficients across the scale. The relationship between the wavelet coefficients across the scale is described by HMM, and each wavelet coefficient is modelled by a Gaussian mixture having multiple means and variances. Experimental results demonstrated that the proposed algorithm yields images that are sharper compared to several other methods in noisy and noiseless scenario.

Collection @ chosun

조선대학교
CHOSUN UNIVERSITY

Chapter 8
Conclusions

This thesis presented a new class of algorithm for the reduction of noise in CFA sensor images. Since, the proposed algorithm works by properly analyzing the pixel statistics and applying the filter appropriate for pixels of different class, It is aimed to reduce the noise by preserving the original edge details. The experimental results have shown that this algorithm has satisfactory performance on a wide variety of images. Due to its non iterative and low complexity property, it can be applied for denoising in low power devices such as mobile phones and PDAs with minimal requirements of computational cost. Moreover, with the application of optimal MMSE filter it has provided good results in both subjective and objective quality metrics. At the same time, the proposed thesis presented efficient up-sampling algorithm based on the wavelet transform based interpolation. Through out this dissertation we proposed three types of wavelet transform based interpolation methods namely, ADL based, hybrid DWT and DCT based and DT-CWT with HMM method. The proposed up-sampling methods yields much better visual quality in high resolution color images and better PSNR for both the color and gray scale images compared to current state of the art in the literature of high-resolution display systems. The better performance comes at the expense of increase in complexity. However it is not a significantly high. We believe, many modifications can be done on the proposed method that can further improve its performance and reduce computational complexity. Finally, owing to the combined DT-CWT and HMM concept of the proposed method, it can be efficiently used for the interpolation of HD images.

Collection @ chosun

조선대학교
CHOSUN UNIVERSITY

Bibliography

[1] P. B. Denyer, U. Kenshaw, W. Guoyu, and L. Mingying, *CMOS image sensors for multimedia applications*, Proceedings of IEEE Custom Integrated Circuits Conference, vol. 2415, 1-4, May 1993.

[2] E. R. Fossum, *CMOS image sensors: electronic camera on a chip*, IEEE Trans. on Electron Devices, vol. 44, no. 10, 1689-1679, October 1997.

[3] E. R. Fossum, *Active Pixel Sensors: are CCD's dinosaurs?*, Proceedings of SPIE Electronic Imaging Conference, vol. 1900, 2-14, 1993.

[4] T. Yamada, Y.-G. Kim, H. Wakoh, T. Toma, T. Sakamoto, K. Ogawa, E. Okamoto, K. Masukane, K. Oda, and M. Inuiya *A Progressive Scan CCD Imager for DSC Applications*, Proceedings of the 2000 International Solid State Circuits Conference, vol. 43, 110-11,2000.

[5] B. E. Bayer, *Color Imaging Array*, U. S. Patent, 3, 971, 965, 1976.

[6] R. Lukac and K. N. Plataniotis,*Color filter arrays: design and performance analysis,* IEEE Trans. Consum. Electron., vol. 51, no. 11, 1260-1267, Nov. 2005.

[7] R. Lukac, *Single-sensor imaging in consumer digital cameras: a survey of recent advances and future directions*. J. Real Time Image Process, 1, 45-52, 2006.

[8] K. Hirakawa, X.-L. Meng, and P. J. Wolfe, *A framework for waveletbased analysis and processing of color filter array images with applications to denoising and demosaicking*, in Proc. ICASSP, Apr. 2007, vol. 1, pp. I-597-I-600.

[9] K. Hirakawa, and T. W. Parks, *Joint demosaicking and denoising*, IEEE Trans. Image Process. vol. 15, no. 8, 2146-2157, 2006.

Collection @ chosun

조선대학교 CHOSUN UNIVERSITY

[10] K. Hirakawa and X.-L. Meng, *Spatially adaptive color filter array interpolation for noiseless and noisy data*, in Proc. Int. Conf. Image Process., 1453-1456, Oct. 2006.

[11] D. Paliy, V. Katkovnik, R. Bilcu, S. Alenius, and K. Egiazarian, *Int. J. Imaging Systems and Technology, Special Issue on Applied Color Image Processing*, vol. 17, pp. 105-122, 2007.

[12] D. Paliy, M. Trimeche, V. Katkovnik, and S. Alenius, *Demosaicking of noisy data: spatially adaptive approach*, Proc. SPIE, vol. 6497, 64970-64970, 2007.

[13] R. Ramanath and W. E. Snyder, *Adaptive demosaicing,* J. Electron. Imag., vol. 12, no. 4, 633-642, Oct. 2003.

[14] D. L. Donoho, *De-noising by soft thresholding,* IEEE Trans. on Info. Theory, 41, (1995) 613-627, 2006.

[15] U. Bal *Wavelet Dual tree complex wavelet transform based denoising of optical microscopy images,* Biomedical optics express, vol. 3, no. 12, 2012.

[16] D. Donoho and I. M. Johnstone, *Ideal spatial adaptation by wavelet shrinkage,*Biometrica, vol. 81, no. 3, 425-455, 1994.

[17] X. Wang, *Moving Window-Based Double Haar Wavelet Transform for Image Processing,*IEEE Trans. on Image Processing, vol. 15, no. 9, 2771-2779.

[18] S. G. Chang, B. Yu, and M. Vetterli, *Adaptive wavelet thresholding for image denoising and compression,*IEEE Trans. on Image Process., vol. 9, no. 9, Sep. 2000

[19] M. Kazubek, *Wavelet domain image denoising by thresholding and Wiener filtering,* IEEE Signal Processing Letters, vol. 10, no. 11, 324-326, 2003.

[20] N. G. Kingsbury, *Image processing with complex wavelets,* philos. Trans. R. Soc. London A, Math, phus. Sci., vol. 357, no. 1760, 2543-2560, Sep. 1999

Collection @ chosun

조선대학교
CHOSUN UNIVERSITY

[21] W. Selesnick, R. G. Baraniuk, and N. C. Kingsbury, *The dual-tree complex wavelet transform,* IEEE signal processing magazine, vol. 22, no. 6, 123-151, 2005.

[22] A. Buades, B. Coll, and J. M. Morel, A review of Image denoising algorithms, with new one, Multiscale Model Simul., vol. 4, no. 2, Jul. 2005.

[23] L. Zhang, R. Lukac, X. Wu, and D. Zhang, *PCA-Based Spatially Adaptive Denoising of CFA Images for Single Sensor Digital Cameras,* IEEE Trans. on image processing, vol. 18, no. 4, Apr. 2009.

[24] T. Tasdizen, Principal components for non-local means denoising, Proc. Int Conf. Image Proc, 1728-1731, 2008.

[25] L. Zhang, X. Wu, and D. Zhang, *Color reproduction from noisy CFA data of single sensor digital cameras,* IEEE Trans. Image Process., vol. 16, no. 9, pp. 2184-2197, Sep. 2007.

[26] K.I. Diamantaras and S.Y. Kung, *Principal Component Neural Networks,* Wiley, New York, 1996.

[27] A. Foi, S. Alenius, V. Katkovnik, and K. Egiazarian, *Noise measurement for raw-data of digital imaging sensors by automatic segmentation of nonuniform targets,* IEEE Sensors J., vol. 7, pp. 1456-1461, 2007.

[28] H. J. Trussell and R. E. Hartwig, *Mathematics for demosaicking,* IEEE Trans. Image Process., vol. 11, no. 4, pp. 485-492, Apr. 2002.

[29] K. Hirakawa and X.-L. Meng, *An empirical bayes EM-wavelet unification for simultaneous denoising, interpolation, and/or demosaicing*, in Proc. Int. Conf. Image Process., Oct. 2006, pp. 1453-1456.

[30] C. C. Koh, J. Mukherjee, and S. K. Mitra, *New efficient methods of image compression in digital cameras with color filter array*,IEEE Trans. Consum. Electron., vol. 49, no. 11, pp. 1448-1456,Nov. 2003.

Collection @ chosun

조선대학교
CHOSUN UNIVERSITY

[31] K. Hirakawa and T. W. Parks, *Adaptive homogeneity-directed demosaicing algorithm,*IEEE Trans. Image Process., vol. 14, no. 3, pp. 360-369, Mar. 2005.

[32] B. K. Gunturk, J. Glotzbach, Y. Altunbasak, R. W. Schafer, and R. M. Mersereau, *Demosaicking: Color filter array interpolation in singlechip digital cameras,* IEEE Signal Process. Mag., vol. 22, no. 1, pp. 44-54, Jan. 2005.

[33] J. E. Adams, *Intersections between color plane interpolation and other image processing functions in electronic photography,* Proc. SPIE, vol. 2416, pp. 144-151, 1995.

[34] T. M. Lehmann, C. Gonner, and K. Spitzer, *Survey: Interpolation Methods in Medical Image Processing,* IEEE Trans. on Medical Imaging. 18, 1999.

[35] P. Thevenaz, T. Blu, and M. Unser, *Survey: Interpolation Methods in Medical Image Processing,* IEEE Trans. on Medical Imaging., vol. 18, 1999.

[36] S. E. El-Khamy, M. M. Hadhoud, M. I. Dessouky, B. M. Salam, F. E. A. El-Samie, *Efficient implementation of image ineterpolation as an inverse problem,* Digital Signal Processing, 137-152, 2005.

[37] S. W. Lee and J. K. Paik, *Image interpolation using adaptive fast B-spline filtering,* IEEE International Conference on Acoustics, Speech and Signal Processing, vol. 5, 177-180, 1993.

[38] Q. Wang and R. Ward, *A New Edge-Directed Image Expansion Scheme,* in Proc. Int. Conf. Image Processing, vol. 3, 899-902, 2001.

[39] X. Li and M. T. Orchard, *New Edge-Directed Interpolation,* IEEE Trans. Image Processing, vol. 10, 1521- 1527, 2001.

[40] M. Li and T. Q. Nguyen, *Markov Random Field Model-Based Edge-Directed Image Interpolation,* IEEE Trans. Image Processing, vol. 7, 2008.

[41] W. S. Tam, C.W. Kok, and W. C. Siu, *Modified edge-directed interpolation for images,* Journal of Electronic Imaging, vol. 19, 2010.

Collection @ chosun

조선대학교
CHOSUN UNIVERSITY

[42] A. P. Pentland, *Interpolation Using Wavelet Bases,* IEEE Trans. on Pattern Analysis and Machine intelligence, vol. 16, 1994.

[43] M. S. Crouse, R. D. Nowak, and R. G. Baraniuk, *Wavelet-Based Statistical Signal Processing Using Hidden Markov Models,* IEEE Trans. on Signal Processing, vol. 46, 1998.

[44] K. Ratakonda and N. Ahuja, *POCS-based adaptive image magnification,* in Proc. IEEE Int. Conf. Image Processing, 203-207, 1998.

[45] C. H. Kim, S. M. Seong, J. A. Lee, and L. S. Kim, *Win scale, An Image Scaling Algorithm Using an Area Pixel Model,* IEEE Transaction on Circuits and Systems for Video Technology, 13, 2003.

[46] E. Aho, J. Vanne, K. Kuusolonna, and T. D. Hamalainen, *Comments on Win scale, An Image Scaling Algorithm Using an Area Pixel Model,* IEEE Transaction on Circuits and Systems for Video Technology, 15, 2005.

[47] N. G. Kingsbury *Image processing with complex wavelets,* philos. Trans. R. Soc. London A, Math, phus. Sci., 357, 25433-2560, 1999.

[48] K. Kinebuchi, D. D. Muresan, and W. Thomas, and T. W. Parks *Image interpolation using wavelet based hidden Markov trees,* in procedding (ICASSP'01), 3, 1957-1960, (2001).

[49] J. K. Romberg, H. Choi, R. G. Baraniuk, and N. G. Kingsbury, *Hidden Markov tree modeling for complex wavelet transforms,* in Proc. ICASSP, 1, 133-136, 2000.

[50] W. S. Tam, *Modified edge-directed interpolation,* proceeding of 17th European Signal Processing Conferrence, 283-287, 2009.

[51] W. X.-Yuan and C. Z. Feng, *An Improved Image Interpolation Algorithm,* Multidim. System Signal Processing, 20, 385-396, 2009.

[52] G. Jeon, J. Lee, W. Kim, and J. Jeong *Edge Direction-Based Simple Resampling Algorithm,* in Proc. Int. Conf. Image Processing, 7, 397-400, 2007.

Collection @ chosun

조선대학교
CHOSUN UNIVERSITY

[53] R. K. Lama, M. R. Choi, J.- W. Kim, J. Y. Pyun, and G. R. Kwon *Color image interpolation for high resolution display based on adaptive directional lifting based wavelet transform,* in Proc. Int. Conf. on Consumer Electronics (ICCE), 219-221, 2014.

[54] M. E. Wall, A. Rechtsteiner, and L. M. Rocha, *Singular Value Decomposition and Principal Component Analysis,*In A Practical Approach to Microarray Data Analysis., 91-109, 2014, Kluwer: Norwell, MA (2003).

[55] N. Muller, L. Magaia and B. M. Herbst, *Singular Value Decompostion, Eigenfaces, and 3D Reconstrucitons.*SIAM REVIEW, 46, 518-545.

[56] A. R. Webb and QinetiQ Ltd. *Statistical Pattern Recognition. Second Edition,* John Wiley and Sons, Ltd, Malvern, UK, 2002.

[57] N. G. Kingsbury, *Complex wavelets for shift invariant analysis and filtering of signals,* Applied and Computational Harmonic Analysis, 10, 234-253, 2001.

[58] I. W. Selesnick, R. G. Baraniuk, and N. C. Kingsbury, *The dual-tree complex wavelet transform,* IEEE signal -processing magazine, 22(6), 123-151, 2005.

[59] S. Mallat, *A theory for multiresolution signal decomposition: The wavelet representation,* IEEE Transactions on Pattern Analysis and Machine Intelligence, 11(7), 674-693, 1989.

[60] Daubechies and W. Sweldens, *Factoring wavelet transforms into lifting steps,* Journal of Fourier Analysis and Applications, 4(3), 247-269, 1998.

[61] N. Ahmed, T. Natarajan and K. R. Rao, *Discrete Cosine Transform,* IEEE Transactions on Computers, C-23(1), 9093, 1974.

[62] K. Gallo and G. Assanto, *All-optical diode based on second-harmonic generation in an asymmetric waveguide,* J. Opt. Soc. Am. B, 16(2), 267269 (1999).

Collection @ chosun

조선대학교
CHOSUN UNIVERSITY

[63] D. Yelin, D. Oron, S. Thiberge, E. Moses, and Y. Silberberg, *Multiphoton plasmon-resonance microscopy,* Opt. Express 11(12), 13851391 (2003).

Collection @ chosun

조선대학교
CHOSUN UNIVERSITY

Acknowledgement

I would like to express my deep and sincere gratitude to my supervisor, Prof. Goo-Rak Kwon. His invaluable support, encouragement, supervision, personal guidance, and useful suggestions throughout the course of my research have provided a good basis for the completion of this thesis. I owe my most sincere gratitude to Prof. Jae-Young Pyun for his precious support and cooperation. I wish to express my warm and sincere thanks committee members, Prof. Sung-Jo Han, Prof. Sung-Won Jung and Prof. Jong Woo Kim for their detailed and constructive comments, and for their important support throughout this work. I also like to express thanks to all my lab mates of Digital Media Computing and all friends in Korea for their support and cooperation. I owe my loving thanks to my parents. They have lost a lot due to my research abroad. Without their encouragement and understanding it would have been impossible for me to finish this work. My special gratitude is due to my brother, my sisters and their families for their loving support for this study. The financial support of the National Research Foundation (NRF) of Korea and Chosun University is greatly acknowledged.

Collection @ chosun